A novel zonal adaptive DG anti-islanding protection scheme to enhance future system stability using real-time inertia estimates

Xue Cao

A thesis presented in fulfilment of the requirements for the degree of Doctor of Philosophy

Advanced Electrical Systems Group
Institute of Energy and Environment
Department of Electronic and Electrical Engineering
University of Strathclyde

2016

This thesis is the result of the author's original research. It has been composed by the author and has not been previously submitted for examination which has led to the award of a degree.

Signed: Date:

Acknowledgements

First and foremost, I would like to express my deepest gratitude to my principle supervisor Prof. Graeme Burt, for giving me such a fantastic opportunity to conduct this research, and for his invaluable guidance, generous support and kind encouragement throughout my studies.

Secondly, I would also like to give my sincere thanks to my second supervisor Dr Campbell Booth. The practical considerations and challenges Dr Booth posed to my work at each stage, pushed me to think about the wider picture with a deeper understanding of the problem.

In particular, I must express my profound gratitude to Dr Ibrahim Abdulhadi for his continuous knowledgeable guidance from the very first day of my PhD research and Dr Bruce Stephen for his selfless support in reference to Chapter 4 of this work.

Completing this research would have been more difficult were it not for the intent listening, encouragement and friendship from my dear friends and colleagues. They are, Dr Jianing Cao, Dr Ran Li, Dr Abdullah Emhemed, Dr Xinyao Li, Jennifer Shaw, Zhen Shi, Dr Yunhai Shan, Dr Li Li, Dr W.H. Siew, Dr Adam Dysko, Prof K.L. Lo, Dr Tianyu Luo and Yu Zhao.

Most importantly, millions of thanks go to my beloved parents, who are thousands of miles away but love me and believe in me unconditionally. Their understanding and endless care are invaluable especially during the period of this research.

Abstract

Emerging power system designs are driven towards supporting the diversity of generation supply through increased flexibility and progressive employment of renewable resources [1], in order to fulfil sustainable and low carbon energy development strategies. The resulting impact on system response, especially during and following disturbances, can incur negative power system stability issues. With particular attention given to the anticipated reduction and variation of system inertia, concerns are growing with respect to power system frequency stability following large disturbances. This is attributed to the potential involvement of acceleration and magnification in frequency excursions due to reduced inertia and differences in generator (particularly converter-interfaced source) control and responses to disturbances.

Despite the fact that new techniques, such as those that produce "synthetic" inertial responses, are evolving to compensate for the absence of inherent inertia from renewable resources, their practical integration into the existing grid is limited at the present stage. This is attributed to the uncertainties underlying when and how these techniques should be applied, with a major barrier to their deployment being a lack of prevailing system inertia information. As the exact amount of real-time response required cannot be known with a high degree of confidence, a risk of "over-responding" would be incurred if inertial responses are deployed widely throughout the system. Moreover, the suitability of adopting present-day frequency-based protection settings in conjunction with aforementioned techniques in future power networks has not been fully investigated, where frequency stability margins, necessitating active regulation, could dynamically vary. As such, the work reported in this thesis focuses on evaluating the impact of variable inertia on the performance of existing frequency-based protections and the feasibility of introducing adaptive solutions as a flexible and reliable approach to improve the performance of affected frequency protection schemes, thereby enhancing future system frequency performance.

There are two major contributions in this thesis. Firstly, a Switching Markov Gaussian Model (SMGM) has been proposed with which the real-time inertia estimates can be profiled from observed frequency variations during normal system operation. An optimised error of lower than 10% (taken for a system of an overall inertia equal to 3 seconds) was produced for 95% of the daily estimation if being calibrated with the equivalent inertia derived from generation dispatch data on a half-hourly basis and its robustness can be maintained for a period of up to two hours when losing frequency observations. Secondly, a zonal adaptive Distributed Generation (DG) anti-islanding protection scheme has been developed and demonstrated with protection settings being adjusted in response to estimated levels of system inertia. Enhancement of the performance of DG anti-islanding protection has been tested and demonstrated on a reduced GB power network model. Validity and robustness have been analysed, along with discussions of configuration adjustments and practicalities of adopting reliable adaptive protection schemes.

Table of Contents

List of Figures

List of Tables

List of Abbreviations

AIC	Akaike's Information Criterion
BIC	Bayesian Information Criterion
BMU	Balancing Mechanism Unit
CCGT	Combined Cycle Gas Turbines Generation
CFR	Commercial Frequency Response
DG	Distributed Generation
DSFR	Demand Side Frequency Response
DSM	Demand Side Management
EM	Expectation Maximisation
EMS	Energy Management System
ES	Energy Storage
ETYS	National Grid's Electricity Ten Year Statement
EVs	Electric Vehicles
FCDM	Frequency Control by Demand Management
FFR	Firm Frequency Response
FR-GFAs	Frequency Responsive Grid Friendly Appliances
GB	Great Britain
GL	Glasgow
GMM	Gaussian Mixture Model
IEDs	Intelligent Electronic Devices
LN	London
LoM	Loss of Mains
MFR	Mandatory Frequency Response
MN	Manchester
MSE	Mean Squared Error
NDR	Non-Detection Risk
OC	Overcurrent
OCC	On-line Calibration Cycle
PDC	Phasor Data Concentrator

PMU	Phasor Measurement Unit
Z-APS	Zonal Adaptive Protection Scheme
RoCoF	Rate-of-Change-of-Frequency
SG	Synchronous Generator
SMGM	Switching Markov Gaussian Model
SNR	Signal-to-Noise Ratio
SOC	States of Charge
SYS	National Grid Electricity Transmission System Seven Year Statement
UFLS	Underfrequency Load Shedding
WAMPAC	Wide Area Monitoring, Protection and Control
WTGs	Wind Turbine Generation Units

List of Symbols

D	System damping constant
df	Frequency deviation
f_t	Frequency observation at time t
Δf	Sum of frequency increments (on a 20 ms resolution) throughout the 5-minute period
Δf_{GL_20ms}	Frequency change at Glasgow on a 20 ms basis
Δf_{MN_20ms}	Frequency change at Manchester on a 20 ms basis
Δf_{LN_20ms}	Frequency change at London on a 20 ms basis
G_{steam_f}	Frequency-responsive steam turbine generator
$\Delta(df/dt)$	Sum of increments in the rate of change of system frequency on a 20 ms basis over 5-minute period
G_{steam_nf}	Non-frequency-responsive steam turbine generator
G_{gas_f}	Frequency-responsive gas generator
G_{gas_nf}	Non-frequency-responsive gas generator
H_g	Inertia constant of a generation unit
H_{est_t}	Estimated system inertia constant at time t
$H_{north_{eq}}$	The equivalent inertia for the labelled north region
$H_{south_{eq}}$	The equivalent inertia for the labelled south region
H_0	Latest observed system inertia
H	System inertia constant
H_t	System inertia constant at time *t*
H_{t-1}	System inertia constant at time prior to *t*
H_{t_0}	System inertia constant at time t_0
H_{t_0+5min}	System inertia constants at 5 minutes after t_0
ΔH	Change of system inertia constant on a 5-minute basis
$\Delta H_{est\_t\|\Delta f}$	Estimated change of system inertia conditional on an observed system summed frequency variation average Δf on a 5-minute basis
$\Delta(dH/dt)$	Increments in the rate of change of system frequency on a 20 ms basis over 5-minute period
I_S	Current at sending end
I_R	Current at receiving end

J	Combined moment of inertia of generator and turbine
K_{pf}	Frequency coefficient for real power
K_{qf}	Frequency coefficient for reactive power
L	Load reference setpoint
np	Voltage exponents for active power
nq	Voltage exponents for reactive power
P_e	Electric power
P_0	Rated real power
$P_{o/p}$	Output of the generator under various load reference setpoint
P_{PL_N}	Renewable generation in the labelled north region
P_{PL_S}	Renewable generation in the labelled south region
P_{tot}	Total power generation
P_m	Mechanical power
P_R	Real power at receiving end
P_S	Real power at sending end
ΔP	Change of power output
$\Delta P_{p.u.}$	Change of real power in per unit
Q_0	Rated reactive power
Q_R	Reactive power at receiving end
Q_S	Reactive power at sending end
R	Speed-droop character
R_e	Equivalent transmission line resistance
R_{PL}	Penetration level of renewable resources in the entire GB system
R_{PL_N}	Penetration level of renewable resources in the labelled north region to the total renewable penetration level in the entire system
R_{PL_S}	Penetration level of renewable resources in the labelled south region to the total renewable penetration level in the entire system
r_C	Correlation coefficient
r-square	Coefficient of determination
S_f	Sample standard deviation of frequency
S_H	Sample standard deviation of inertia
S_n	Machine rating
t_0	The initial counting time from when the frequency measurements start to be summed up

V	Instantaneous voltage
var	A variance filter with moving window
w_m	Mixing weight or probability of the mixture component m occurring,
ω_o	Rated angular velocity of the rotor
ω_S	Rotor speed
Δw	Rotor speed change
X_e	Equivalent transmission line reactance
Y_e	Equivalent transmission line admittance
$\widehat{y_i}$	The estimates
y_i	The true value
δ	Rotor angle
μ	Mean vector
μ_1	The mean vector of the variable to be predicted
μ_2	The mean vector of the variable already known
μ_m	The Gaussian mean of m^{th} mixture component
$\sum$	Variances
Σ_m	The Gaussian covariance of m^{th} mixture component
$COV(f, H)$	Covariance between frequency and inertia
$P(f \cap H)$	Joint probability between frequency and inertia
$P(H\|f)$	Conditional probability between frequency and inertia

1. Introduction

1.1 Research Context

Future power systems will be more complex and less predictable through the widespread introduction of renewable resources, often interfaced via power electronic converter devices. To meet GB's 'green energy target', which states that 15% of the electricity supplied must come from renewable resources by 2020 to reduce the emissions of CO_2 [2], a large amount of renewable generators will have to be accommodated throughout the transmission system and distribution networks. Driven by the growing size of nuclear generators being commissioned, the largest infrequent infeed loss in the GB network, which refers to the acceptable level of power infeed loss on the occurrence of which the system frequency would not deviate outside the range 49.5 Hz to 50.5 Hz for more than 60 seconds, has been increased from 1320 MW to 1800 MW [3]. Moreover, intelligent domestic energy management systems which are computer-aided system monitoring and management tools, since being initially introduced in the 1980s [4], were applied to dynamically control and optimise energy consumption to achieve more economic power balance. As a direct consequence of this paradigm shift, great challenges have been placed on power system dynamic operation in terms of it becoming more active in nature and being pushed closer to its operating limits.

In addition to the potential network reinforcement required as a result of system expansion, one of the most pressing challenges stems from witnessing not only a gradual reduction of system inertia level but also through the fact that system inertia will have higher volatility and variability in the future [2]. This is attributed to the progressive retirement of large conventional fossil-fuel generation plants with their replacement by renewable resources which generally are intermittent in nature. These renewable units, unlike large synchronous machines (which naturally provide valuable damping torque to any system frequency excursion based upon their inertia constants), are decoupled by power electronics from the grid, therefore, unable to

deliver inherent inertial frequency response. The future systems, involving high levels of renewable penetration, will therefore experience accelerated and magnified frequency excursions more frequently in comparison with the behaviour of present-day power networks.

Due to the fact that the frequency variations are upset with system inertia constants, future power systems, especially their frequency stability, could benefit considerably from having a continuous real-time estimate of system inertia. However, the dependency between frequency and inertia and the significance of such relation in identifying potential system instability and issuing effective strategies (e.g. adequate proactive control and protection) in future networks have not been clearly addressed and quantified. Current practices in deriving system inertia are only effective upon the occurrence of a disturbance coupled with analysis of the transient data gathered during and after the disturbances [5-8]. Therefore, it is unrealistic to gain instantaneous access to system inertia information prior to any disturbances, which, as a consequence, limits its practical application for taking proactive actions to mitigate the negative effects. As such, it is necessary to evaluate and establish a valid means of estimating system inertia continuously and in real time.

Underlying the upset of inertia reduction and variations on system frequency response, an adverse effect will potentially be imposed on the stability and sensitivity of frequency-based protections, such as Rate-of-Change-of-Frequency (RoCoF) based DG anti-islanding protection and under-frequency load shedding (UFLS) [9, 10], jeopardising required performance levels. This could be exacerbated by a subsequent increase of any initial power imbalance if further power sources are unexpectedly disconnected due to protection mal-operation. Such a cascade event could severely affect power system stability and consequently lead to a blackout. Adaptive protection, which exhibits flexibility and adjustability by tuning protection settings to be best suited to prevailing system conditions, could be a potential solution to the increased challenges posed by reduced system inertia. There are many adaptive protection schemes that have been widely discussed in literature [11-16]. However, a majority of the proposed adaptive frequency-based protection functions,

such as [14-16], focus on achieving optimised automatic load disconnection with few of them concerning RoCoF-based DG Loss of Mains (LoM) protection. Moreover, the strategies in the proposed adaptive protection schemes typically involve increasing/decreasing protection thresholds with one unique value applied across the entire network. It is clear that there are zonal variations in frequency response across a network, as outlined in [17-19]. Such schemes, if adopted in a practical network, could desensitise/over-sensitise the operation of protection systems in a certain way. This is due to the fact that protection settings are fixed and normally set with factors applied considering the variations across the network to cope with most of the scenarios.

Given the overwhelming significance of inertia reduction and variation on system frequency response as well as the performance of system frequency-based protections, estimating system inertia, if realised, will be valuable to minimise or even avoid erroneous behaviour in system operation. Such information could be used for proactive control or protection schemes, where the settings or the operating strategies are regulated for the system dynamics, thereby reducing the risk of incorrect operations and potentially system blackouts. Moreover, a more accurate and dedicated performance of protection systems will be achieved if taking into account the local frequency variations when actively profiling the protection settings. To achieve these objectives, the work reported in this thesis focuses on addressing the following three questions:

- What is the quantitative impact of changes in system inertia on frequency response across the entire network and the performance of frequency-based protections?
- Is there a valid approach capable of estimating real-time inertia from dynamic frequency observations?
- Are adaptive protection techniques an effective means to diminishing the risk of mal-operation of frequency-based protections in future networks and would they be enhanced by real-time estimates of inertia in their deployed region being made available? If so, how can such schemes be designed and what are the resultant accommodated levels of increased flexibility and

enhancement of network performance (e.g. in terms of the amounts of renewable generation that may be connected)?

1.2 Research Contributions

The main research contributions reported in this thesis are as follows:

- A real-time inertia estimation algorithm has been formulated for the first time to express the underlying correlation between system frequency and inertia variations. This algorithm fills the gaps in continuous real-time inertia estimation practices – that existing techniques need transient events to perform their estimation. The accuracy and reliability of the developed algorithm have been examined against recorded historical events, and tested using cases where the frequency observations have been lost and with various levels of system noise. It has been designed as a system monitor to dynamically monitor system stability margins, as well as in this case an enabler of adaptive protection scheme to actively mitigate the risk of frequency-based protection mal-operation in the future.
- A zonal adaptive DG anti-islanding protection scheme has been firstly proposed to mitigate the unexpected tripping of RoCoF-protected DGs when subjected to large infeed loss in future networks, without jeopardising its protection sensitivity. The local generation mix and the geographic distance from the locations of disturbances to each measurement point were considered when evaluating the frequency performance against a large infeed loss, in association with the influence of prevailing system inertia constants. A three-layer adaptive protection architecture proposed and formalised in previous work [20, 21] was fitted to implement the designed adaptive protection scheme in a practical network with alterations made for specific functions assigned to each layer in this research.
- Quantification of the marginal inertia constants that cause frequency instability issues and the mal-operation boundaries of the RoCoF-based DG anti-islanding protection system and UFLS scheme. The analysis was performed using a

reduced GB model with a range of system conditions, including various renewable penetration levels and distribution patterns, locations of disturbances and sizes of infeed loss. The main objective of the work reported in this thesis is to solve the protection issues identified from the simulation results.

- A generic system modelling and validation process has been presented. Based on the proposed process, an 11-node reduced GB network model has been built by fine tuning the typical parameter values, such as droop value, lead/lag time constants, in the light of recorded historical events. Performance of the reduced model has been validated against the historical events given a valid GB dynamic model for assessing future frequency response.

1.3 Publications

The following papers have been published over the course of this research:

Journal papers:

- X. Cao, B. Stephen, I. Abdulhadi, C. Booth, G. Burt, "Switching Markov Gaussian Models for Dynamic Power System Inertia Estimation", IEEE Transactions on Power Systems, vol. PP, pp. 1-10, Issue 99, Dec. 2015.

Conference papers:

- X. Cao, I. Abdulhadi, A. Emhemed, C. Booth, and G. Burt, "Evaluation of the impact of variable system inertia on the performance of frequency based protection," in Developments in Power System Protection (DPSP 2014), 12th IET International Conference, 2014, pp.1-6.
- X. Cao, I. Abdulhadi, C. Booth, G. Burt, "Defining the Role of Wide Area Adaptive Protection in Future Networks", in Universities Power Engineering Conference (UPEC 2011), 47th International, 2011, pp. 1-6.

1.4 Thesis scope

The layout of chapters in this thesis is presented as follows:

Chapter 2 - presents an overview of power system frequency stability followed by a discussion of the challenges that may impact upon power system frequency stability in the future due to a number of reasons. This chapter presents a theoretical concept of power system frequency stability and the practical frequency regulation mechanisms used in the GB network. This chapter analyses the impact of future system developments on frequency response to events and the performance of frequency-based protection practices in present networks, including RoCoF-based LoM protection for DGs and UFLS as the last line of defence against system collapse during severe disturbances. The potential risks of protection mal-operation associated with existing performance quantitative practices are discussed at the conclusion of the chapter.

Chapter 3 - presents a detailed analysis and quantification of the erosion of system inertia constants in the future and the associated variability with respect to future system frequency response. The impact this may have on the performance of frequency-based protections is fully quantified and demonstrated. A reduced GB power network model has been created through the presented model building methodologies. The reduced model has been validated to carry out the investigations undertaken in a range of system conditions, including a range of inertia levels, sizes of infeed loss, different locations of infeed loss coupled with different renewable generation dispatch patterns. Based upon the simulation results, this chapter concludes by identifying two protection issues and builds the argument relating to the need for real-time inertia estimation and adaptive protection scheme to mitigate the risk of identified protection mal-operations in future system.

Chapter 4 - formulates a multidimensional probability model based on historical frequency and generation dispatch data where real-time inertia estimates can be generated for observed dynamic frequency variations. This chapter initially contains a review of existing inertia estimation approaches from which the need for continuous on-line inertia estimation is identified and developed. Subsequently, the concepts of Gaussian Mixture Model (GMM), Markov Chain and some other fundamental statistical terms are introduced, and these are coupled to formulate a

Switching Markov Gaussian Model as a valid means for real-time inertia estimation. The proposed methodology is implemented on the GB system model where the validity of the formulated SMGM is also assessed through its performance of estimating system inertia pre- and post-disturbance. This is carried out in conjunction with an evaluation of its robustness against loss of frequency observations input into the model and the presence of system noise. Finally, the sources of estimation errors and practical aspects associated with the implementation of the method in future networks are discussed.

Chapter 5 - verifies a new adaptive protection scheme as a flexible approach to take real-time system inertia as an incentive to effectively mitigate the mal-operation of the RoCoF-based DG LoM protection (identified with case studies in chapter 3). The allocation of the designed functions into a three-layer adaptive scheme (proposed in [20] and further developed in [21]) are presented in association with implementing the zonal DG anti-islanding protection on the scheme. The improvements in the performance of DG anti-islanding protection scheme gained through employing the adaptive feature are proven through stability tests under large infeed loss scenarios and an associated assessment of its risk of undetected islanding. Discussions are included at the end of the chapter incorporating the potential barriers of its implementation in a real system, the configuration of protection settings and issues associated with potential loss of communications facilities and how this can be dealt with.

Chapter 6 - summarises the major novelty and contributions inherent in the reported research as well as issues that are worthy of being taken forward as future work. It focuses on contributions made to the formulation of a continuous real-time inertia estimation model and the verification of using zonal adaptive protection scheme to enhance the performance of DG anti-islanding protection in future networks. Future work is identified, focusing on improving the accuracy of inertia estimation and implementing the proposed protection algorithm within a practical situation.

2. Power System Frequency Stability

2.1 Chapter Overview

Power system frequency is a continuous system-wide variable (that is essentially constant at all locations in an interconnected power system, although during transient events instantaneous frequency measurements could be different as different elements of the system and generators "swing" against each other and the system loads) that essentially is reflective of the dynamic balancing condition between system generation and demand. During power system dynamic operation, system frequency stability is seen very important as it determines whether the system will withstand the occurrence of severe system upsets. This chapter firstly reviews the concept of power system frequency stability and its frequency regulation mechanisms used in the present-day GB power system. On-going and future developments in the GB power system are then described, from which the potential frequency stability issues caused by the mal-operation of the existing frequency-based protections that may also impact upon future system operation are discussed. Questions with regards to the existing quantification practices on system frequency response are summarised at the end and this will act as a platform for the quantitative evaluation of future system frequency response that is presented later in the dissertation.

The main contributions of this chapter are listed below:

- Review of the power system frequency stability concept and frequency regulation practices in present-day GB power networks.
- Review of the system developments.
- A preliminary assessment of examples given as the impact of incorporating wind turbine generation units (WTGs) and demand side management (DSM) on system frequency response.
- Review of the existing frequency-based protections and a preliminary discussion on the risk of mal-operation of such schemes in future networks.

- Raising concerns on the shortfalls of existing practices to quantify system frequency instability in future networks.

2.2 Frequency Stability

Frequency stability is stated as: 'the ability of a power system to maintain steady frequency following a severe system upset resulting in a significant imbalance between generation and load' [22]. It defines two criteria that the performance of a system must meet in order to be classed as stable from a frequency perspective: remaining stable during normal operation and after being exposed to disturbances.

In general, instability issues are associated with a lack of adequate frequency response, improper coordination among control and protection systems or insufficient energy reserves in the system [22, 23]. In the presence of frequency instability, some protective actions which are designed to cope with excessive excursions of system voltage or frequency would be activated. As a result, a large integrated power system could potentially be split into small islanded networks (which is generally not permitted in the GB system) that further poses challenges to system frequency stability as there could be a need for generation/load disconnection and ultimately system blackout.

During frequency excursions, there are sometimes associated significant changes in voltage magnitudes that activate other protective functions apart from the frequency-based functions. In addition to automatic generation control and regulation, there is also a need to schedule power reserve manually when the automatic actions are no longer able to bring frequency back to the limits.

2.3 Standard Regulation and Trace of Power System Frequency Response

In order to maintain system frequency within an operational range (±1% of the nominal 50 Hz in the GB system [3]) for the quality of power supply, operational

policies have been drawn to regulate the dynamic frequency response in the GB power system.

Based on the timeline after the occurrence of power imbalance, the framework of frequency drop can be divided into five stages as listed below [24-26].

- Rotor swing in the first few seconds;
- Inertial response up to 10 seconds;
- Primary frequency response achieved from few seconds up to 30 seconds.
- Secondary frequency response achieved between 30 seconds up to 30 minutes.
- Tertiary frequency response achieved from 15 minutes up to several hours after a request being generated.

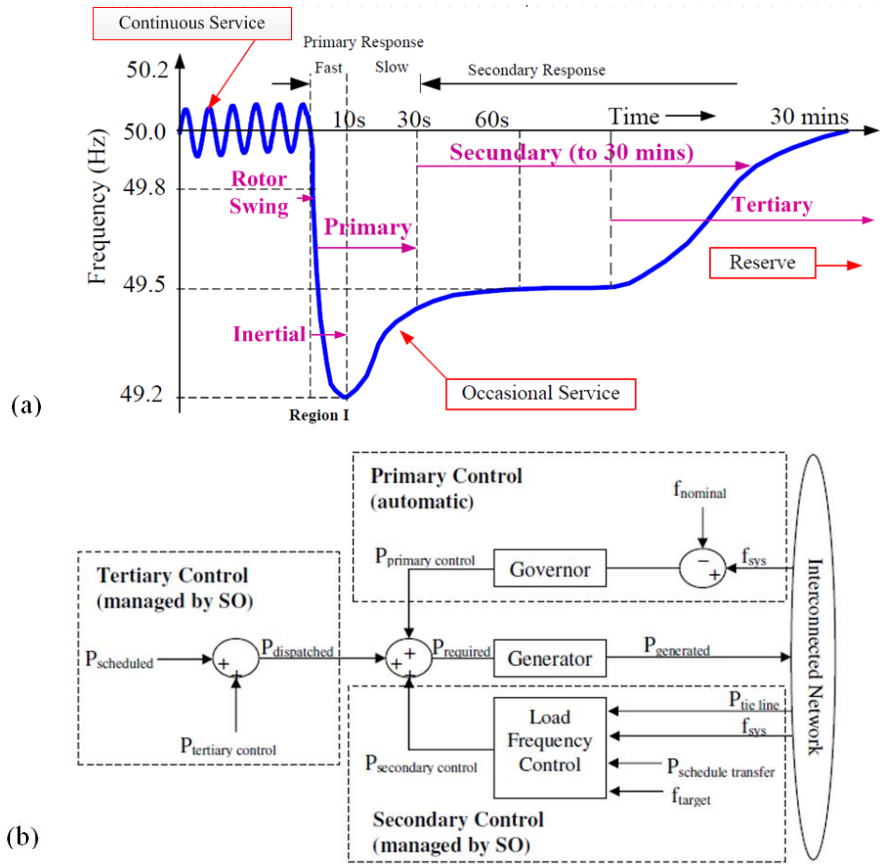

Figure 2-1: General frequency response and regulation: (a) in temporal frame [10], (b) in a schematic overview [27]

The time-series framework of system frequency response and their schematic overviews are presented in Figure 2-1. The lowest constraint for normal operating conditions is 49.8 Hz with 49.5 Hz set as the lowest statutory limit for loss of power infeed less than 60 s [3]. A maximum instantaneous deviation of 0.8 Hz (from the nominal frequency) is permitted in response to an infrequent loss of large generation event [26]. The schematic diagram presents contributors at each stage of the frequency response as stated above.

2.3.1 Generator dynamics

Under steady-state operation, a dynamic balance between mechanical power (P_m) and electric power (P_e) should always be maintained to ensure a consistent power supply (P_e will be slightly less than P_m due to losses). However, this balance will be upset when the system is subjected to disturbances. This will lead to a rotor swing which oscillates around the equilibrium point and is damped over time if the system remains stable.

Oscillations in rotor angle can be explained using the full swing equation as given in (2-1) [28], where H_g is the inertia constant of the generation unit, ω_S is the rotor speed, δ is the rotor angle and D is the damping constant. However, the damping contributed by synchronous machine damper windings is generally ignored for a system to be stable as $d\delta/dt = 0$. This simplifies the equation as well as give a pessimistic transient stability limit. It can be seen that for any net power imbalance, there will be a deviation in the rotor angle.

$$\frac{2H_g}{\omega_S}\frac{d^2\delta}{dt^2} + D\frac{d\delta}{dt} = P_m - P_e \qquad (2\text{-}1)$$

Assuming a generation loss occurs in the system, the process of regaining a new balance point is illustrated in Figure 2-2 (a). The states of all other remaining generators connected to the system move from ‘1’ to ‘2’ due to the increase in assigned power supply. However, the increased electric power output, which is higher than the mechanical power prior to the disturbance, decelerates the rotor speed

until state ‘3’ is reached. As can be seen, a higher mechanical power than the electric power is present in state ‘3’, so the rotor starts to accelerate. After iteratively decelerating and accelerating around the equilibrium point for several cycles, a new steady state (state ‘4’) is reached eventually unless the system becomes unstable. Corresponding oscillations experienced by rotor angle are shown in Figure 2-2 (b). This phenomenon can be explained by the inherent character of the generator – the rotors of remaining generators cannot immediately respond to the disturbances.

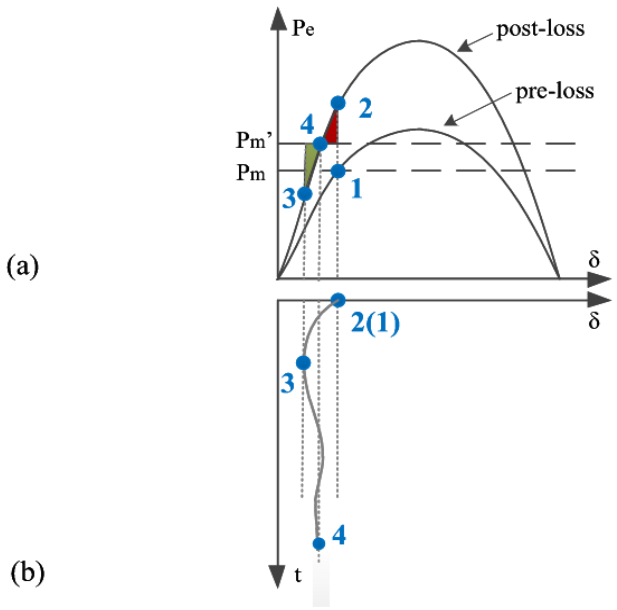

Figure 2-2: Generator dynamics during disturbances: (a) transient power-angle characteristics [24]; (b) rotor swing.

In general, the Equal Area Criterion is widely applied to assess system transient stability and calculate the critical fault clearance times [24, 28]. A stable system must satisfy the criterion that the size of acceleration area (filled in red on the diagram) should equal to the deceleration area (filled in green) as shown in Figure 2-2 (b) before the rotor angle reaches 180 degrees.

2.3.2 Inertial response

Inertial response is a natural active response of synchronous generators reacting to any power imbalance that is observed as a frequency change in the system where the

generators are connected to. It is essentially the release or absorption of kinetic energy stored in (or input to) the rotating mass of electric machines. Inertial response contributes to limiting the rate of change of system frequency following event and effectively allows more time for frequency response to begin and take action [29].

The effectiveness of inertial response on reducing the impact of sudden power imbalances and frequency deviations is determined by the inertia constant. It is defined as the kinetic energy stored in the rotating parts of a machine at synchronous speed over the rating of the machine [30, 31], expressed as in (2-2). Typical values of the inertia constants locate between 2 s to 9 s with variations attributed to diverse generation fuel types and the sizes of generation units [32].

$$H_g = \frac{J{\omega_o}^2}{2S_n} \tag{2-2}$$

where,

H_g is the inertia constant of a generation unit
J is the combined moment of inertia of generator and turbine
ω_o is the rated angular velocity of the rotor
S_n is the machine rating

For a power system consisting of more than one generation unit with their different inertia constants, the system inertia (H) should be calculated using (2-3) considering that all the generation units are operating in parallel. It takes into account the contribution from various generation fuel types and different ratings of generators in service. It is derived through summing the product of installed capacity of each individual generation unit (S_i) and its corresponding inertia (H_i) and dividing this by the total installed generation capacity [33, 34].

$$H = \frac{\sum_{i=1}^{n} H_i \cdot S_i}{\sum S_i} \tag{2-3}$$

A system of a higher overall inertia will be less susceptible to frequency variations, and vice versa. This phenomenon can be explained using the Swing Equation as in (2-1) where the frequency variation is inversely proportional to power imbalance assuming a constant inertia constant.

2.3.3 Primary frequency response

Primary frequency response is regulated by the controllers/governors of generation units in response to a change in turbine speed, which is of course reflective of changes in system frequency in a synchronous machine [35]. As shown in Figure 2-3, the governor follows a speed-drop characteristic to prevent the conflict among multiple generation units during dynamic load changes.

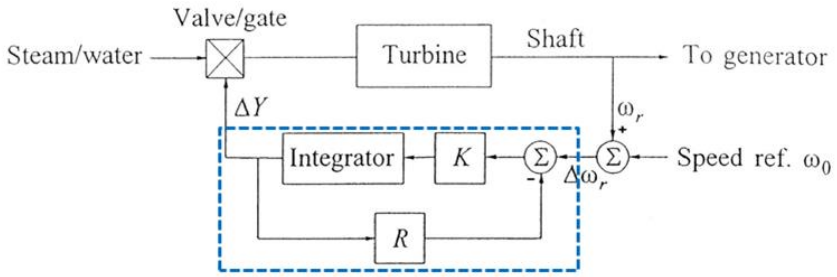

Figure 2-3: Schematic diagram of governor with steady-state feedback [30]

The theory is illustrated in Figure 2-4 where the change of power output (ΔP) is inversely proportional to rotor speed change (Δw) or frequency variation (Δf) with a slope of $1/R$. After sensing system power imbalance from the changes in rotor speed, the feedback loop in the governing system (marked in blue) regulates the power output from the generator in a ratio of 1/R to the rotor speed deviation.

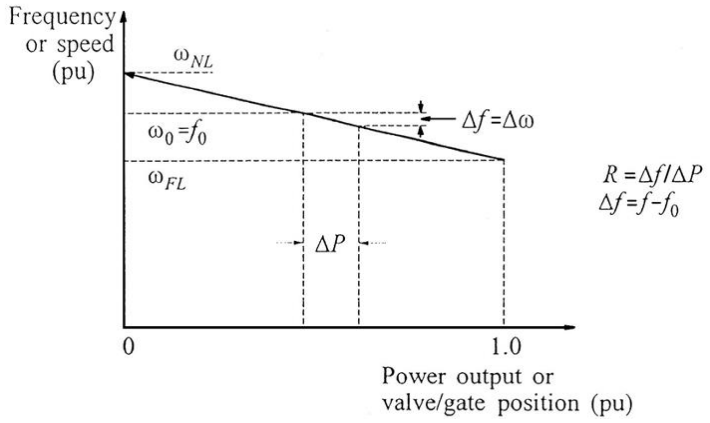

Figure 2-4: Steady-state characteristics of a governor with speed droop [30]

For a multi-unit system, a load sharing phenomena is evident, where the output of each generation unit is increased/decreased according to their individual speed-droop

characteristic with the total amount of variation from generation output equal to the amount of total load change [24, 30].

2.3.4 Secondary frequency response

Primary frequency response, as shown in Figure 2-1, should bring system frequency back to a new stable equilibrium point by increasing (or decreasing) generator outputs after any disturbance if the overall system remains stable. However, the system at this stage cannot return back to its initial frequency without additional intervention. In order to bring the system frequency back to its statutory limits, secondary frequency response should act.

Secondary frequency response is normally achieved by adjusting load reference setpoint (highlighted with red circle) as depicted in Figure 2-5. This manipulation can be applied manually by local operators or from a grid control centre.

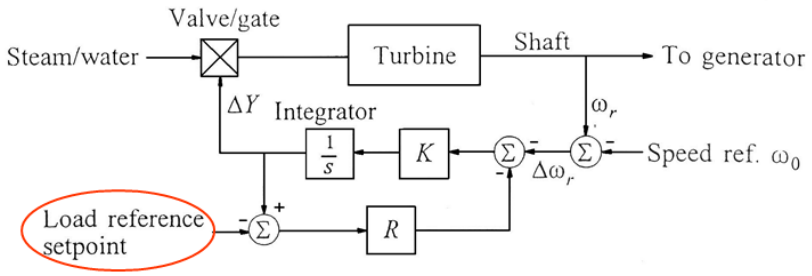

Figure 2-5: Schematic diagram of governor with load reference setpoint [30]

The paralleled lines shown in Figure 2-6 represent the shifting of speed-droop characteristic by adjusting load reference setpoint (L). With the change of load reference point from L_{ref_1} to L_{ref_1n}, the percentage of generator output is increased from P_{o/p_1} to P_{o/p_1n}, leading to a frequency rise.

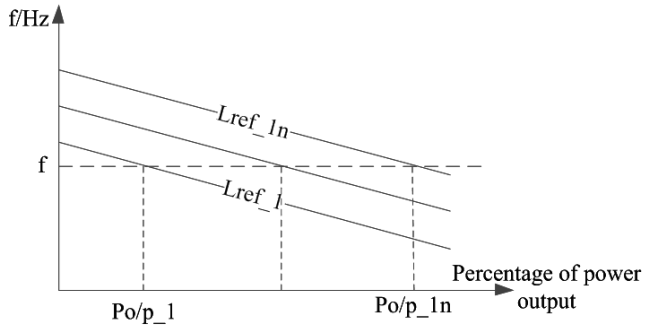

Figure 2-6: Load reference setpoint on generation output

2.3.5 Tertiary frequency response

Tertiary frequency response contributes to restoring frequency after the primary and secondary response by rescheduling the dispatch and commitment of generation units [24, 36]. The referenced operating point of an individual unit is manually/automatically adjusted by system operators based on economic dispatch or, more generally, optimal power flow to ensure adequate reserve for frequency restoration [37]. The regulation of tertiary frequency response, either achieved from on-line spinning reserve or off-line non-spinning reserve (e.g. interruptible load), should be delivered within 15 minutes according to the Grid Code .

2.3.6 Balancing services regulated by National Grid

In GB, National Grid is obligated to provide (by procuring from service providers) services to ensure the dynamic power balance between generation and demand, as well as to coordinate all infrequent risks. The followings are two balancing services procured by National Grid to maintain system frequency within operational and statutory limits [38]:

- Mandatory frequency response (MFR)
- Commercial frequency response (CFR)

MFR is defined as: ‘the ability of selected generation units to provide continuous modulation of power output in response to system frequency change’ [39, 40]. Primary response, secondary response and high frequency response are three MFR

approaches adopted in the present GB power system [41]. In addition to the time-scale of delivery, the distinction between primary and secondary frequency response can also be reflected from the operation hierarchy as the primary response controls local generation units individually while the secondary response is a regional or system wide management among multiple units [35].

CFR is a service with terms negotiated on a bilateral basis between system operators and customers. Firm frequency response (FFR) and frequency control by demand management (FCDM) are two types of CFR. FFR is a commercial service through which balancing mechanism units (BMU) and non-BMU participants, generation and demand, existing MFR providers and new providers are all committed to providing a specific measure of response [42]. A bid and offer method is employed to settle the cost from each FFR provider with a proven delivery capability, contracted in a period of single month, multi-month or long-term tenders [42, 43]. FCDM is delivered through immediate disconnection of demand when system frequency drops [44, 45]. The participants are paid on a contract basis during the accepted availability periods (e.g. a contracted 30 minutes' duration for approximately 10 to 30 times per annum) [45].

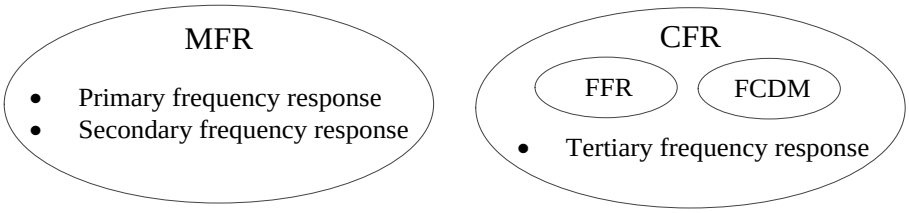

Figure 2-7: Classification of frequency response with balancing mechanisms

Figure 2-7 classifies the aforementioned frequency response that delivered at different timescales from their roles as balancing services. Both primary and secondary frequency response refer to frequency deviations in a dynamic and automatic approach through the adjustments of generation output or flexible demand. In comparison, tertiary frequency response is delivered in a non-dynamic (static) way through contracted units in the system with some specific system operation strategies [46].

2.4 Transformation of the UK Power System

2.4.1 Overview of future UK power system scenarios

Future power system, as meticulously documented in the reports from both National Grid and European Energy Committee, targets on limiting the emissions of CO_2 [2, 47]. This involves the emerging concepts of renewable resources, high-voltage direct current (HVDC) links, DSM, along with the controllable flexible AC transmission system (FACTS), etc. With more operational flexibility achieved, the system now transits towards a smarter, more efficient and diverse future [48].

According to National Grid's electricity ten year statement (ETYS) Gone Green scenario [2], the percentage of installed renewable generation capacity will rise to 29% (to a total of 90.5 GW) in 2020 and 43% (to a total of 127.3 GW) in 2035. Among all types of renewable resources, the installed capacity of wind tops with a level of 25 GW in 2020 and will reach to 51 GW in 2035. This refers to a corresponding 21%/40% of the total installed generation capacity in National Grid "Gone Green" scenario. This installed and planned renewable resources aim to meet the target of achieving 15% renewable supply is set for year 2020 to reduce the emission of CO_2.

In order to relieve the burden of power transfer congestion and improve the efficiency of power transfer, HVDC links are integrated in the power system to achieve more flexible power transmission through controllable power electronics. In addition to the already-built HVDC links (e.g. BritNed, Moyle, UK and France cross-channel HVDC), there are several HVDC links under planning and/or to be commissioned in UK, such as the Western Boostrap [49] and between UK and its neighbouring countries/islands, such as Norway and Iceland [2].

Due to the increase in the installed capacity of some large generation plants (e.g. combined cycle gas turbines generation (CCGT), large wind farms, nuclear power stations) and the upgraded transfer capacity of HVDC links, the largest secured infrequent infeed loss has been increased from 1320 MW to 1800 MW since April 1st

2014 [3]. This necessitates a faster frequency response to reduce the frequency excursions, which will be exaggerated because of the reducing inertia and a larger amount of power reserve against any sudden frequency curtailment that could possibly occur in the system.

Controlling of system demand will be required more frequently to achieve system optimisation, such as peak demand shifting and system contingency management [50]. Some form of future system demand is invited by system operators to respond to system frequency anomalies. This can be achieved by controlling the participation of system demand, such as Electric vehicles (EVs) and electrical appliances (e.g. washing machines, fridges), through incentives like cost or system optimisation (e.g. maximise the utilisation of power output from renewable resources) [51]. In National Grid 'Gone Green' scenario [47], the mass roll-out of smart meters, providing real-time information for active load response, is expected to cover 95% of UK homes by 2020 and the amount of EVs connected to the grid will increase to 0.6 million in 2020 and 5.4 millions in 2035 from the original 0.01 million in 2013.

As such, the continuous evolving of the modern techniques and advanced control strategies stimulates more dynamics in future power system frequency response. Their impact on system frequency stability needs to be study extensively for a reliable power supply.

2.4.2 Wide area monitoring, protection and control

Security and reliability need to be ensured in future upgraded system where all the functional sectors should operate appropriately and be well-coordinated to achieve desired system optimisation. Wide area monitoring, protection and control (WAMPAC), utilising of system-wide information and synchrophasor techniques, is an effective means to provide such a system-level supervision [52].

Figure 2-8 presents a three-layer architecture of WAMPAC, including measurements taken at local areas, the energy management system (EMS) at the top layer and the

phasor data concentrator (PDC) in between. Advanced functionalities, such as system real-time monitoring and control applications, dynamic recording, congestion and optimal flow management, are enabled through high-level comparisons among synchronised measurements. To achieve the real-time information transfer between local and remote sites, one of the most important requisites is a fast and reliable communication path. Such path can be selected from microwave, phone lines, satellite and InternetWPN [52, 53].

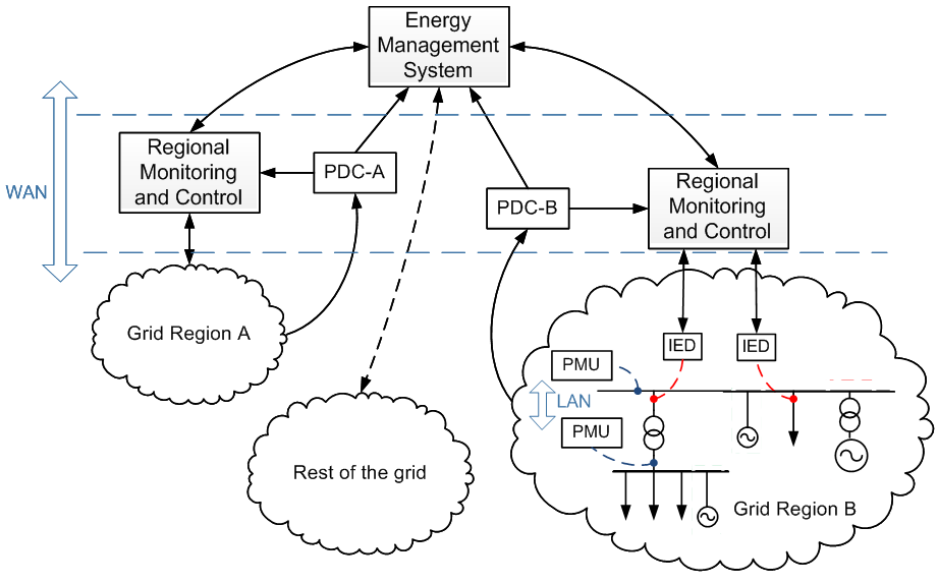

Figure 2-8: Generic architecture of WAMPAC [52]

As a promising enabler of WAMPAC, Phasor Measurement Units (PMUs) provide a synchronised time stamp for comparisons made among all the measurements taken at the same time while multiple locations. A basic overview of this technique is presented in [54] and its enabling of real-time control and protection applications are discussed in [55, 56]. With the assistance of PMUs as well as advanced dynamic simulation and estimation techniques, WAMPAC is able to retain a safer and more stable power system for a more economic dispatch, even under stressed conditions or operating near the limits of its constraints.

2.5 Impact of System Development on Frequency Response

Due to the fact that the inertia constant is derived from the kinetic energy stored in the rotating mass, renewable resources, such as photovoltaic and wind, that are decoupled from the grid through power electronics cannot contribute to system inertia. As a result of the growing renewable penetration and its contribution in power supply, system inertia decreases and only equals to one third of current level 20 years later as shown in Figure 2-9. However, the contribution to the system inertia from the demand side should not be ignored where motors with rotating mass are embedded as well as intelligent control strategies that are introduced to participate in system dynamics. In order to study the implications of system development on future system frequency response, two examples – the active incorporation of WTGs and responsive loads, are given among various generation techniques and the methods of demand side control.

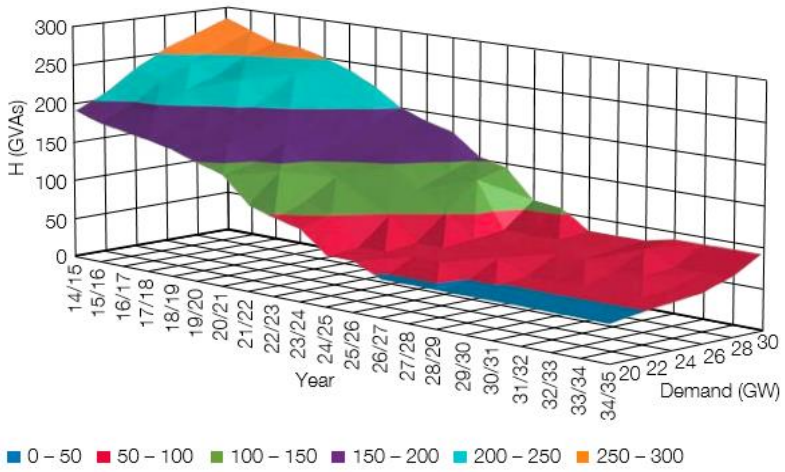

Figure 2-9: System inertia changes for Gone Green scenario at 70% wind power output [2]

2.5.1 Impact of WTGs on system frequency response

WTGs are typically connected to the grid through power electronics (e.g. HVDC links) where considerable benefits can be achieved through, for example, the

dynamic control of power output at the terminals of the HVDC links, isolation from the disturbances on grid side, connecting two systems that operate at different frequencies. Unlike large synchronous machines, WTGs are unable to naturally provide a desired damping effect to any system frequency excursions. This is due to the fact that by implementing through power electronics, WTGs are decoupled from the grid [57], leading to an isolation of any inherent inertial frequency response. With the increasing percentage of WTGs in supplying system demand, the actual system inertia will drop gradually. Such concerns have also been raised by National Grid Frequency Workgroup [58].

[59-62] presents detailed comparisons of system frequency response for wind integration scenarios against sudden power imbalance. An example of the impact of WTGs penetration on system frequency response is presented below, conducted with the following three cases as per [59].

- Case 1: with no replacement of synchronous generators (SGs), WTGs contribute to 30%, 60% and 90% of the demand respectively. System inertia level remains unchanged.
- Case 2: with replacement of SGs, WTGs contribute to 30%, 60% and 90% of the demand respectively. System inertia level reduces.
- Case 3: with replacement of SGs, WTGs contribute to 30%, 60% and 90% of the demand respectively. However, the moment of inertia remains the same by adjusting the inertia constant.

The performances of system frequency under these three different system conditions are depicted in Figure 2-10. Increased frequency drops are observed when comparing Case 1 and Case 2 and 3. It claims a penalty placed on the performance of system frequency if replacing SGs with WTGs in the system. Given the fact that the moment of inertia remains the same in Case 1 and Case 3, larger frequency excursions are generally observed in Case 3 but with very close frequency response for the first few seconds. Therefore, the replacement of SGs with WTGs, even without reducing system moment of inertia, still degrades system frequency response but the inertial frequency response remains nearly the same. In other words, the penetration of

WTGs would not influence system frequency regulation at all unless the conventional SGs are replaced.

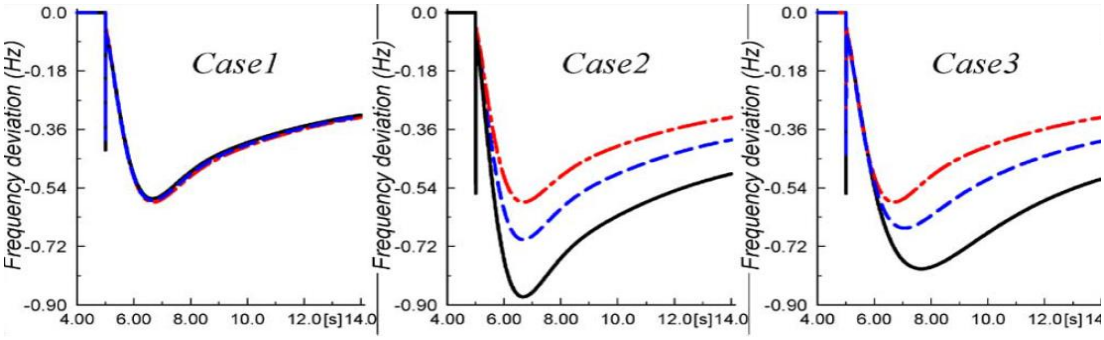

Figure 2-10: Impact of WTGs penetration on system frequency excursions during power imbalance where WTGs supply 30% (red), 60% (blue) and 90% (black) of system load [59]

It should be noted that WTGs of fixed speed have an inherent inertial response but much slower than frequency dynamics due to the mechanical time constant of pitch actuators [57, 60]. Considering the fact that it is limited to a certain operational wind speed and has poor performance on voltage stability [63], only a minority of fixed speed WTGs are still in service today. Therefore, their contributions to the inertial frequency response is negligible.

2.5.2 Impact of DSM on system frequency response

Transitioning towards more flexible and efficient power networks is not only limited to the diversity of energy resources but also incorporating intelligent management strategies. This includes applying certain strategy to optimise energy utilisation while maintaining system stability [64].

This section focuses on the frequency response provided by DSM (hereafter referred to demand side frequency response (DSFR)) when system frequency stability is jeopardised. DSFR belongs to the CFR as one of the balancing services reviewed in Chapter 2.3.6, maintaining system frequency stability through active regulation and control of power system demand either as an emergency plan or energy-balancing service. It is achieved by technologies like two-way communication and smart

metering infrastructures that enable interactions between end appliances and electricity suppliers. Decisions are generally made complied with certain operational strategies, such as financial incentives or economic dispatch [64]. The three main forms of DSFR are listed below:

- Frequency responsive "grid-friendly" appliances (FR-GFAs). This refers to the domestic electrical appliances, such as refrigerators, washing machines and air conditioners, which are sensitive to frequency excursions and operate accordingly through certain control logic [65].
- Electric vehicles. It has shown that system frequency response depends on the type of battery of EVs, as well as its charging mode [66, 67].
- Energy storage (ES). This can be realised through batteries, flywheels or storage system such as pumped hydroelectricity. When the grid has more generation than demand, the redundant energy will be stored in ES system. Such stored energy will be released back to the grid for a temporary energy shortage.

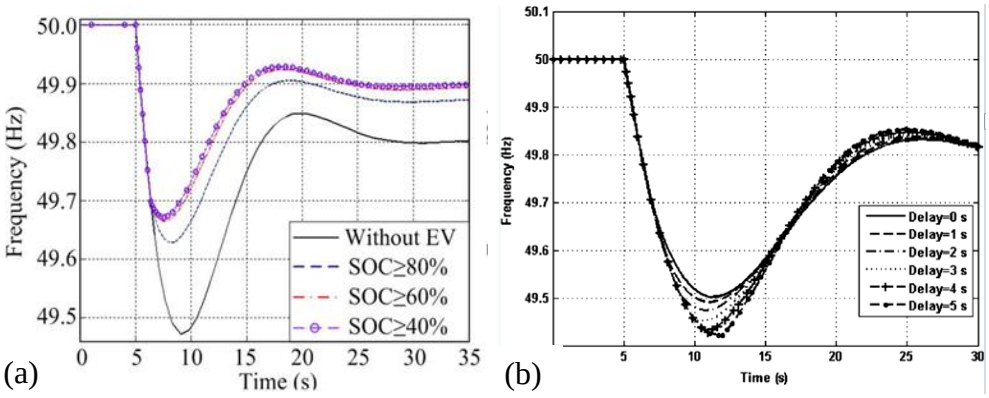

Figure 2-11: Examples of DSFR provided by (a) EVs [66]; (b) FR-GFAs [68]

Figure 2-11 demonstrates two examples of DSFR. Figure 2-11 (a) compares system frequency response with and without contributions from EVs, and among various states of charge (SOC) of EVs. The impact of time delays in switching on/off of FR-GFAs on frequency curtailment is shown in Figure 2-11 (b). Both of them prove that the DSFR could act as an effective means to reduce frequency excursions.

Although examples given above have shown that DSFR can be actively regulated to provide system frequency response, there still exists some concerns in implementing DSFR into the real systems. For example, the inconvenience brought to customers who are on agreement with system operators for the disruptions from time to time, the cost for system operators to compensate the contracted disruptions, large space occupation and high cost on installation and maintenance of batteries, etc. Most importantly, although DSFR, such as EVs and batteries, can provide fast response contributing to primary frequency response, they still cannot compensate the absence of inertial frequency response from renewable resources, considering the time spent on sending signals till all the DSFR units starting taking effect to system frequency excursions. In addition, the coordination achieved among all kind of DSM and the total amount delivered by them need to be accurately adjusted to avoid over-response or under-response.

2.6 Impact of System Development on Present-day Frequency-based Protections

The challenges brought by the generation mix and more dynamic demand side management have raised wide awareness and been addressed by the UK transmission system operators [2, 19, 69]. This is not limited to the constraints they have placed on the desired output from renewable resources but also the adverse impact on power system integrity and frequency stability. Moreover, the target of providing a more flexible and efficient power supply continuously pushes power system closer to its operating limits.

In addition to the control strategies aiming to maintain desired system frequency response during disturbances, protection system also plays a significant role without which a secure and reliable power supply cannot be achieved. Considering the emerging system operational challenges, attention in this research work is given to the performance of frequency-based protections. With particular regards to the reduction and variation of system inertia, the mal-operation risk of frequency-based

protection would be highly increased. Such protection mal-operation, if incorporated into future grid, would lead to a more critical system-wide issue due to the increasing dynamics.

This section therefore will review frequency-based protections currently in the GB system, along with discussions of the potential negative impact brought by system development on their performance.

2.6.1 Loss-of-Mains protection for distributed generators

LoM refers to the situation where part of the system remains energised by DGs after being isolated from the main grid. IEEE standard, as well as the GB grid, requires disconnecting DGs from the network within 2 seconds, in the light of the safety of both system infrastructure and human beings, along with the stability of the islanded system [70]. Hazardous conditions typically result from the loss of earthing in a part of the system following the LOM event.

Under the condition where the local load closely matches the output of DGs, the detection methods using the deviations in power magnitude or direction could therefore be inaccurate. Moreover, the applied detection method should be able to resist a remote fault being cleared by the utility system. Considering the sensitivity and reliability the system asks for, voltage vector shift and RoCoF are two most widely used criteria for islanding detection.

RoCoF as an indicator for LoM protection is calculated through averaging the changes over certain consecutive cycles of frequency measurements. In this research work, the RoCoF values were calculated using the frequency simulation results over three consecutive cycles based on the MiCOM P341 algorithm same as in [71], expressed as :

$$RoCoF = \frac{f_t - f_{t-3\Delta t}}{3 \cdot \Delta t} \tag{2-4}$$

where,

f_t and $f_{t-3\Delta t}$ are the frequency observation at time *t* and at the time three cycles before

Δt is the cycle length between two frequency measurements

Due to the integration of renewable resources, the RoCoF threshold in the GB power system has been permitted to be upgraded to 1 Hz/s with 500 ms delay [72] for DGs with installed capacity ranging from 5 MW to 50MW. This setting is developed through research work presented in [18] in association with the practical industrial advise. However, concerns still remain as applying a fixed setting across the entire network could still desensitise the performance of RoCoF-based LoM protection practices on moving towards renewable dominated future grid [18, 19] due to the variations in the inertial frequency response from one place to another.

Moreover, as a result of renewable penetration, the gradually reduced system inertia level could accelerate and magnify frequency oscillations that could result in persistent potential false operations of DG anti-islanding protection relays. This could be caused due to an unacceptable large RoCoF measured just after the disturbances or a false RoCoF value and largely depend on measurement algorithm. As shown in Figure 2-12, there is also a certain percentage of risk throughout the year in 2024 onwards that the RoCoF values would be higher than the 1 Hz/s new threshold due to high renewable penetration. Subsequently, the unexpected trip-off of DG units would further increase power imbalance that incurs adverse consequence on system stability.

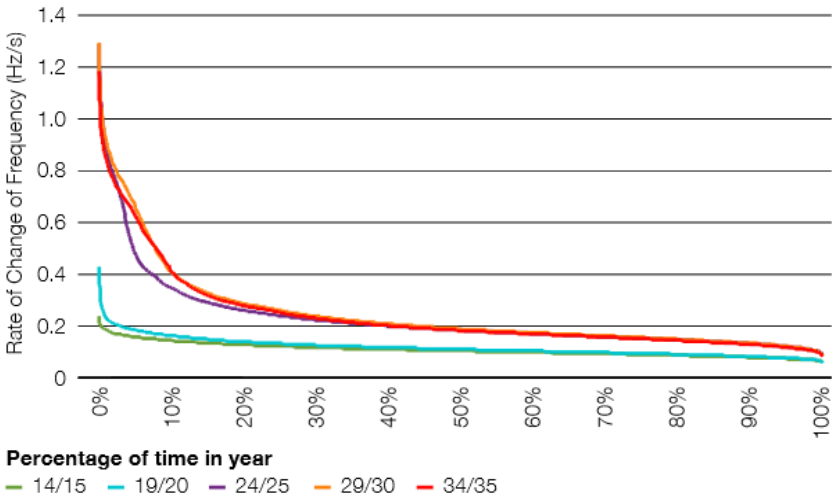

Figure 2-12: Exposure to high RoCoF – Gone Green [2]

2.6.2 Under-frequency load shedding scheme

In the situation where system frequency drops lower than the UFLS threshold, an automatic disconnection of system demand would be scheduled as a last defence to prevent further decrease of system frequency as well as the potential damage to system devices, such as generator assets and variable speed drives [73].

According to the Grid Code [25], the present UFLS strategy in the GB power system has been divided into nine stages and executed individually in three identified transmission areas. The amount of load to be disconnected at each stage and at specific transmission area in the GB system are stipulated as in Table 2-1. They are expressed in percentage to the peak demand forecasted in each area. NGET is short for National Grid Electricity Transmission Ltd., SPT refers to Scottish Power Transmission Ltd. and SHETL is Scottish Hydro-Electric Transmission Ltd.

Table 2-1: Settings of UFLS scheme in UK Grid Code [25]

Frequency (Hz)	% Demand Disconnection for each Network Operator in Transmission Area		
	NGET	SPT	SHELT
48.8	5		
48.75	5		
48.7	10		
48.6	7.5		10
48.5	7.5	10	
48.4	7.5	10	10
48.2	7.5	10	10
48.0	5	10	10
47.8	5		
Total Demand (%)	60	40	40

However, the fixed amount of load to be shed at specific area in a pre-defined sequence could cause an issue of effectiveness as it does not take the size and location of the disturbance into consideration and may over-/under-estimate the amount of load to be shed. In reality, system demand dynamically varies over the course of a day, with distinctive load patterns (e.g. industrial, commercial and residential). Therefore, a more flexible shedding strategy could potentially increase the effectiveness of load disconnection in the light of the location and size of a

disturbance [74]. The development of microprocessor-based techniques and integrated communication system nowadays could facilitate the delivery of such a more flexible and dynamic load shedding scheme.

However, observations of magnified frequency excursions infer the increasing probability of UFLS being activated more often in future low inertia network, especially when experiencing large disturbances in a stressed system [10, 19]. As a matter of fact, this would not only indicate the increasing interruptions to the customers, but also bring potential instability to the system operation if 'hidden generation' (refers to generation units connected at distribution level that cannot be directly measured and monitored from the transmission level) are disconnected as a result of load shedding.

2.7 Shortfalls of Existing Quantification Practices of Future System Frequency Response

As seen the potential performance issues system development imposed to the existing frequency-based protections, there is an urgent need to quantify such negative impact in order to deliver a more flexible while reliable frequency protection. However, existing publications such as [10, 58, 62, 75-77], assess frequency response via an integrated system, represented by a single busbar system or only a frequency responsive model, where local variations have never been recognised. Such variations in frequency response largely depend on the local generation-demand structure and the level of local renewable penetration (given various local inertia). While in an informal conversation, the interests of getting to know such variations across the system and their potential effects emerge. To provide a reliable power supply, future system frequency response, especially the local variations should be well understood and quantified.

Projects, such as National Grid's 'Enhanced Frequency Control Capacity' (EFCC) Project [78], Scottish Power's 'Visualisation of Real Time System Dynamics using

Enhanced Monitoring' (VISOR) Project [79] and Ofgem's Kent Area System Management (KASM) [80], are presently invested to tackle system instability challenges brought by the system development. However, they focus on delivering more flexible frequency control and system management rather than investigating the potential mal-operation risk of frequency-based protections. To quantify such risks, quantitative assessments on the suitability of existing frequency-based protections should be conducted and can be achieved from answering the following two questions:

- Can existing frequency-based protections still be able to cope with the increasing dynamics in future systems and deliver desired protection performance?
- If existing frequency-based protections are insufficient to maintain system frequency stability, what are their mal-operation boundaries?

2.8 Chapter Summary

Prevailing power system frequency stability which is secured through the interoperation between frequency control and protection schemes will subject to challenges in future. Attributing to the increasing penetration level of renewable resources and their intermittent nature, the system inertia decreases gradually and may vary over a wider range as generation and demand changes. The conventional frequency-based protections that have not been designed to accommodate such changes will potentially face sensitivity and stability issues when subjected to system disturbances, thereby, further degrades system frequency stability.

This chapter reviewed the fundamentals of frequency stability and the practical frequency regulation mechanisms in the GB power system. Based on the study of future system development trends, their impact on system frequency response has been demonstrated from examples of integrating WTGs, EVs and FR-GFAs presented in published works. Concerns were drawn thereafter on the adverse impact imposed to the performance of frequency-based protections as a result of system development. Associated with analysis given to the stipulations of existing RoCoF-

based LoM protection and UFLS scheme, the risk of potential protection mal-operation has been concluded. However, discussions at the end of this chapter have shown there is no such extensively quantification studies on future system frequency response associated with the performance of frequency-based protections, therefore, placing an urgent need.

There necessitates an extensive study of system frequency stability and the potential instability boundaries, if they are found to exist, to be addressed and quantified. Detailed discussions and quantitative investigation will be carried out in the following chapters where the impact these aforementioned contributors have on frequency stability in future low inertia network will be investigated using the GB power system.

3. Evaluating the Impact of Inertia Reduction and Variability on the Dynamic Frequency Response of the GB Power Networks

3.1 Chapter Overview

The overview and discussion in previous chapter have preliminarily addressed and demonstrated the potential frequency performance issues associated with the suitability of existing frequency-based protections in future low inertia networks. By recognising the need of further quantification analysis of the potential challenges, the underlying objective of this chapter is to assess and quantify system frequency response from which opportunities to improve the performance of implicated protection schemes can be identified.

In order to study power system frequency dynamics, a reduced GB dynamic network model has been developed and validated against historical events for its suitability to carry out studies of frequency stability to be demonstrated. Using the reduced model, case studies are undertaken to exhibit system frequency response in future GB power systems against the sudden large loss of infeed. Through analysing the observed frequency behaviour, mathematical equations are then fitted in specific cases to extract the deterministic quantitative relationship between each pair of investigated system variables to predict the marginal values of the maximum sudden infeed loss and the minimum system inertia with which the system operational limits will not be exceeded. Based on the simulation results, discussions are made on the performance of RoCoF-based LoM protection and UFLS scheme to arbitrate the suitability of applying their current protection settings in future scenarios.

The main contributions of this chapter are:

- Development of a generic system modelling and validation process.
- Creation of reduced model of the GB power network which is capable of representing the dynamic frequency performance of the actual full GB grid.
- Quantifying the impact of system inertia variation on the maximum frequency drop and RoCoF value when subjected to a 1800 MW infeed loss.
- Quantifying the impact of the size of infeed loss on the maximum frequency drops and RoCoF values for a system inertia of 3 s (as an approximation of system inertia in 2020 [81]).
- Quantifying the impact of renewable penetration levels and their dispatch patterns on the maximum frequency drops and RoCoF values to a 1800 MW infeed loss.
- Identifying the mal-operation boundary of the size of the sudden infeed loss and the system inertia for DG anti-islanding protection in a low inertia GB network.
- Identifying the mal-operation boundary of the size of the sudden infeed loss and the system inertia for UFLS scheme in a low inertia GB network.

3.2 System modelling and validation methodology

In order to evaluate the frequency response under various and low inertia system conditions, a valid model is necessary to conduct the studies. A generalised process to build such model is shown in Figure 3-1. The system data needs to be firstly collected regardless of whether it is a full model or a reduced model. Depending on the type of study and available data, certain model reduction methodologies can be applied to achieve a desired level of model reduction. Methodologies of model reduction are classified as physical reduction, topology reduction and modal reduction [24]. Physical reduction refers to the simplification of the inner structure of any individually selected system elements, while topology reduction targets a part of the network to eliminate and/or aggregate system nodes. Modal reduction using linearized models for reduction is rarely used due to the difficulties in achieving the standardisation of the software. To ensure the model is representative of the system to be assessed, it needs to be verified against the true system performance before

further investigation can be carried out using the model. If the response of the developed model is not acceptable, reselection of the modelling methodology is required as well as verifying the validity of the collected data. With the recognition of the system dynamic operation constraints, the validated model can then be used to evaluate the impact of one system variable on another. In this thesis, the GB grid model was selected to assess the impact of system inertia reduction on frequency response.

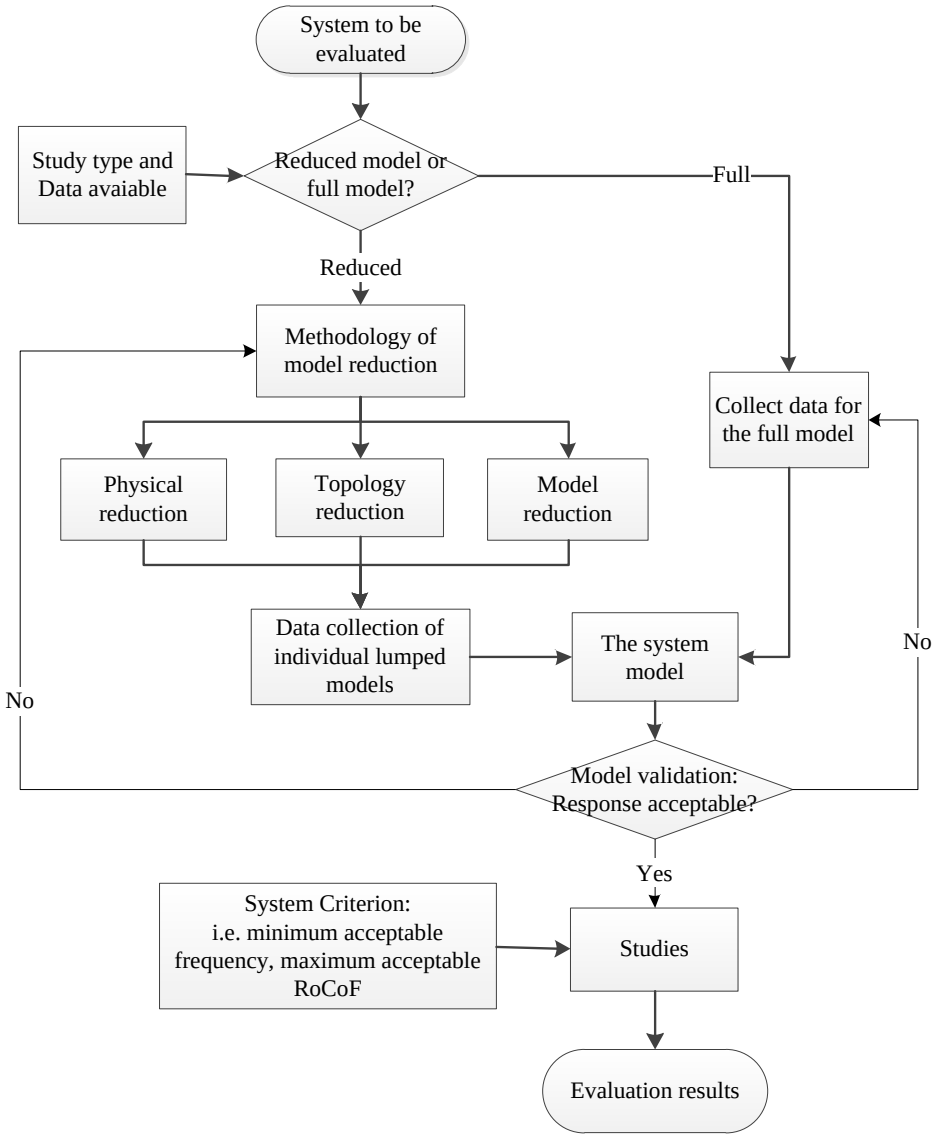

Figure 3-1: System modelling and validation flowchart

3.3 Modelling of a Reduced GB Power System

Instead of modelling every single detail of the GB power system using time domain analysis, a reduced model has been developed in this research. This is mainly due to the following facts: limitations on the access to all the commercial data of the system blocks and the commercially marketed power system analysis packages which make it impossible to build the entire GB network for research analysis; no need to replicate the enormous GB power system as the impact of inertia to be investigated is at system level and the frequency is also a system level variable.

In this modelling process, the concept of physical reduction is applied to represent the grouped generation and loads in each newly-defined study zone. This is due to the fact that the physical reduction is generally applied to linearize external subsystems without creating extra nodes as per the topology reduction. The equivalent transmission lines connecting the zones are derived based on the concept of topology reduction.

3.3.1 Zoning of the GB power system

In this research, the reduced GB network model was initially built referencing the 17 study zones partitioned in the National Grid Electricity Transmission System Seven Year Statement (SYS) [82]. In order to get a more simplified yet adequate model, further reduction has been achieved by grouping the zones with similar power flow patterns as seen in the average cold spell winter peak in 2011/2012 [82]. It should be noted that although a further nine local boundaries and three wider boundaries have been introduced in recent ETYS [2], these changes were not made correspondingly in the reduced model. This is attributed to the fact that the ETYS had not been released at the time the model was developed and the new zones were added with considerations given to the integration of renewable resources and the potential reinforcements required for transmission system that are out of scope in this research work.

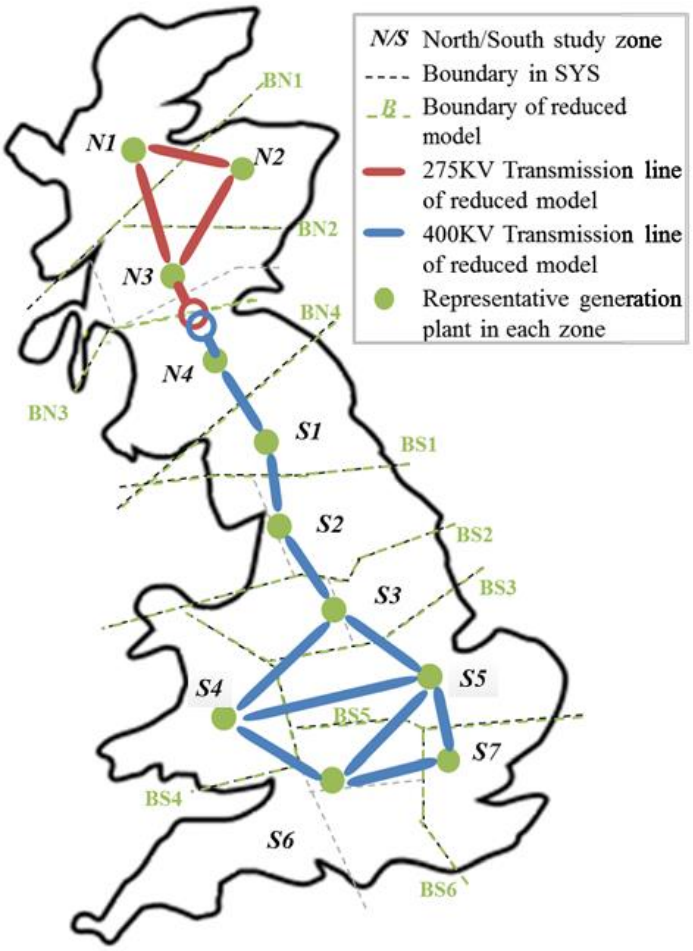

Figure 3-2: Boundary map of the 11-node reduced GB model

The geographic diagram of the reduced GB power system is shown in Figure 3-2. Zones prefixed with 'N' represent the northern part, while the remaining zones prefixed with 'S' stand for the south. A 275/400 kV transformer linking SHETL and SPT is placed across N3 and N4, considering the fact that Scotland is mainly comprised by voltage level less than or equal to 275 kV. The boundaries of the 17 study zones stated in SYS are depicted with black dotted lines in contrast to the newly-defined zones highlighted in green. For example, the original zones 14, 16 and 17 in the SYS model were lumped as S6. This has taken into account the same power flow direction they have where more demand than generation appears in these zones and the fact that synchronous generation dominates in these areas, giving the potential similar frequency response. Future development, where the frequency response would potentially be affected, has also been considered during the reduction, e.g. the fact that more offshore wind will be connected at zone 12 in SYS, therefore,

it has not been further lumped with adjacent zones but remained as separate zone S4 to accommodate system development strategy [2].

3.3.2 Generation model

In each newly-defined zone, aggregated steam (from coal and nuclear) and gas-fired generation units were employed to supply the demand, along with providing sufficient frequency response. Generating units, like hydro were not modelled in this research as they are not responsible for providing inertial and primary frequency response in real system due to their longer response times. In this research, 10% of the aggregated units were set with frequency response according to the minimum frequency response requirement in [25, 58]. Moreover, the reduced GB model does not include models of renewable resources due to the complexity in their control and regulation strategies where a significant number of power electronics units are involved. Alternatively, the influence of integrating renewable resources on system inertia level was simulated by reducing the inertia of non-frequency-responsive generators. It was also assumed that there was no synthetic inertia injected from renewable generators.

An IEEE standard AC1A exciter and generic steam turbine and governing system were used to represent steam turbine driven generators [30]. The gas turbine model validated in [83] was used to regulate the frequency response of gas turbine driven generators. Typical values of the control parameters [30, 84] were used and adjustments were made to fine tune the inertial and primary frequency performance of the developed model so that the model behaved in a similar fashion to the recorded first stage system frequency response as in [85]. For example, the speed relay time constant (T_{SR}) of the steam turbine model was tuned from 0.1 s to 0.5 s to match the time for the frequency to drop to its minimum, the value of the governor droop was tuned from 20 (typical) to 29 [30] to match the frequency value at the new steady state.

Detailed models of the exciter, turbine and governor and their parameter values applied in this research are provided in Appendix A. It was assumed that the generators in each defined zone belong to the same coherent group and can therefore be "lumped" and represented as one aggregated generator.

3.3.3 Transmission line model

Topology reduction was applied to transform all lines crossing the same boundary between two adjacent zones to one equivalent line, regardless of the limits arising from line thermal capacity and transfer capacity. As no extra fictitious branches or shunt admittances were created, this direct equivalent method is simpler than Dimo's and Zhukov's method [24].

For power system study involving long transmission lines, the nominal PI model [86] shown in Figure 3-3 is the most appropriate way to represent the equivalent overhead lines between zones where hyperbolic corrections are included without making approximations. The attenuation and shunt conductance (representing the corona loss and the leakage current) were neglected [24, 30].

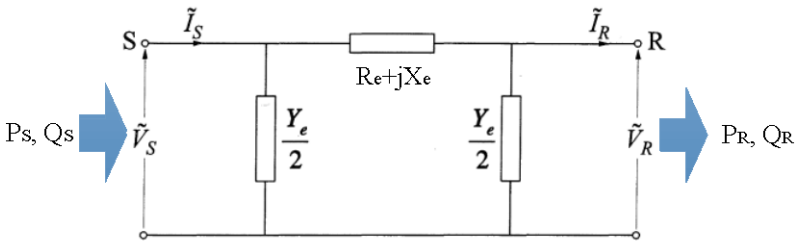

Figure 3-3: PI model representing for the equivalent transmission line

The loop current method [24] was employed to calculate the equivalent line parameters R_e, X_e and Y_e in the PI model. Equations for parameter calculations are expressed in (3-1) and (3-2), where each parameter value was calculated based on the power flow crossing the border of the study zones in the average cold spell winter peak in 2011/2012 [82]. It should be noted that the voltages were taken as vectors with their magnitudes and phase angles derived from the solved power flow in PSSE

[87]. Values of each equivalent transmission line are provided in Appendix A Table A-6.

$$\left(\frac{P_S + jQ_S}{3V_S}\right)^* + \frac{Y_e}{2}V_S + \frac{Y_e}{2}V_R = \left(\frac{P_R + jQ_R}{3V_R}\right)^* \quad (3\text{-}1)$$

$$V_S - V_R = (I_R - I_S)(R_e + jX_e) \quad (3\text{-}2)$$

where,

P_S, P_R	are the real power at the sending end and receiving end
Q_S, Q_R	are the reactive power at the sending end and receiving end
V_S, V_R	are the voltages at the sending end and receiving end
I_S, I_R	are the currents at the sending end and receiving end
R_e	is the equivalent line resistance
X_e	is the equivalent line inductance
Y_e	is the equivalent line admittance

It was assumed that all of the lines crossing the defined zone boundaries will still be in service in 2020 regardless of any reinforcements or the de-commissioning of some transmission lines. This attributes to the fact that transmission line has negligible impact on the frequency response, only on the power flow direction, losses and the voltage performance at the remote ends and these are out of the research scope.

3.3.4 Load model

A typical PQ load model was used to represent the lumped load in each defined zone. The real power and reactive power are calculated in an exponential manner, expressed as in [30, 88]:

$$P = P_0 \cdot \left(\frac{V}{V_0}\right)^{np}(1 + K_{pf} \cdot df) \quad (3\text{-}3)$$

$$Q = Q_0 \cdot \left(\frac{V}{V_0}\right)^{nq}\left(1 + K_{qf} \cdot df\right) \quad (3\text{-}4)$$

where,

P_0, Q_0	are the rated real and reactive power
V	is the instantaneous voltage
np, nq	are the voltage exponents for real and reactive power
df	is the frequency deviation
K_{pf},K_{qf}	are corresponding frequency coefficients for real and reactive power

Only the voltage-dependent indexes of the load are defined in this study where np and nq were set to 2 and K_{pf} and K_{qf} were set to 0 [30]. This is to reduce the complexity of the reduced GB model in the case that the frequency response of the developed model only needs to be tuned to match the real system response from adjusting turbine and governor control parameter values based on historical events.

3.3.5 Integrated zonal model

As shown in the blue box in Figure 3-4, after the above network reduction and aggregation process, each zone has been simplified with aggregated frequency-responsive generation unit, aggregated non-frequency-responsive generation unit, a lumped local load and a PI-model transmission line connecting between zones. As such, the final zonal model is composed of four generators and one load, dynamically importing/exporting power from the remaining network. The subscripts of steam or gas in Figure 3-4 represent the fuel type of the generator and f/nf specifies generator with/without frequency response duty.

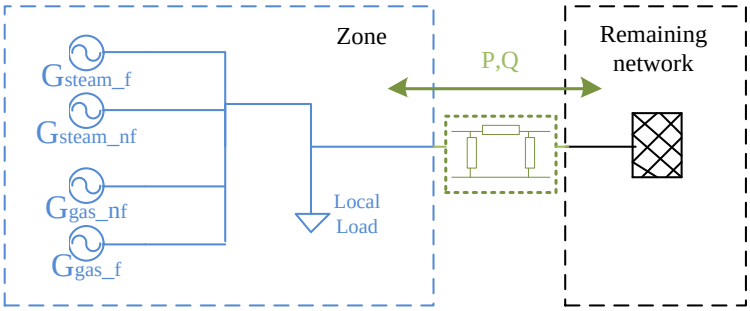

Figure 3-4: Zonal generation distribution and load diagram

3.4 Validation of the Reduced Model

With the GB grid model now fully developed following the selected model reduction methodologies, the performance of the reduced model needs to be validated for a truly representative model of the real grid. Due to limited access to commercial data for both cross-boundary transmission line parameter values and the variables of the generator turbine and governor in the GB system when the model was constructed,

validating the developed model against known historical events is the feasible approach for its representation of the real GB dynamic power system. In this research work, the control parameters of the reduced model (e.g. droop value and governor time constant) was firstly fine tuned based on the first-stage frequency behaviour in May 2008 UK blackout [85]. In order to build a generic model that is valid to simulate the frequency response of the GB system, the reduced model was further tuned according to the following two historical events. From the comparisons made between real system response and the simulation results, the accuracy of the developed model and the suitability of using this model for investigations relating to system frequency response have been validated.

Both of the historical events were recorded by a number of PMUs installed across the GB system [89]. The frequency measurements taken in Glasgow (GL), Manchester (MN) and London (LN) are available from the archives at the University of Strathclyde and were used for assessing the performance of the reduced model. RoCoF values were calculated using (2-4). On the basis of the peak demand on the average cold spell winter peak in 2011/2012 [82], a de-rating factor was applied to all load and generation load reference point in each zone to match the total system demand published on [90] at the time the event occurred.

3.4.1 Event 1: Loss of interconnector between UK and France (28/09/2012)

The first event described below is the disconnection of HVDC link between UK and France on the 28th of September 2012. The event took place at around 1:48 UTC and approximately 1 GW power import was lost at a total demand of 27.59 GW.

Figure 3-5 (a) and (b) show the recorded frequency and its corresponding RoCoF during the first 20 s of the event. The simulated results, as displayed in Figure 3-5 (c) and (d), show a very close overlap to the actual data, but the behaviour is “smoother” than shown in the recorded data: a maximum of 0.25% error in frequency is evident within the first 7 s after the loss while a maximum of 0.06% error is displayed during

the subsequent time period where frequency recovery is taking place; the RoCoF dip value just after the interconnector loss is 2.7% less at LN and the RoCoFs observed in GL and MN are generally smaller with a difference of around 0.1 Hz/s for both locations.

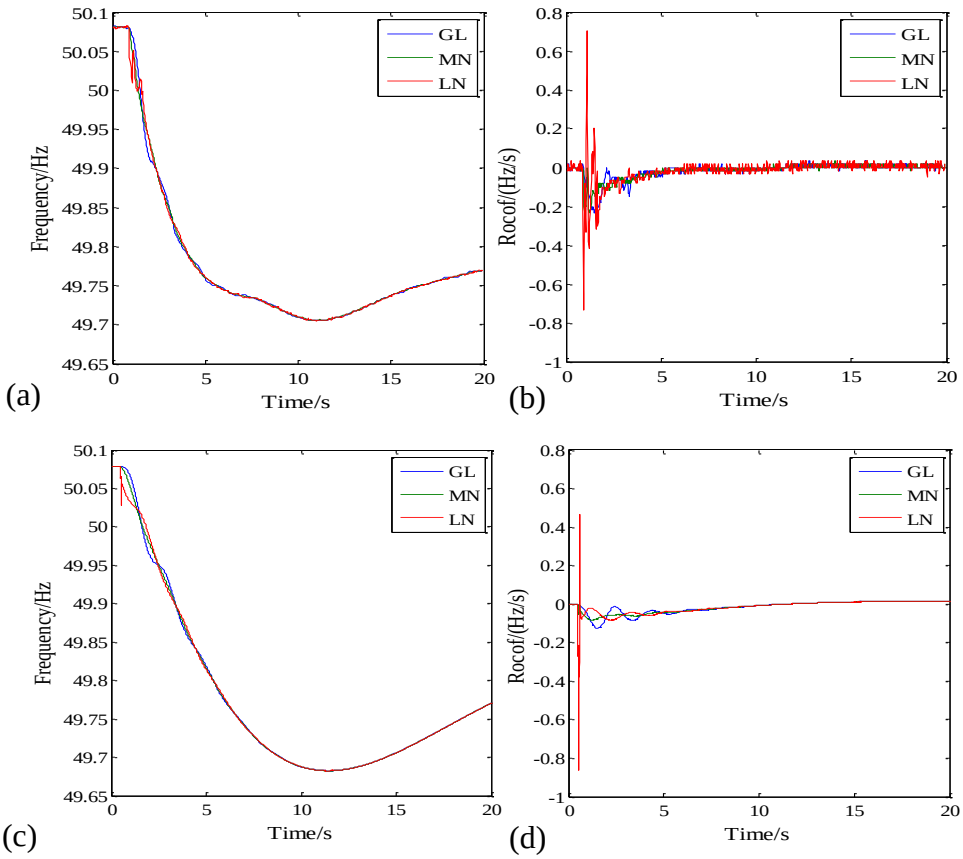

Figure 3-5: Event1: (a) recorded frequency response, (b) recorded RoCoF performance, (c) simulated frequency response, (d) simulated RoCoF performance.

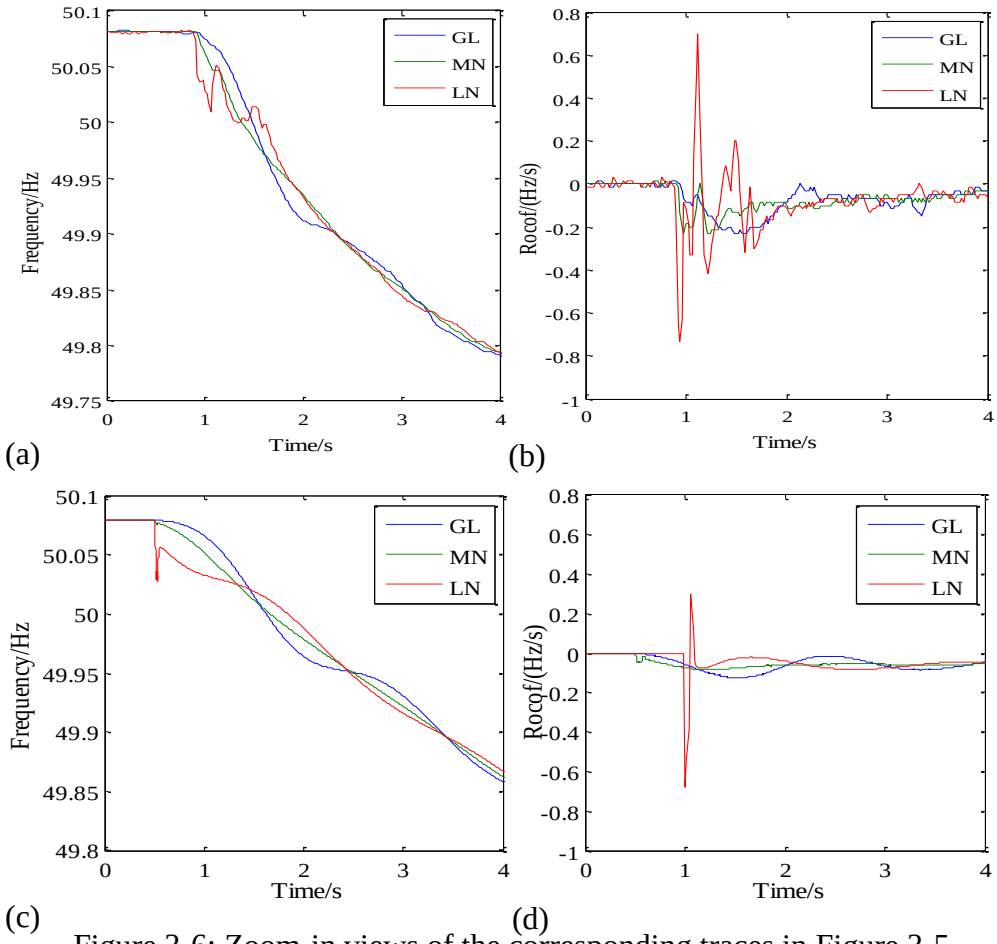

Figure 3-6: Zoom-in views of the corresponding traces in Figure 3-5

3.4.2 Event 2: Generation disconnection (19/04/2011)

This event occurred on the 19th of April 2011 at around 8:41 UTC. There was a sudden disconnection of a large generator at the far north of the British system. It was believed that the generator lost was Peterhead, as around a 1 GW power difference was seen on [90] between the two adjacent records (which are recorded with a 5-minute resolution) during that period of time.

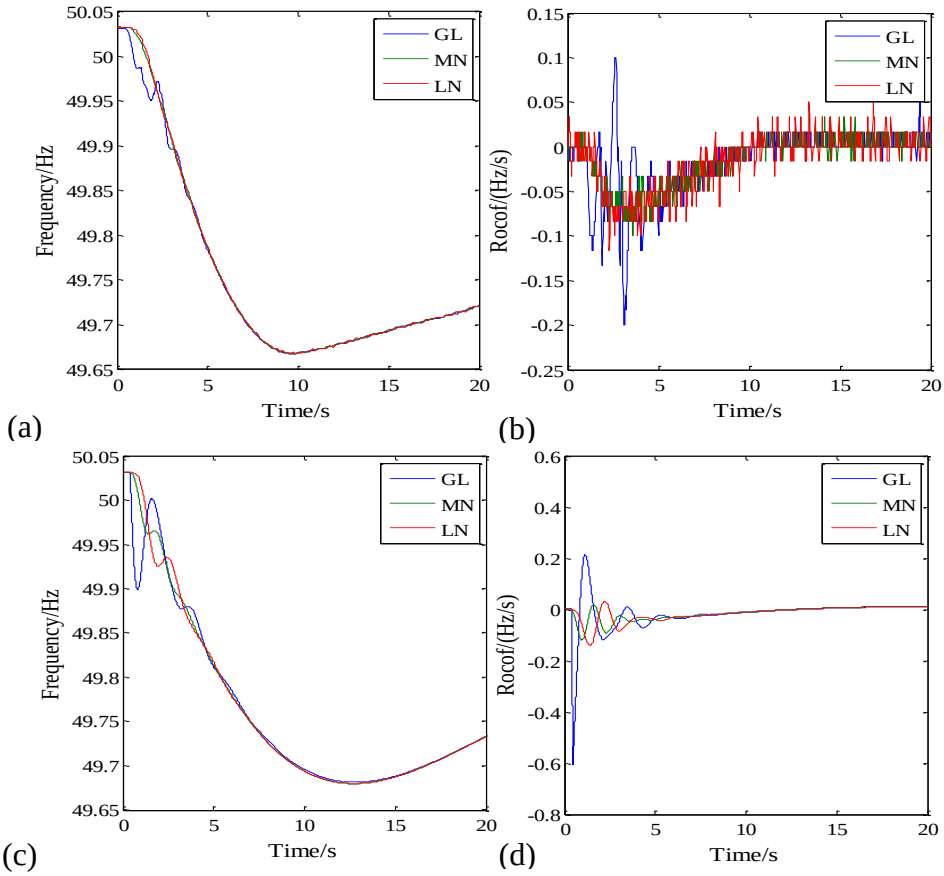

Figure 3-7: Event 2: (a) recorded frequency response, (b) recorded RoCoF performance, (c) simulated frequency response, (d) simulated RoCoF performance.

Figure 3-7 presents the frequency and RoCoF performance. The simulated system frequency drops to the same minimum point at approximate 49.67 Hz while takes 5 s longer than the recorded data. Abnormal frequency response was recorded at GL where the graph shows frequency trying to recover at 2 s after the occurrence of the event. This is believed to be due to the fast response from the system that tried to recover system normal operation but failed. The maximum RoCoF appeared at GL, which is the closest measurement point to the loss, was recorded as 0.17 Hz/s which only equals to one third of the simulated RoCoF value. This is due to the inaccurate simulation of the frequency recovery at approximate 1 s after the loss. However, the RoCoF values are reduced to within 0.2 Hz/s after the first swing.

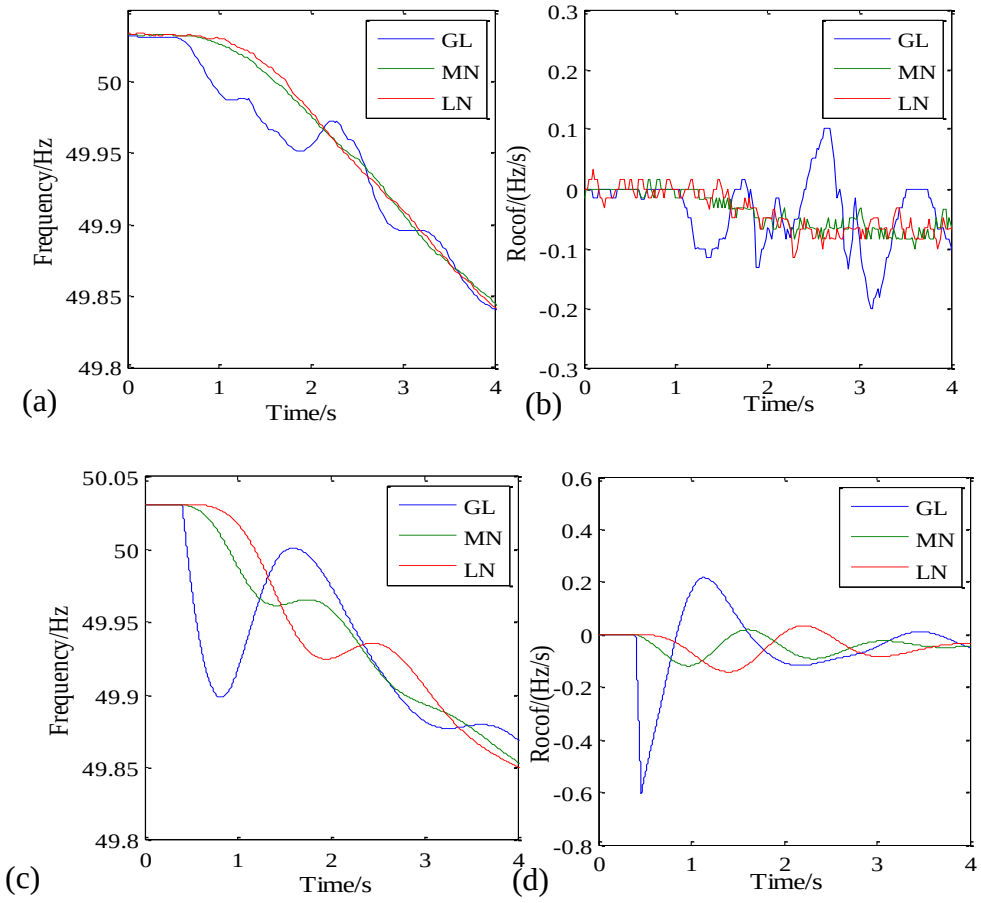

Figure 3-8: Zoom-in views of corresponding traces in Figure 3-7

The simulation results in Figure 3-7 (d) show larger oscillations within the first 3 s after the event compared to the actual data. It is suspected that the swing in the north was caused by relatively less generation in service and typically a net power flow toward the south. It should also be noted that [91] has stated that "several power system stabilisers (PSS) should be installed between generators in England and Wales and Scotland for the purpose of oscillation stabilization". While in this case, there is no power system stabiliser included in the reduced model and this could be a reason for causing such large oscillations at the start of the event. In addition, the disturbance which was located closer to GL than the other two measurement points should theoretically has larger impact on its local frequency performance. The simulation results show the frequency drop in the reduced model also reaches 49.67 Hz but takes a longer time (in this case, approximate 4 s more). This could be as a result of the tight headroom of the remaining frequency-responsive generators to increase

their loading upon the loss in the simulation while the headroom is relatively higher in the real system.

With regards to the magnitude of frequency deviations, the first event shows a 0.023 Hz difference from the recorded data while the second event reaches the same minimum frequency value. The time for the model to reach to its minimum frequency was relatively longer than for the recorded event. Due to the fact that the initial RoCoF values in the replayed historical events are close to the recorded data, the reduced model is clearly capable of providing representative frequency performance in the time periods subsequent to sudden large infeed loss events.

3.5 Studies: Frequency response in low inertia networks

In order to evaluate the frequency performance and the zonal variations in future GB power system, the reduced model which has been validated will be used as the basis for the following three case studies. The system criterion selected in order to criticise the pessimistic operation condition in this case took into account the 49.2 Hz minimum instantaneous frequency limit and the maximum infrequent infeed loss of 1800 MW. However, these could vary in different networks.

In order to simulate the worst case scenario where the severest frequency drop may occur, a system of potential minimum system demand should be assessed when experiencing the potential largest infeed loss. In this study, a typical minimum demand of 25.5 GW [58] was modelled against a 1800 MW loss (largest secured infrequent infeed loss [3]) and this was simulated from scaling down the generation and demand in reference to the power flow in the average cold spell winter peak in 2011/2012 [82]. Although there is a minimum amount of 19 GW stated in [1], it was not released at the time when the studies were carrying on, therefore, this level of demand is not considered in this research.

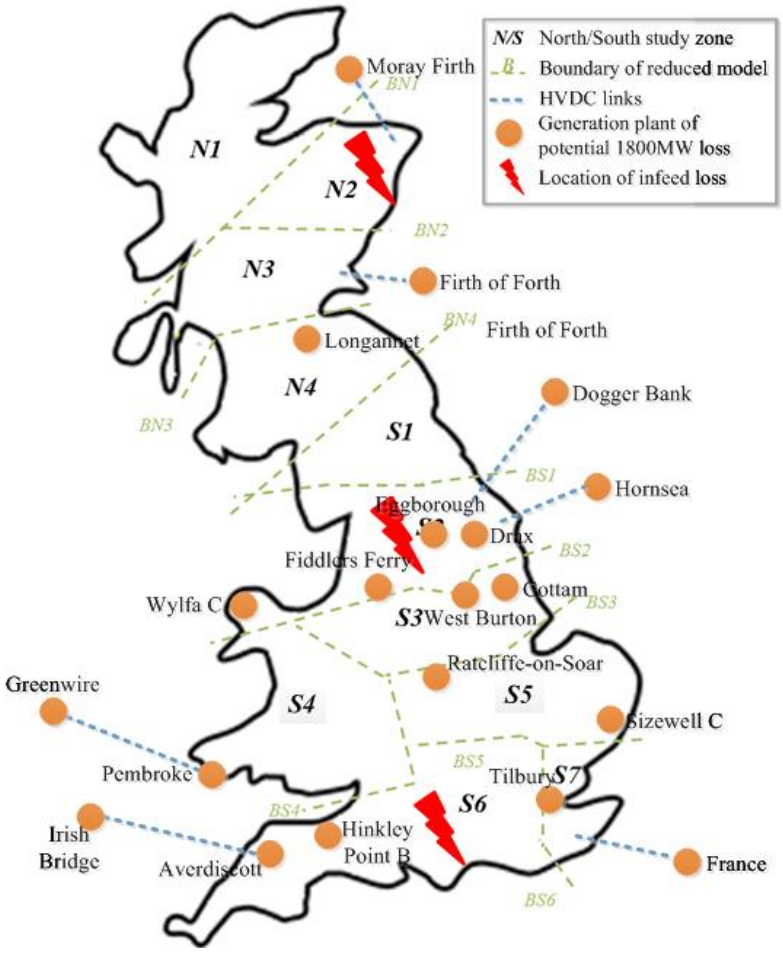

Figure 3-9: Locations of a potential 1800 MW infeed loss

Locations of generation plants or interconnectors with an installed capacity equivalent to or higher than 1800 MW are highlighted with orange dots in Figure 3-9 [2]. It shows that for some of the study zones, there is more than one location which is capable of acting as the loss of infeed location. It is not necessary to simulate multiple infeed loss scenarios within one zone as their local frequency response (identified with only one zonal frequency curve) and their impact on the remaining zones would be broadly similar. The performance of the entire system, in this research, is evaluated by simulating the loss representatively in the north, midlands and the south due to the similarity in generation and demand structure within each region. Moreover, these three locations denote the locations of future highest renewable penetration levels, geographic central of the entire network and the areas with relatively higher demand. Therefore, the infeed loss event will only be

simulated in zone N2, S2 and S6 to assess system zonal frequency response and the performance of frequency-based protections.

The framework here presents the overall frequency response and the zonal variations when the GB system is subjected to a sudden infeed loss as there is insufficient quantification of how zonal frequency will respond to various system inertia. The marginal values of the system variables (including system inertia, size of the infeed loss, etc.) where system frequency stability can still be preserved are also assessed. The first two case studies focus on the system-wide impact of inertia reduction, the location and the size of infeed loss on GB system frequency response, assuming the renewable resources are equally distributed in the system. In contrast, the third study considers the practical operation where the renewable resources are unequally distributed in the network from time to time. The investigations will be carried out using a 70% renewable penetration level referencing the ETYS of 2012 [81] but with an uneven distribution of renewables connected across the network. Moreover, instead of splitting renewable production by 10% and 70% as in [81], this research undertakes a consistent assessment of increasing the renewable production from 0% up to 70% in steps of 10% (of the total renewable penetration) for a more comprehensive quantification of performance. It should be noted that in these three cases, the 1800 MW infeed loss will not be simulated in zone N2 but in S2 and S6 as the total output generated in zone N2 is lower than 1800 MW based on the scaled power flow from the average cold spell winter peak in 2011/2012 [82].

3.5.1 Study 1: Frequency response for a sudden loss of 1800 MW infeed under various system inertia

The first study simulates and compares the frequency response for a 1800 MW infeed loss in S2 and S6 respectively under various system inertia constants. In this research, system inertia constants ranging from 2 s to 7 s are assessed as a reasonable range to reflect the variability caused by different levels of renewable penetration [2, 92].

As shown in Figure 3-10 (a) and (c), with the decrease of system inertia constant from 7 s to 2 s, the minimum frequency that the system experiences after the disturbance becomes progressively lower coupled with an increasingly longer time to reach the lowest value. For the loss occurs at both locations, higher RoCoFs are generally experienced in the north of the GB network. Such phenomena can be explained as a relatively weaker power network in the north where the generation units remain in service do not have enough headroom to schedule sufficient power to meet the demand in the south when subjected to the loss (in the case of the GB power system, the overall power flow is generally from north to south all year around) .

The system-wide minimal RoCoF value is observed in the midlands for the loss in S6 and gradually increases towards north and south ends of the GB network. This can be attributed to the fact that there is relatively more generation (than demand) in these central zones. Among these generation units, a majority are conventional thermal plants (including CCGT, coal and nuclear) which contribute relatively strongly to system inertia. Therefore, the system stability in the midlands are strengthened.

The principle that the closer the measured area is to the disturbance, the higher the impact will be in that area than the rest of the system is followed for the loss occurs in both S2 and S6. As shown in Figure 3-10 (b), a relatively higher RoCoF value appears at S2 than its two adjacent zones. For the appearance of infeed loss in S6 shown in Figure 3-10 (c), the zonal RoCoFs at its neighbouring zones (i.e. S5, S7) are lower than in S6 while there is a local peak in zone S4. S6, specifically, has a net power inflow from its neighbours (i.e. S4, S5 and S7) and the mis-match between generation and demand would be further pronounced when a local generation loss is experienced in that area, leading to a higher ROCOF than for losses occurring elsewhere.

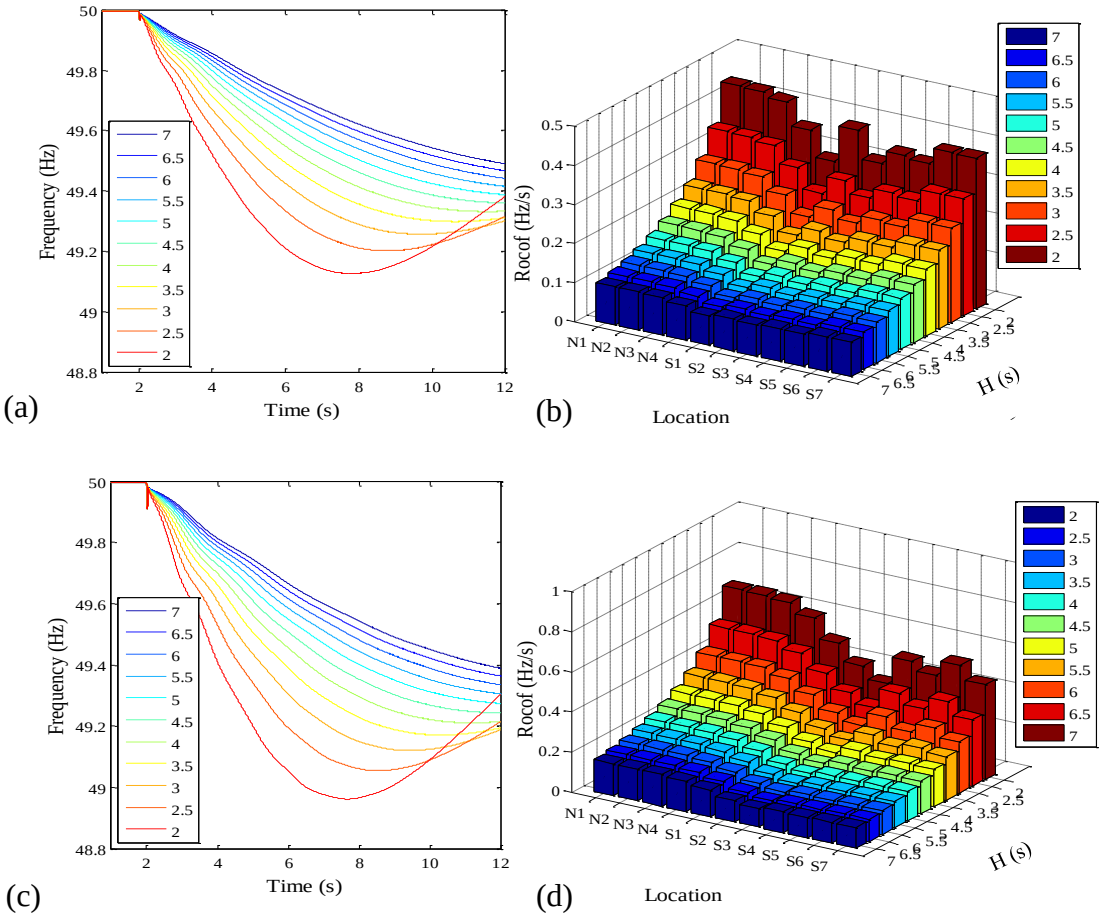

Figure 3-10: Frequency response for 1800MW infeed loss in (a) S2, (c) S6 and corresponding maximum RoCoF in (b) S2, (d) S6 under various system inertia constants

The existing GB power system, if taking from the system level, is more robust against disturbances occurring in the midlands as seen a system-wide reduction on the frequency drop and the maximum RoCoF values for loss in S2 than S6. For example, when the loss occurs in S2 for system inertia lower than 3 s, the frequency stays above 49.2 Hz while drops below 49.2 Hz for loss in S6. Moreover, in contrast to loss in S6, the north region of the GB system experiences an average 35% reduction in maximum RoCoFs when it takes place in S2. These figures are calculated based on simulation results available in Appendix B.

As seen from Figure 3-10, there exists a high risk for system frequency dropping below the 49.2 Hz minimum instantaneous frequency constraint [93] for both of the losses when the system inertia gets low. To quantify such an inertia borderline which

cannot be directly read from the investigated values (in a step of 0.5 s), a quantitative benchmark shall be established other than just analysing system performance from simulation trial and error. In order to achieve this with limited data, curve fitting was applied [94].

Performance of the curve fitting process is presented in Figure 3-11 where attempts are made among linear, quadratic and cubic polynomial curves with their corresponding R-square values given in the brackets. R-square is a coefficient that indicates how accurately the curve fits the data (a R-square value closest to 1 gives the most precise indication). Taking Figure 3-10 (a) as an example, the cubic fitting curve is selected given a R-square value of 0.9991. Although it is desirable to have a R-square value closer to 1 if fit with a higher-order polynomial curve, the complexity the higher-order fitting would introduce and the uncertainty of being either a lumpy or a smooth curve make no guarantee to delivery an accurate fitting with the limited data. Moreover, the differences between cubic polynomial and higher-order ones, in this case, are in a negligible term of 10^{-3}, which is insignificant to quantify frequency drop for the system inertia between 2 s and 7 s as it runs to the second decimal of the value. As such, the cubic polynomial fitting was selected and the corresponding fitting equations are formulated as:

$$\Delta f_{S2} = -0.0028 \cdot H^3 + 0.046 \cdot H^2 - 0.23 \cdot H + 1.31 \quad (3\text{-}5)$$

$$\Delta f_{S6} = -0.0036 \cdot H^3 + 0.059 \cdot H^2 - 0.38 \cdot H + 1.58 \quad (3\text{-}6)$$

where,

Δf refers to the frequency drop from initial value to the minimum post-disturbance frequency

$s2/s6$ is the subscript identifying the location of disturbance

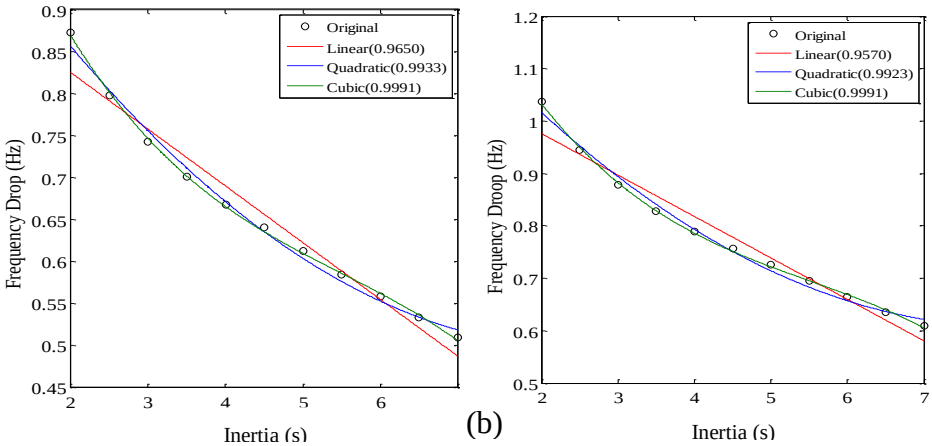

Figure 3-11: Polynomial fitting for the relationship between the frequency drop and the system inertia for a 1800 MW infeed loss in (a) S2 and (b) S6

According to above figures, the system inertia constant should not be lower than 2.52 s for the loss in S2, while not lower than 3.83 s for the loss in S6, to ensure that the frequency drop would not exceed the 49.2 Hz minimum instantaneous frequency constraint upon a sudden 1800 MW infeed loss. The inverse proportional relation between inertia and profiled frequency drop can also be verified from the swing equation.

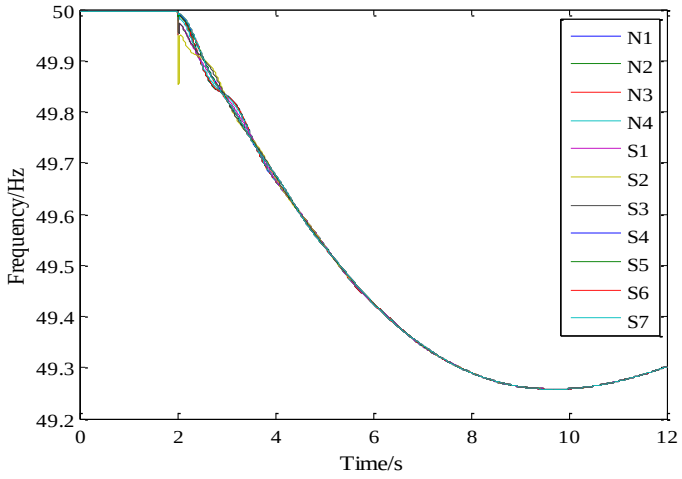

Figure 3-12: An example of zonal frequency response for 1800MW infeed loss in S2 for a system inertia constant of 3 s

It should be noted that the frequency performance curves especially during the first few seconds varies from one zone to another as an example given in Figure 3-12.

This introduces a concept of zonal frequency, which is affected by the local generation-demand structure where a higher percentage of frequency-responsive synchronous generation units could stem the frequency variations. In this chapter, the frequency response shown in the simulation results (above and in the other two case studies) were plot by averaging the frequency performance over the total 11 zones in each scenario.

3.5.2 Study 2: Frequency response for various sizes of sudden infeed loss in a system of 3 s inertia

The previous study focuses on the impact from system inertia to the frequency response which takes the size of sudden infeed loss as a fixed amount equals to the largest secured infrequent infeed loss. Although the worst case scenario is derived from the 1800 MW maximum sudden infeed loss, in reality, the size of the loss is unpredictable and the system faces higher risk of being subjected to a loss smaller than 1800 MW. Therefore, there is also a concern for the system frequency response when experiences such a loss in a low inertia system.

This study investigates the dependency of frequency response on the size of disturbances, taking a fixed system inertia constant of 3 s (on the basis of 25.5 GW demand). This value is selected as a typical system inertia level in future networks and scaled from [19] where system inertia is expected to reach approximately 3.2 s for a 20 GW demand and 2.5 s for a 35 GW demand under high levels of renewable penetration. Therefore, a system inertia constant of approximately 3 s is derived for a 25.5 GW demand system. The sizes of infeed loss are simulated from 300 MW [3] up to the largest secured infrequent infeed loss of 1800 MW.

Figure 3-13 shows the zonal frequency performance across the GB network. The growing size of infeed loss increases both the frequency drop and the maximum RoCoF value. Similar to the results in Study 1, the RoCoF values are generally higher in the north of the GB power system for both of the locations of disturbances and the RoCoF values in the midlands are mostly lower than the remaining system.

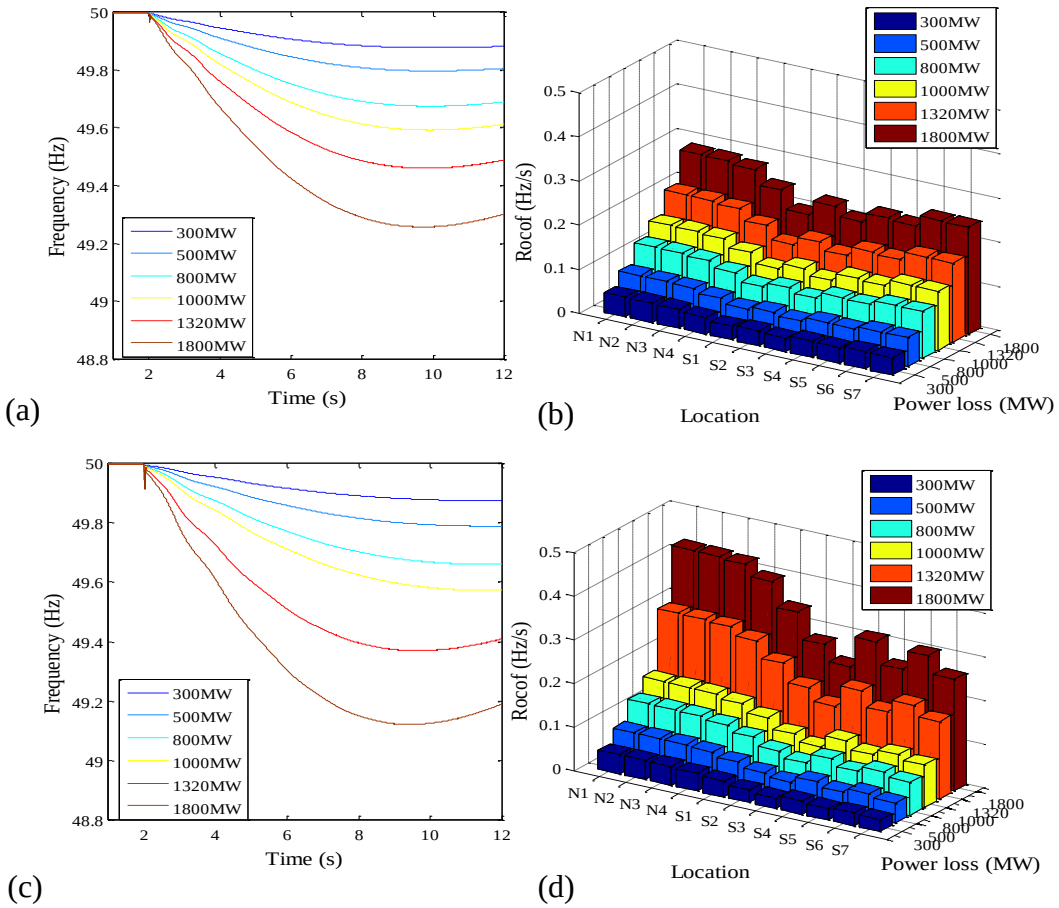

Figure 3-13: Frequency response for different sizes of infeed loss in (a) S2, (c) S6 and corresponding maximum RoCoF in (b) S2, (d) S6.

However, there also exists a risk of frequency drop higher than the defined safety range of 0.8 Hz [93] for loss in S6. To identify such an unstable boundary of the size of the loss under which the frequency drop will reach to 0.8 Hz, curve fitting analysis was also processed.

As shown in Figure 3-14, the total of three curve fitting approaches present a very close result with the R-square value all above 0.99. Due to the fact that the cubic polynomial fitting preserves higher accuracy and would not create too much complexity, it was selected to profile the dependency between the frequency drop and the size of loss as expressed in (3-7). According to the fitted curve, the sudden infeed loss in Zone S6 should not exceed 1644 MW with a system inertia of 3 s to ensure the instantaneous minimum frequency stay within the acceptable 49.2 Hz.

$$\Delta f_{S6} = -8.882e^{-11} \cdot \Delta P^3 + 3.448e^{-7} \cdot \Delta P^2 - 1.187e^{-4} \cdot \Delta P + 6.751e^{-2} \qquad (3\text{-}7)$$

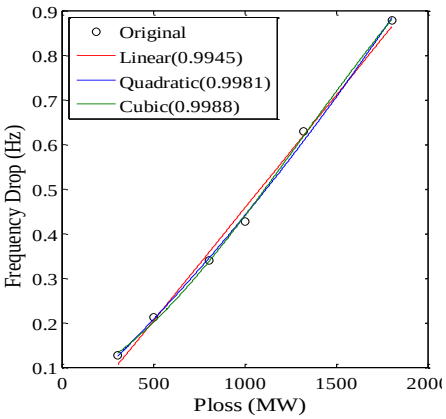

Figure 3-14: Polynomial Fitting for the relationship between the frequency drop and the size of infeed loss in S6

3.5.3 Study 3: Frequency response for various levels of renewable penetration under different generation dispatch patterns

The impact of system inertia level on frequency response, which varies as a result of the growing penetration of renewable resources and their nature of intermittence, has been evaluated in Study 1. However, that study was taken under the assumption that the renewable resources are uniformly distributed in the system. This is not the case in practical system operation where the renewable resources are not equally distributed and more WTGs are scheduled to be connected in the north and west coast (Appendix C). Therefore, the impact of inertia variations from one place to another needs to be addressed and demonstrated through various generation dispatch scenarios considering contributions from both conventional and renewable units locally.

To this end, this section investigates the impact of the percentage of regional generation dispatched from local renewable resources on system frequency response against the 1800 MW largest infeed loss. Studies have been conducted for renewable penetration levels from 30% to 70% in steps of 10% and unevenly distributed in the system, indicating system conditions that could occur in future GB grid. It was assumed that the minimum demand in the future system is 25.5 GW and the

distribution of the demand remains the same, therefore, the same load condition as in previous studies was adopted which was scaled from the average cold spell winter peak in 2011/2012 [82]. The transmission lines built in the reduced model were assumed still capable of transferring the simulated amount of power in all of the scenarios.

Attributing to the uncertainties in local generation structure (as some of them are only at planning stage) and the dynamic generation schedule, the equivalent inertia in each zone is not accessible at this stage thereby presented with the regional inertia.

The dispatch patterns of renewable resources from labelled north (N1-N4) and south (S1-S7) parts of GB are shown in Table 3-1 with a further classification into 3 scenarios:

- Case 1: 0% of the generation in the north is from renewable resources
- Case 2: 50% of the generation in the north is from renewable resources
- Case 3: 100% of the generation in the north is from renewable resources

Variable R_{PL} in Table 3-1 represents the penetration level of renewable resources in the entire GB system. For example, if the overall renewable penetration is 30% and none of it comes from the labelled north part (N1-N4) (Case 1), that means the contributions from renewable resources are all located in the labelled south (S1-S7) and the amount equals to 30% of the total power generation in the GB power network. The specified level of 14.86% is the maximum generation that the north can reach to as referenced from SYS with a system demand of 25.5 GW.

Table 3-1: Renewable resources dispatch patterns

	North Region	South Region
Case 1	0%	$R_{PL} - 0\%$
Case 2	7.43%	$R_{PL} - 7.43\%$
Case 3	14.86%	$R_{PL} - 14.86\%$

Detailed regional inertia constants which refer to various renewable penetration levels associated with different renewable dispatch patterns are presented in Table

3-2. The equivalent inertia constants are approximate values calculated according to renewable penetration level and the generation distribution as expressed in (3-8) to (3-11). The generic equations take the renewable resources dispatch patterns into account and assume inertia constants of renewable and non-renewable generation units are 0 s and 6 s respectively.

Table 3-2: System inertia for different renewable penetration levels under different generation dispatch patterns

Unit (s)	Case1	Case 2	Case 3
R_{PL}= 30%			
H_{eq_N}	6.00	3.00	0.00
H_{eq_S}	3.89	4.41	4.93
R_{PL}= 40%			
H_{eq_N}	6.00	3.00	0.00
H_{eq_S}	3.18	3.70	4.23
R_{PL}= 50%			
H_{eq_N}	6.00	3.00	0.00
H_{eq_S}	2.48	3.00	3.52
R_{PL}= 60%			
H_{eq_N}	6.00	3.00	0.00
H_{eq_S}	1.77	2.30	2.82
R_{PL}= 70%			
H_{eq_N}	6.00	3.00	0.00
H_{eq_S}	1.07	1.59	2.11

$$H_{eq\_S} = \frac{6 \cdot (1 - 14.86\% - R_{PL\_S}) \cdot P_{tot}}{P_{tot} \cdot (1 - 14.86\%)} \tag{3-8}$$

$$H_{eq\_N} = \frac{6 \cdot (14.86\% - R_{PL\_N}) \cdot P_{tot}}{14.86\% P_{tot}} \tag{3-9}$$

$$R_{PL\_S} = \frac{P_{Rew\_S}}{P_{tot}} \tag{3-10}$$

$$R_{PL\_N} = \frac{P_{Rew\_N}}{P_{tot}} \tag{3-11}$$

where,

H_{eq_N}, H_{eq_S}	are the equivalent inertia constants for the labelled north and south regions
P_{tot}	is total power generation
R_{PL}	is the total renewable penetration level
R_{PL_N}, R_{PL_S}	are the renewable penetration levels in the labelled north and south regions to the total renewable penetration level in the

	entire system
P_{PL_N}, P_{PL_S}	are the renewable generation in the labelled north and south regions

Figure 3-15 summarises frequency responses for a 1800 MW sudden infeed loss in both zone S2 and S6 where larger frequency drop and higher maximum RoCoF are experienced across the entire network with the increasing penetration of renewable resources. The performance of frequency and RoCoF can be concluded as follows:

- The amounts of frequency drop in S6 is generally 15% higher than in S2 for the same size of sudden infeed loss.
- The maximum RoCoF values for loss in S6 are generally 26% higher than the loss in S2 from zone N1 to S1 while 18% higher from zone S4 to S7.
- The maximum RoCoF values for loss in S6 are generally 19% higher than the loss in S2 in zone S2 and S3 when renewable penetration is lower than 60% while generally 3% lower when renewable penetration equals to and higher than 60% in Case 1.
- For loss in S2, the maximum RoCoF values are generally 8% higher in Case 2 than Case 1 in zone N1 to S1 while 22% lower in zone S2 to S7.
- For loss in S2, the maximum RoCoF values are generally 17% higher in Case 3 than Case 2 in zone N1 to S1 while 3.5% lower in zone S2 to S7.
- For loss in S6, the maximum RoCoF values are generally 12% higher in Case 2 than Case 1 in zone N1 to S1 while 32% lower in zone S2 to S7.
- For loss in S6, the maximum RoCoF values are generally 15% higher in Case 2 than Case 3 across the zones.
- The worst case scenario is experienced under 70% renewable penetration in Case1 where the RoCoF values in zone S4 to S7 exceed the 1 Hz/s threshold of the RoCoF-based LoM protection. This would unexpectly trip 55% DGs in the GB network according to the recorded DG distribution in [18].

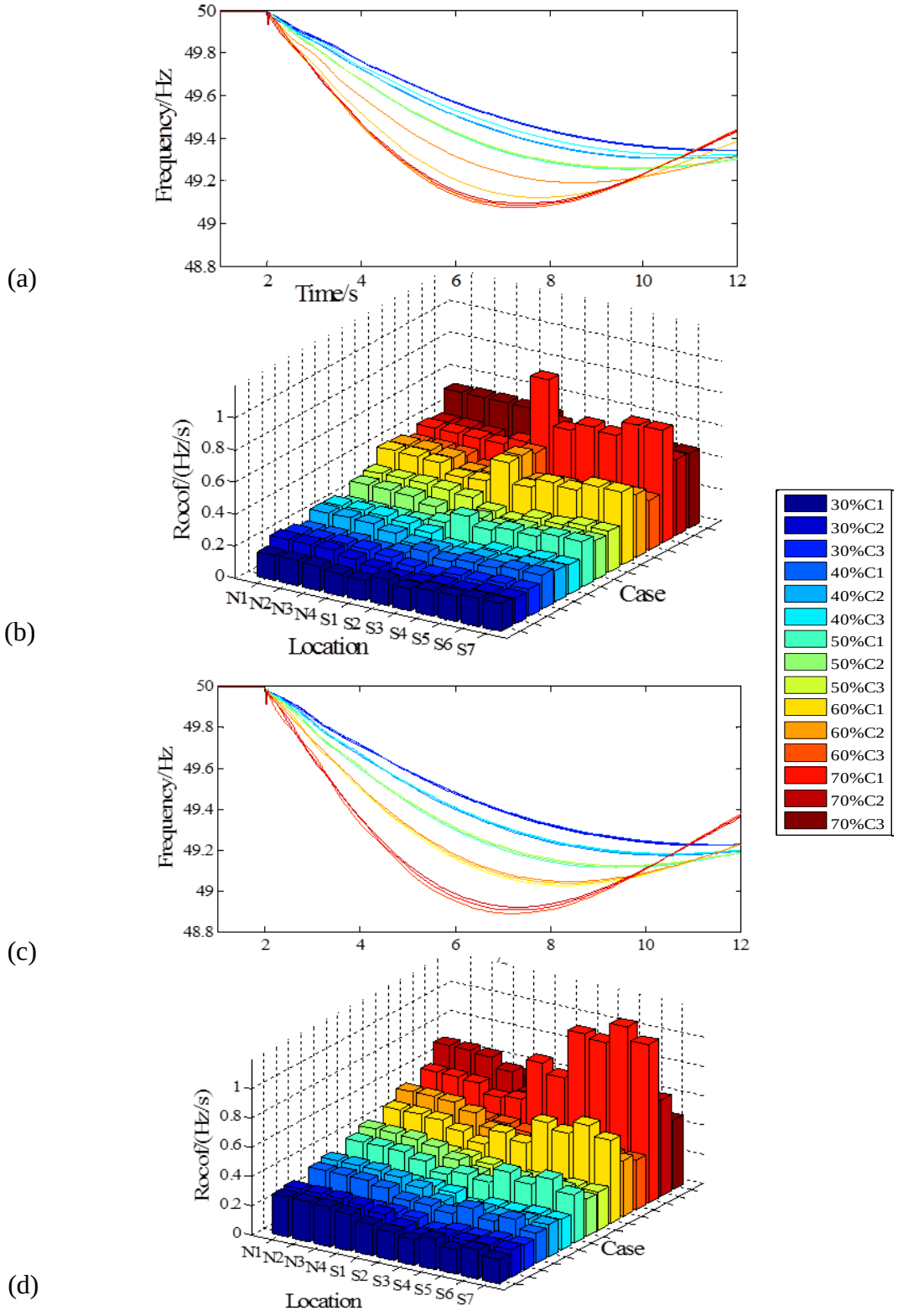

Figure 3-15: The impact of renewable penetration levels and dispatch patterns on the performance of system frequency for a 1800 MW loss infeed in (a) S2, (c) S6 and corresponding RoCoF in (b)S2, (d)S6.

3.6 Evaluating the Performance of Frequency-based protections

3.6.1 Identification of protection issues

Taking the reduced GB grid model, three case studies have shown that system frequency response and its corresponding maximum RoCoF values vary under different system inertia constants, different sizes of infeed loss, different renewable dispatch patterns, as well as different locations of disturbances. These studies were carried out with the recognition of the system dynamic operation constraints: the 49.2 Hz minimum instantaneous frequency limit, a maximum infrequent infeed loss of 1800 MW and an anticipated RoCoF-based LOM protection threshold of 1 Hz/s. The same process can also be applied in any other networks to evaluate the impact of system inertia reduction on system frequency performance.

By assessing the simulation results (Appendix B) in association with the current protection settings reviewed in Chapter 2.6, the following potential protection issues are identified in future GB grid due to the accelerated and magnified frequency excursions:

- Under 70% renewable penetration, the RoCoF based DG anti-islanding protection in zone S4 to S7 will mal-operate for a 1800 MW infeed loss in zone S6 if all the renewable outputs are from the south region of GB as the simulated maximum RoCoF values are higher than 1 Hz/s. Given the DG distribution recorded in [18], 55% of the DGs will be false tripped due to the high RoCoF values caused by low system inertia.
- Under 70% renewable penetration, the first stage UFLS will be issued if system frequency prior to the 1800 MW infeed loss in zone S6 is lower than 49.84 Hz as the simulated system frequency will drop below 48.8 Hz which is the threshold of the first stage load shedding.

3.6.2 Discussion on the impact of identified protection issues

The underlying threats of system inertia variations to system frequency stability are induced by the absence of an inherent inertial frequency response from renewable resources and variability introduced by the intermittent nature of renewable resources. As a result of the magnified frequency variations, operation performance of the conventional frequency-based protections would be degraded.

If the RoCoF-based DG anti-islanding protection mal-operates undesirably, the overall power imbalance due to the original infeed loss could be exacerbated by a further loss of power supply from DGs. Consequently, the frequency will drop even lower and the system will be more unstable. Eventually, system frequency could collapse followed by the automatic low frequency load disconnection. Taking the GB system as an example (Figure 3-16), the second stage frequency drop was caused by the unexpected tripping of DGs due to the large RoCoF value after the loss of generator B, leading to the frequency collapse [85].

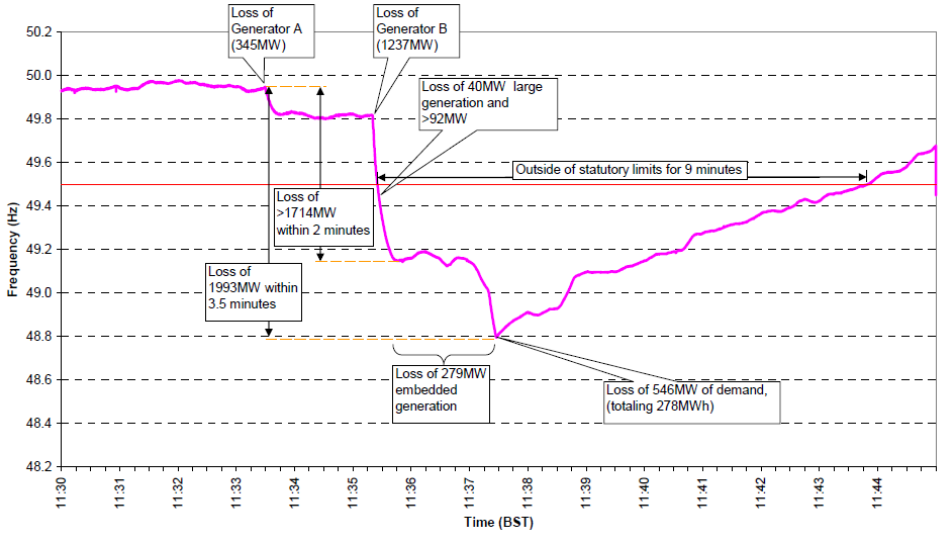

Figure 3-16: GB system frequency deviation following exceptional generation loss (1993 MW) during the blackout on 27th of May 2008 [85]

With regards to the UFLS issue raised from the case study, its initialisation could take place in a weak system (where the initial system frequency before the infeed loss is below 50 Hz, but above 49.8 Hz) for a 1800 MW infeed loss. The operation of

unexpected UFLS due to the lower system inertia will result in interruptions to customers. Furthermore, if the frequency keeps decreasing, the potential disconnection of DGs which are exporting power and connected downstream of the contracted UFLS disconnection points could also initiate a second stage frequency drop. One protection mal-operation could lead to a cascading event that further degrades system stability and consequently end up with a system-wide blackout.

The increase of RoCoF threshold, which targets to reduce the unexpected trip of DGs due to more frequent and severe system dynamics brought by renewable resources, inevitably compromises protection sensitivity and introduces a certain degree of blindness for the real LoM event. In the case studies presented in this chapter specifically, only a 70% renewable penetration can lead to a sudden and severe frequency drop that gives a RoCoF value higher than 1 Hz/s. And there lays a fact that the probability of reaching a 70% renewable penetration is very low in prevailing GB grid and the coming decades. With reliance on the fixed 1 Hz/s RoCoF setting, the protection system is not designed to cope with such variable system conditions, consequently denotes high risks of undetected real LoM events in the future.

The evaluation work gives quantified reference to seek for more reliable protection settings for the potential issues identified for the future networks. As seen the root cause of system inertia reduction and variation, a flexible approach, which is sensitive to dynamic system inertia level and also reflective to the zonal variations of frequency response, if realised, could effectively protect future GB power system from deterioration.

3.7 Potential adaptive solution to enhance future system frequency stability

Through applying the generic modelling and validation process, potential system stability issues now have been characterised where effective solution can be seeking for to mitigate system deterioration. In this case, it has shown through extensive

simulation that the growing renewable resources in future GB grid will act to reduce system inertia that places negative impact on system frequency stability as a result of potential protection mal-operation. The setting of RoCoF-based LoM protection, for example, although has been adjusted could still lead to high risks in protection failure as a result of non-detection. This attributes to the significant desensitisation of protection schemes, by increasing threshold while still remains as a fixed value, to cope with the high renewable penetration which would occasionally happen during practical system operation [21]. However, if the protection system is designed to only cover scenarios that could possibly happen during normal operating conditions, any of the cases that beyond this scope will lead to protection mal-function. Therefore, future protection system should be designed to not only meet the requirements for its robustness but possess a certain degree of flexibility on account of the uncertainties in system dynamic operation, as in this case the variations in system inertia as well as the zonal maximum RoCoF values.

On measuring primary system condition synchronously, adaptive protection provides an active means of updating protection settings for any detected changes in the light of pre-designed operational rule. The flexibility exhibited in adaptive protection has manifested itself effective on improving protection sensitivity [74, 95, 96], discrimination [97-100] and coordination [101-103] which are limited in conventional protection schemes where fixed protection settings are applied.

Adaptive protection started to draw attention since 1980s and was initially proposed for protecting transmission lines [104, 105]. A commonly used definition can be found in [106] describing adaptive protection as "a protection philosophy which permits and seeks to make adjustments automatically in various protection functions in order to make them more attuned to prevailing system conditions". It allows settings to be automatically populated after fine tuning to best fit to prevailing primary system conditions. Therefore, it could act to mitigate pre-identified protection mal-operations, which in other words, enhancing the operational performance of future system.

This hypothesis will be examined throughout the course of the following chapters. It should follow the objective that protection settings are adapted to the ones that best suit for prevailing system conditions as a balance between protection stability and sensitivity. To achieve this, system inertia, as the root cause of initiating the mal-operation of conventional RoCoF-based LoM protection and UFLS, shall operate as the variable that activates and facilitates to realise adaptive protection functionality. The observed zonal variations in system frequency response will also be considered for a more dedicated and sensitive protection performance.

3.8 Chapter Summary

This chapter assessed the impact of the increased largest infrequent infeed loss and the growing integration of renewable resources have on the frequency response in future GB power system as well as the performance of frequency-based protection practices. A pronounced influence of system inertia level on frequency response has been observed, along with potential protection mal-operation issues.

A generic system modelling and validation process has been presented following which the evaluation of system performance can also be carried out in any networks in a software environment. Based on the proposed process, an 11-node reduced GB model has been built in PSCAD/EMTDC as an example to assess the impact of inertia reduction and variation on system frequency response. Each newly-defined zone was composed by two types of aggregated generation (thermal, gas), lumped voltage dependent PQ load and equivalent PI model to connect adjacent zones. A range of modelled elements was analysed to illustrate how the reduced model has been produced based on logical assumptions made for model simplification. Validation of the model in terms of its capability to exhibit representative frequency response has been achieved through comparisons of its performance in simulating historical events with the data recorded for the actual events.

The largest frequency drops and the resulted maximum RoCoF values have been quantified under a range of combined system conditions, including various

penetration level and distribution patterns of renewable resources, different locations and sizes of sudden infeed loss. The GB network was observed more resilient for the loss in zone S2 than in S6 as seen the amounts of frequency drop in S6 were generally 15% higher than in S2 for the same size of sudden infeed loss and the maximum RoCoF values for loss in S6 were generally 26% higher than the loss in S2 from zone N1 to S1 while 18% higher from zone S4 to S7.

The cubic polynomial has been employed to best articulate the relations of the investigated pairs. The extreme conditions have been criticized for reaching system operating limits, assuming the outputs from renewable resources are equally distributed in the GB system:

- The system inertia constant should not be lower than 2.52 s for the loss in S2, while not lower than 3.83 s for the loss in S6, to ensure that the frequency drop would not exceed the 49.2 Hz minimum instantaneous frequency constraint upon a 1800 MW sudden infeed loss.
- The sudden infeed loss in Zone S6 should not exceed 1644 MW with a system inertia of 3 s to ensure the instantaneous minimum frequency stay within the acceptable 49.2 Hz.

The stability and sensitivity issues of conventional protection schemes have exposed from simulating frequency response under more practical system operating conditions where renewable outputs are unevenly distributed in the GB system:

- Under 70% renewable penetration, the RoCoF based DG anti-islanding protection in zone S4 to S7, which is equivalent to 55% of the RoCoF-protected DGs, will mal-operate for a 1800 MW infeed loss in zone S6 if all the renewable outputs are from the south region of GB as the simulated maximum RoCoF values are higher than 1 Hz/s.
- Under 70% renewable penetration, the first stage UFLS will be issued if system frequency prior to the 1800 MW infeed loss in zone S6 is lower than 49.84 Hz as the simulated system frequency will drop below 48.8 Hz which is the threshold of the first stage load shedding.

This chapter finally posed a potential of using adaptive protection as a flexible approach to enhance protection stability without compromising its sensitivity. Both prevailing system inertia level and the zonal frequency variation characteristic should be considered for delivering such flexible feature in the protection schemes. Ways of achieving real-time system inertia estimation will be introduced in Chapter 4 and the hypothesis of introducing a zonal adaptive protection scheme as the flexible while more stabilised protection operation approach will be investigated in Chapter 5.

4. Real-time System Inertia Estimation using Switching Markov Gaussian Model

4.1 Chapter Overview

System inertia is the key factor that alters dynamic frequency response in a deterministic way. In future systems which inherently feature inertia reduction associated with the uncertainties in its dynamic variations, deteriorated performance of frequency-based protections could be incurred as evaluated in Chapter 3. The hypothesis that adaptive protection can effectively mitigate such protection mal-function requires a continuous awareness of system inertia in assisting the recognition of any potential instabilities where protection settings can be adjusted accordingly. However, existing methods are limited to the presence of system events, such as generation loss [5, 6], or based on a simplified system [7, 8] which cannot fully express the complex and quasi-stochastic system in reality. Moreover, the requisites of instantaneous system measurements during disturbances and high sensitivity to system noise all manifest to provide undesirable inertia estimates pre-disturbance.

This chapter introduces a Switching Markov Gaussian Model (SMGM) through which system inertia can be, for the first time, estimated continuously on-line during normal operating conditions [107]. By training with historical frequency and inertia measurements, the complexity and underlying frequency-inertia dependencies in system dynamics can be learnt and extracted to formulate a Gaussian Mixture Model (GMM) with temporal dependence encoded as Markov Chains for an improved accuracy. Based upon presently observed frequency variations, system inertia estimates can be simply and continuously generated from the trained SMGM.

This chapter firstly reviews current practices on system inertia estimation associated with discussions on their shortfalls in achieving continuous on-line inertia estimation. The reasons of selecting SMGM that gives best estimation performance are analysed,

followed by reviews of relevant statistical theories and terminologies. The constituent elements required to formulate the SMGM are then brought together through an elaborative selection of components and the parameter values in each element which best fit the GB system are identified.

Conducted with the SMGM formulated for the GB system, its validity has been examined against the historical recordings of system frequency and inertia constants. The reliability of the proposed model in facing the loss of frequency observations or the presence of system noise is tested with discussions on fail-safe strategies that shall be applied for its best performance. An extensive discussion is presented at the end to clarify the impact of SMGM configuration to its estimation accuracy and potential future applications along with requisites for its practical implementation.

The main contributions of this chapter are:

- A consolidating summary of existing inertia estimation practices and their limitations.
- Proposal and formulation of a novel statistical model which is capable of continuously estimating dynamic system inertia on-line through observed steady-state and relatively small frequency variations.
- Capturing temporal dependency between variations of frequency and inertia through a multivariate mixture model encoded with skip-k Markov Chains.

4.2 Current Inertia Estimation Practices

Existing inertia estimation methodologies can be classified into transient frequency based and recursive state-based estimation approaches. Details will be presented in the following subsections where transient frequency based approach is further divided with its reliance on the employment of the Swing Equation or a deformed Swing Equation.

4.2.1 Transient frequency based inertia estimation

In the frequency transient based approach, the Swing Equation is predominantly applied to estimate system inertia in the presence of a system event. It describes the dynamic change in rotor angle when a disturbance on the network upsets the balance between generator mechanical power and electrical power. The instantaneous change in rotor angles (which also refers to frequency change) and power imbalances are restricted due to the characteristics of inertial response which only lasts for the first few seconds after the disturbances.

[5] summarised the relationship between system inertia constant and the total demand on the basis of swing equation using historical outage data. A polynomial approximation was introduced in [108, 109] which incorporates a 500 ms sampling window to identify the start of the event and the suitability for using the event for inertia estimation. However, the accuracy of estimation is shown to be largely affected by system noise, the location of PMUs and the system loading condition. Moreover, the dependency of fitting the frequency polynomial is too critical and has to be aligned with the 20 s data. In contrast, [110] proposed a moving average filter which smooth the active power measurements and the derivative of frequency stored over a certain time period to improve the resilience against system noise. Further improvement was achieved in [6] by introducing a consecutive sum from which the duration of a disturbance and the inertia at that time can be derived.

Despite the realisation of inertia estimation, these methods are all limited in that the onset of a disturbance is required to determine system inertia which can not facilitate the inertia estimation pre-event. This can be reflected as necessitating the instantaneous measurements of system frequency and the power imbalance prior and just after the disturbance. Moreover, the subsequent time needed for inertia computation could delay effective actions that possibly reduce the impact of disturbances on system stability (e.g. through proactive control actions). Furthermore, their applicability to future systems may be negatively influenced from the perspective of measurement accuracy, as a result of the evolving system dynamics.

4.2.2 Deformed swing equations

Inertia estimation, in this approach, is invoked through deforming the Swing Equation to derive a new formula with specific system measurements (e.g. voltage, current, phase angle).

A fifth-order polynomial approximation equation was applied in [111] to fit the rate of change of frequency curve where the estimated coefficients of the polynomial are used to compute inertia. In [7], inertia estimates were obtained from an expression of bus voltage and oscillatory frequency. However, this is only applicable to radial networks, while mesh networks are invariably used in practical power systems. A single machine infinite bus model was used in [8] where the inertia of an individual machine is derived from the division of the change in electrical power by the third derivative of the rotor angle. However, this method is restricted when extended to assess the inertia of a multi-machine system as the needs of converting the system to an equivalent single machine and infinite bus model.

4.2.3 Recursive state estimation

According to real-time selected observations of system topology and measurements (e.g. voltage, phase angle), the states of a statistical model and its parameters, which equivalently represent the investigated network model, are updated in a recursive manner to provide estimates of prevailing system inertia.

The system inertia in a multi-machine system derived in [112] was achieved through the iterative updates based on Least-squares and Newton-Raphson methods. However, the dynamic states of each generation model need to be known for deriving the sensitivity matrix and analysing eigenvalues to provide inertia estimates. In practice, generation plant is rarely monitored in the control centre and not all the generation units in the system are responsible for inertial frequency response, meaning this method could under/over-estimate system inertia by missing or wrongly accumulating contributions from the generation units. An Extended Kalman Filter

was applied in [113, 114] to calibrate the system inertia as a prediction correction process by minimising the errors between the predicted and the actual values of inertia. In practice, actual inertia measurements are not available or available in a finer time resolution indicating that the reference to correct the prediction cannot be retrieved every iteration therefore breaking off the process, limiting the practical applicability of this approach. Such kinds of methods could be unsatisfactory for real-time applications in terms of the long executing time and the risk of failure to derive the inertia estimates during iteration.

Relying on the occurrence of system disturbances, estimates generated from above reviewed methods are inconsistent and their accuracy and validity cannot be guaranteed all the time to proceed continuous reflection of dynamic system inertia variations. In order to overcome the limitations inherent in these existing approaches, this chapter, thereby, centres on seeking valid means to achieve real-time inertia estimation during normal system operation.

4.3 Switching Markov Gaussian Model

4.3.1 Motivations for SMGM

As seen the great dependency identified between system inertia and frequency response in previous chapter, there is potential to obtain system inertia information from the frequency measurements. Although the frequency oscillations during normal operation are a result of natural events (i.e. load or network switching), they are similar in their dynamic nature, only proportionally lower in magnitude compared to frequency changes during major system events. If realised, it would be the simplest approach to achieve real-time inertia estimation without relying on the occurrence of system events. The validity of this hypothesis depends on whether such dependency can be expressed in a certain way, and the consistency of such dependency not only existing when subjected to the disturbances but also during normal system operation.

Challenges to fully express such dependency are presented by the non-linear system dynamics (including the variations in system demand over time, generation mix, the corrective responses of control systems and the centralised management of generation dispatch, etc.), where such relations are not typically measured and/or available straight away. Therefore, it relies on being represented as latent or hidden variables that only exist in a model hypothetically [115]. The problem now turns to select a proper model through which the frequency-inertia dependency can be fit more closely.

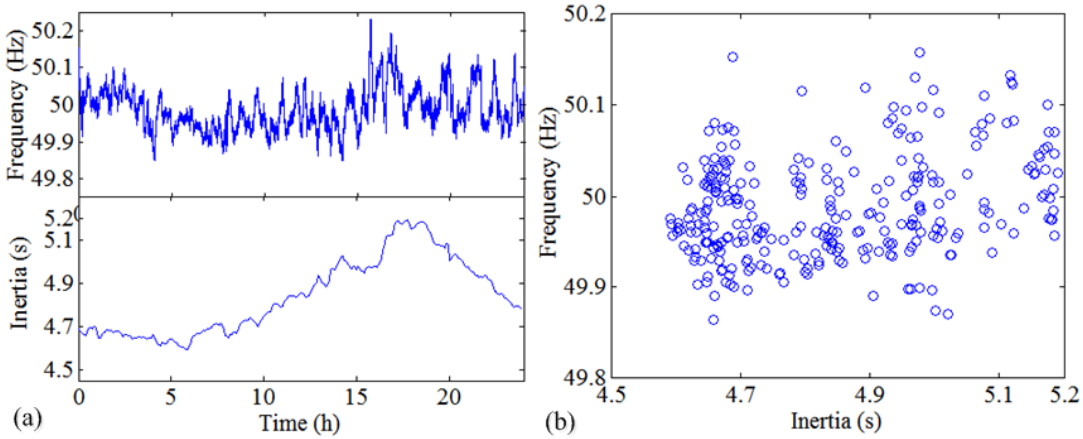

Figure 4-1: Typical mapping of the GB system frequency and inertia variations over the course of one day in: (a) time series, (b) scatter plot.

An example of typical daily frequency and inertia profiles in the GB system is shown in Figure 4-1 where the same group of frequency and inertia data is given for a course of a day separately in (a) while a coordinated scatter plot in (b). The frequency data is recorded from a PMU installed at the University of Strathclyde with a 20 ms reporting rate [89]. The inertia data is derived from historical generation dispatch data from ELEXON [116] using (2-3), with each source assigned to their typical inertia constants listed in Table 4-1. Due to limited access to commercial data, related historical generator dispatch can only be obtained on a 5-minute resolution, meaning levels of historical system inertia used for model training in this study is also limited to a 5-minute interval. In order to preserve consistent data pairs to profile the underlying dependency, the 5-minute interval is also selected to

demonstrate the frequency data where system frequency dynamics within this interval will be recorded and aggregated.

Table 4-1: Typical inertia data for different generation types [30, 119]

Generation Source	Inertia constant (s)
Coal	4.5
Gas	6.5
Nuclear	6.5
Hydro	4.5
Wind	0.0
Interconnector	0.0

In order to express such daily trajectories of frequency and system inertia, a complex model would be necessitated than a single/simple distribution, like linear or exponential. This is due to the observed coupling of non-linearity in their temporal characteristics and non-stationary in the range of observed values. If fitting with a single distribution, there exits a risk of under-fitting that deteriorates the accuracy of real-time inertia estimation. However, the hypothesis would also only valid if such a complex model incorporates a limited number of sub-distribution or sub-model, therefore, introducing an existing concept called finite mixture model. A finite mixture model uses a set of simple parametric distribution which can be linearly combined and weighted to fit the implied distribution of the observed data [117, 118]. The flexibility posed in its switching regimes further stipulated credible approximation for the probability functions, along with generating a wider range of estimates than through a single distribution. Therefore, the features that inter-relate between frequency and inertia can be expressed in greater detail and a more comprehensive way by such a finite mixture model.

To verify the hypothesis that the dependency between frequency and inertia can be expressed using a finite mixture model, a quantitative procedure is required to determine the model form of the mixture distribution and the parameter values of each distribution, if can be formulated. By selecting from the existing form of mixture model, Gaussians Mixture Model is chosen among other mixture models due to its simplicity and computational tractability where it can be inferred without resorting to the computationally intensive Monte Carlo type methods [120].

Moreover, the multivariate Gaussian dependency structure also possesses a higher degree of flexibility over others (few as they are) as it can accommodate the apparent skewness, multimodality and in the case of multivariate distributions, where a known form of parametric distribution rarely fits [121, 122].

To this end, GMM is selected as the most suitable model to express the dependency between frequency and inertia and will be assessed for the validity of realising real-time inertia estimation. To deliver the method explicitly, relevant terminologies and theories in statistics will be firstly introduced in the next section, which assist in justifying the selection of the unknown parameter values in GMM. Accuracy of the formulated GMM will then be verified through its implementation on the GB system. Markov Chain and on-line calibration cycle (OCC) will be introduced and tested afterwards as an effective means to further improve estimation accuracy. Quantification and reasonable justification of estimation accuracy will be presented throughout the selections of constituent elements.

4.3.2 Theory behind SMGM

4.3.2.1 Joint probability and conditional probability

In this research, inertia estimates are hypothesized to be generated through extracting the most likely value from the formulated dependency conditional on a given frequency observation from the mixture distribution. This involves the concepts of joint probability and conditional probability.

Joint probability denotes the probability as a resulted of a series of variables fall in a combined range or discrete set of values specified for each variable. In the case of taking system frequency and inertia as two variables, the notation for joint probability takes the form of $P(f \cap H)$. An illustrative example is given in Figure 4-2, where the joint probability of frequency and inertia constants are expressed as an arbitrarily complex form following a multimodal distribution. This, on the other hand, proves that such a distribution cannot be expressed using a simple distribution in a two-dimensional space.

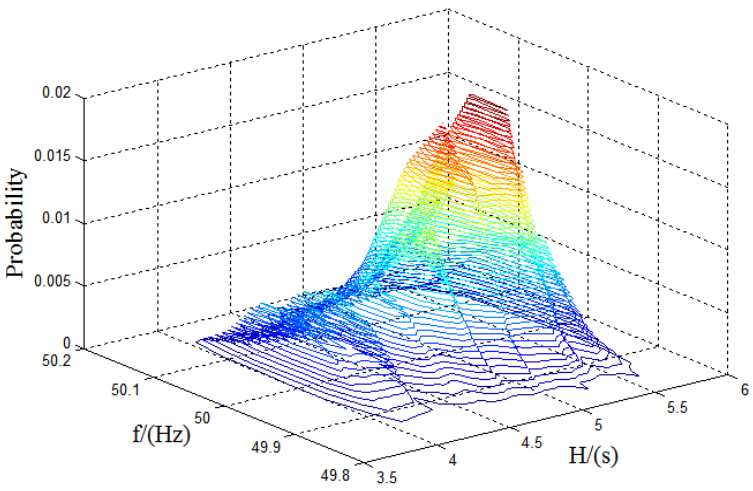

Figure 4-2: Joint distribution of frequency and inertia

Conditional distribution is the probability that one variable equals a certain value given by the occurrence that another variable has been assigned to a specfic value [120, 123]. If system frequency and inertia are still taken as an example, the conditional probability, expressed as $P(H|f)$, is the probability of the inertia constant when frequency equals to a specific value. Figure 4-3 depicts the probability of inertia constants conditional on a frequency observation of a magnitude of 50 Hz taken from the joint distribution in Figure 4-2.

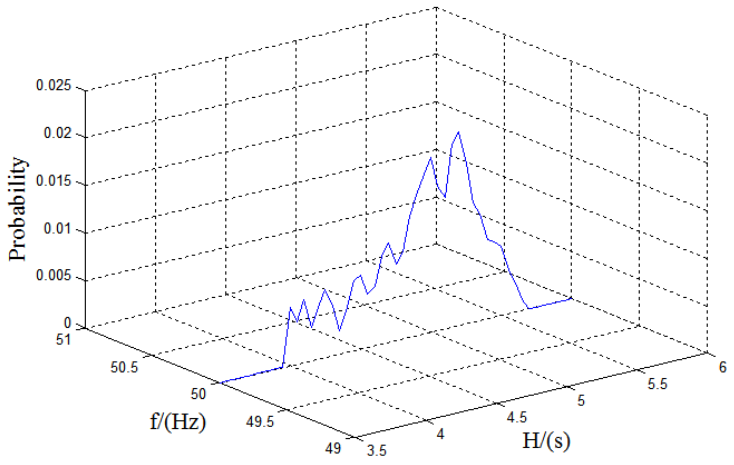

Figure 4-3: Conditional probability of frequency and inertia for a 50 Hz system

The expression of a variable conditional on another is a multivariate normal distribution. Assuming a is the specific value being conditioned on, the mean and variance of this multivariate normal distribution are formulated as [124]:

$$\bar{\mu} = \mu_1 + \sum_{12}\sum_{22}{}^{-1}(a - \mu_2) \quad (4\text{-}1)$$

$$\bar{\sum} = \sum_{11} - \sum_{12}\sum_{22}{}^{-1}\sum_{21} \quad (4\text{-}2)$$

with the parameters for the conditional distribution component being partitioned as $\mu = [\mu_1, \mu_2]$ and $\sum = [\sum_{11}, \sum_{12}; \sum_{21}, \sum_{22}]$.

where,

μ_1 is the mean vector of the variable to be predicted
μ_2 is the mean vector of the variable already known
$\sum_{11}, \sum_{12}, \sum_{21}, \sum_{22}$ are their covariances

4.3.2.2 Correlation

Owing to the fact that the potential dependency underlying system frequency and inertia is unidentified, it requires a logical explanation to select from the existing forms of these two variables (e.g. variance of frequency/inertia, derivative of frequency/inertia) to formulate the dependency pair. Therefore, the term correlation will be applied.

Correlation determines the degree of two variables linearly related to each other, quantified by a correlation coefficient [125]. It is widely used for dependency analysis where the similarity of any two variables (or two sets of variables) can be discovered as a reference to find the best profiling of one dependent on another [126]. For a correlation coefficient equal to zero, the two variables are entirely independent. A positive dependence is indicated if the coefficient is higher than zero, while an inverse relation is identified by its value being negative. It is formulated as [125]:

$$r_C = \frac{COV(f, H)}{S_f S_H} \quad (4\text{-}3)$$

where,

r_C is the correlation coefficient
S_f and S_H are the sample standard deviations of the random variables f and H
$COV(f, H)$ is the covariance between frequency and inertia variables (Appendix D.1)

4.3.2.3 Gaussian Mixture Model

For a finite mixture model with each component taking the form of a Gaussian distribution, a GMM is produced which is of nearly singular covariance matrix that reduces the number of parameters to be estimated. The general form of a mixture of M Gaussians would be used to express the probability of observation x of a dimension d as [121]:

$$P(x) = \sum_{m=1}^{M} w_m \frac{1}{2\pi \left| \Sigma_m^{\frac{d}{2}} \right|} e^{-\frac{1}{2}\{(x-\mu_m)^T \Sigma_m^{-1}(x-\mu_m)\}} \quad (4\text{-}4)$$

where

w_m is the mixing weight or probability of the mixture component m occurring
μ_m is the Gaussian mean of m^{th} mixture component
Σ_m is the Gaussian covariance of m^{th} mixture component
Matrices and vectors are shown bold

An example is shown in Figure 4-4 illustrating the distribution of a GMM attributed from three underlying individual Gaussian components with each Gaussian capturing a stationary range of observations. The mixture distribution now follows a non-Gaussian distribution which is formed with mixed means and variances and overlapped at some points.

With regards to the mean and variance of each Gaussian distribution and the number of Gaussians to represent the observation data set, Expectation Maximisation (EM) algorithm and Bayesian Information Criterion (BIC) are two recognised and defined step to generate such values for a GMM that best profiles the observations [127]. EM algorithm determines the parameters (i.e. mean and covariance) of each Gaussian set by iteratively selecting from the candidate models according to the goodness of fitting a distribution to data [121, 128-130]. Due to the fact there is no restriction on their variance type, the resulted distribution parameter values are of higher flexibility and accuracy. BIC works on maximising the posterior probability of a candidate model given a set of observations while introducing penalty terms to avoid an overly complex model [131-134]. As it can be proceed without the specification of prior distribution, it provides a simpler approach, in this research work, to better

accommodate the hidden dependency between frequency and inertia. Detailed calculation can be found in Appendix D.2.

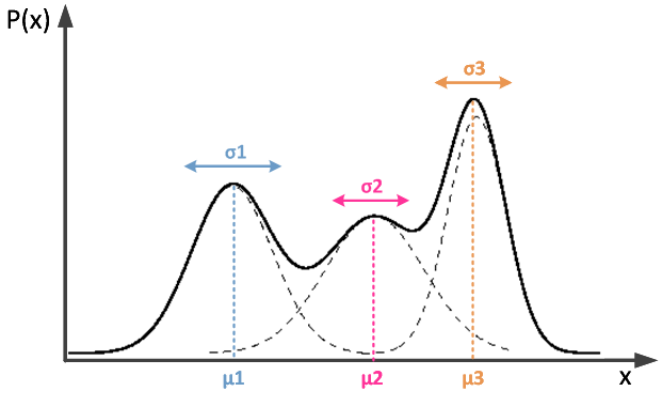

Figure 4-4: Generic distribution of GMM

4.3.2.4 Sampling from a non-Gaussian distribution

The fitted model takes the form of a joint distribution that represents the multivariate relation between the variables in the given data set. Estimating using this model, therefore, necessitates an effective means to take samples from this distribution as the final estimates. This, inevitably, presents a challenge when dealing with non-Gaussian distributions. Slice Sampling is therefore introduced to draw samples from the mixture distribution [135]. This attributes to the higher efficiency it possesses than methods like Metropolis algorithm, while it is simpler than Gibbs which needs extra instructions to sample from a non-standard distribution without losing the generality [136].

Slice Sampling takes samples uniformly from the region under the univariate distribution curve in vertical coordinates and takes the value at its horizontal coordinates, as demonstrated in Figure 4-5. A region of width (W) is identified around the starting point (x_0) and such a width will be continuously added towards both end until reaching out of the distribution curve (x_1, x_2). It has the benefits of allowing distributions of an arbitrary form to be sampled, without any specialisation of the procedure and the size of each sampler can be adapted as required.

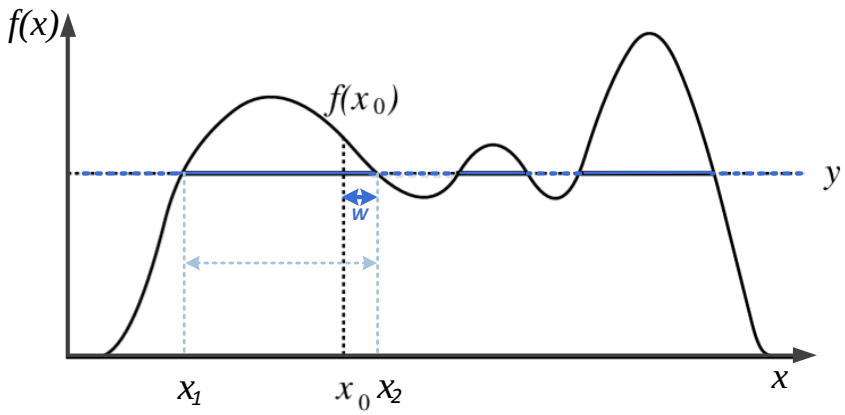

Figure 4-5: An example of slice sampling

4.3.2.5 Contextualising temporal dependency: Markov Chain

Markov Chain refers to a dependency structure where the current state is modelled with a certain degree of dependency on its previous one or more states (possibly temporally discontinuous) in a non-deterministic way [137-139]. As shown in Figure 4-6, the given Markov Chain features a discrete-time character where the state f_t is dependent on f_{t-1} and f_{t+1} (the subscript refer to the state in time series). A time axis has been added on GMM to form an extra dimension for the conditional probability curve. It facilitates a more profound understanding of the dependency structure inherent in the system dynamics from which, the joint distribution can be expressed in association with its temporal distribution in prior states. In addition, by switching among multiple Markov regimes, the encoded GMM (namely SMGM) would be more flexible to accommodate the stochastic complex in system dynamics.

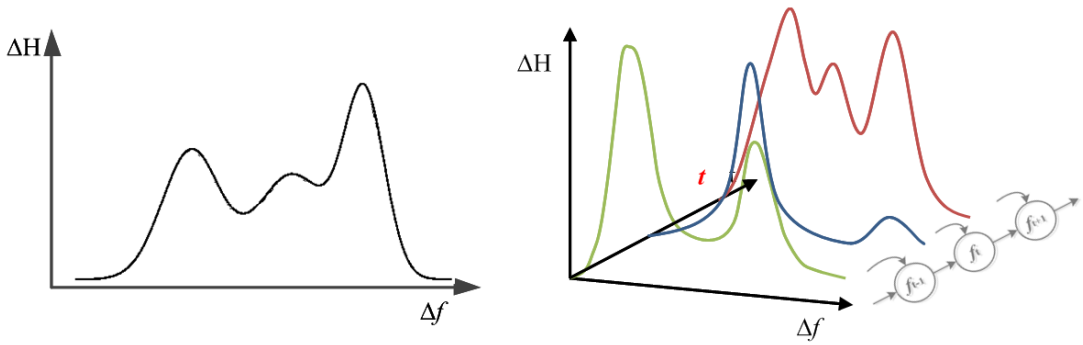

Figure 4-6: An example of encoding of a discrete-time Markov Chain

There are three major techniques of entering/removing independent variables to identify the states of regression for the Markov Chain: forward, backward and the stepwise regression [125]. In this research, the stepwise regression is employed to select the dependent-states of the variables. It can provide higher feasibility and flexibility than the other two techniques through automatically entering/removing variable one by one in a justifiable and reasonable manner [131, 140].

4.3.2.6 Performance evaluation with Mean Squared Error

Mean Squared Error (MSE) is a risk function that reflects the difference between the estimated values and the true values, expressed as:

$$MSE = \frac{1}{n}\sum_{i=1}^{n}(\widehat{y_i} - y_i)^2 \tag{4-5}$$

where,

$\widehat{y_i}$ is the estimate

y_i is the true value

In this research where a statistical model is established, MSE is superior to techniques like sum squared error or mean percentage error as it incorporates both the variance of the estimate and its bias [129]. Therefore, it will be more accurate and representative to determine the suitability of the candidate model to the given data without significantly harming the model's estimation ability.

4.3.3 SMGM algorithm for inertia estimation

This section presents the procedure of how the algorithm is designed to verify the hypothesis of profiling inertia performance from system frequency observations. As depicted in Figure 4-7, there are two-independent phases: off-line training phase and on-line operation phase. Conducted with the historical frequency and inertia data set, the mixture model is formulated through an iterative off-line training where the underlying frequency-inertia dependency will be expressed using the selected model presenting a best performance. The trained model is then commissioned on-line to generate inertia estimates from the frequency measurements taken in the real time.

The estimated inertia constants are monitored continuously through comparisons with the available generation dispatch data as a reflection of real-time system inertia level. The statistical analysis steps included in the off-line training phase are detailed in Figure 4-8 where the corresponding steps are highlighted using the same colour as in Figure 4-7.

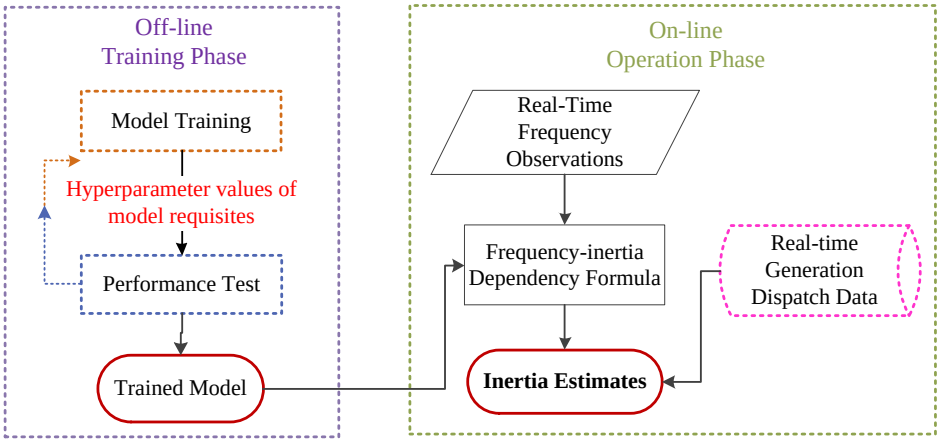

Figure 4-7: Algorithm design procedure

Training of the model starts from exploring the dependency pair where the mixture model can be formulated with ('Step 1'). From the selected dependency structure, a corresponding mathematical equation can be formulated to indicate the underlying relationship of one variable given by the other in the identified pair. An iterative process is executed in 'Step 2' among a finite set of model hypotheses. This incorporates algorithms like EM and BIC to select the number of mixtures and parameter values of each Gaussian which best profile the joint distribution of system frequency and inertia. GMM is then summed from these individual Gaussians in proportion to their corresponding weight factors to identify the contribution of each Gaussian.

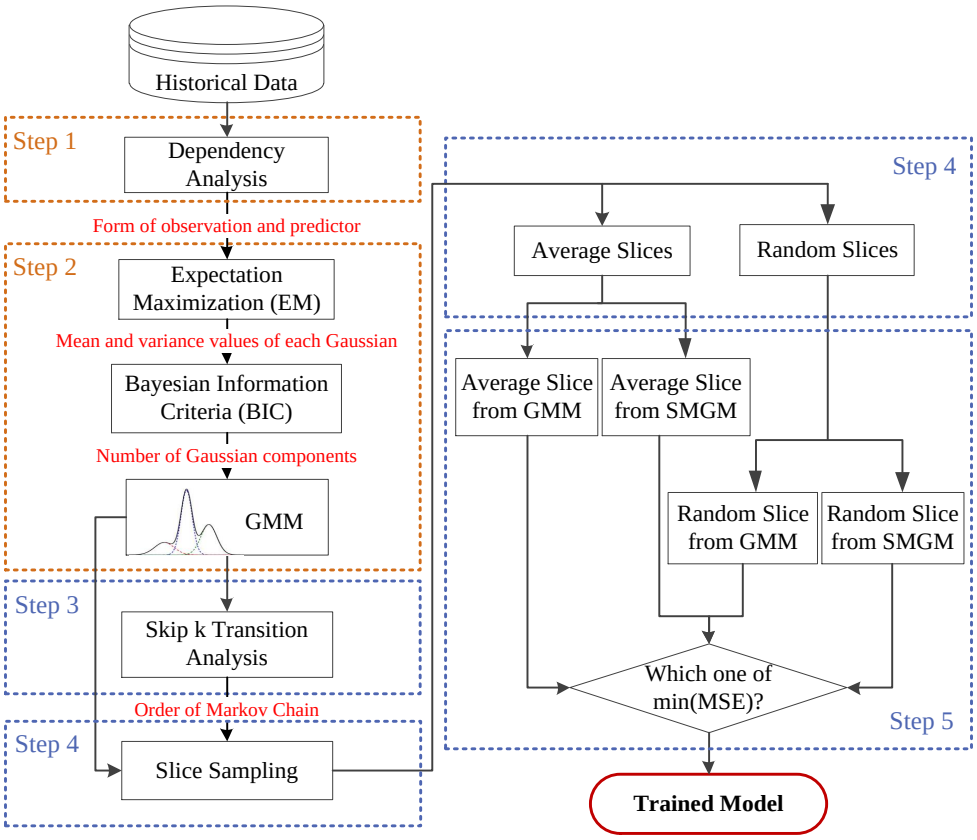

Figure 4-8: Off-line model training process

A temporal dependency, introduced as the mixed-order Markov Chain in 'Step 3', is encoded and assessed as a potential option to improve estimation accuracy. The order of the Markov Chain is selected from Skip k Transition algorithm. This determines the prior states that are relevant to the current state [141, 142] using stepwise regression. This is coupled with 'Step 4' to select the best approach to generate estimates from the fitted SMGM as it takes the form of a joint distribution that gives more than one value for a given frequency measurement. Concerns in choosing the one of the highest probability stem from the potential of losing the generalisation in applying under all conditions. Therefore, two approaches are suggested and will be compared with the first adopting the mean of the entire sample slices whilst the second approach randomly selects from the samples.

The final model is determined in 'Step 5' through analysing the MSEs from a total of four combinations as listed below. The combination which gives the minimum MSE should be selected as the most accurate model for on-line inertia estimation.

- Random sample from GMM
- Random sample from SMGM
- Averaged sample from GMM
- Averaged sample from SMGM

The following sections will continue to provide details of verifying the performance of the proposed inertia estimation algorithm through its implementation onto the real GB system. The parameter values of the mixture model and accuracy of its real-time performance will be assessed throughout the process of formulating such a dependency distribution for the GB power systems.

4.4 Off-line Model Training: Formulating a SMGM for the GB power system

Historical frequency measurements and generation dispatch data of the GB system were used in this research to train the model. The inertia was derived from historical generation dispatch data provided by UK System Operator on ELEXON [116] using (2-3), with each source assigned to their typical inertia constants listed in Table 4-1. The frequency data used was extracted from the available recordings of PMU data at the University of Strathclyde, University of Manchester and Imperial College London which form part of a UK monitoring network with a 20 ms reporting rate [89]. However, the training data set used the average across these three measurement points as this approach gives greater robustness from less reliance on a single source of data due to the potential loss of data measurements or measurement noise. Moreover, the average gives better reflection of true system-level conditions as the single measurement would largely be affected by the local generation dispatch pattern and the location of the disturbance.

The methodology for selecting training data that has been adopted in this work involves randomly selecting 100 days from a window of the past two years, giving 28,800 training samples which encompass daily and seasonal factors that may affect

the analysed variables. According to [143], a minimum sample size of 3,393 is required for a very accurate 99% confidence interval with a marginal error of 0.01. This spread of historical data, thereby, provides sufficient sample data to present the underlying features hidden in system dynamics within the statistical model. It should be noted that the data has been checked to ensure it was taken during normal operating conditions (±0.2 Hz of nominal frequency), given the validity that the formulated SMGM is then only legitimate in generating real-time inertia estimates during normal conditions. As mentioned earlier, resolution of the training data pair was set to 5 minutes and has also been applied for the on-line inertia estimation as the feature learnt by SMGM was based on such a resolution.

The following sections will present the steps of formulating the most suitable real-time inertia estimation model for the GB power system through selecting proper parameter values from first-stage model training and second-stage performance assessment.

4.4.1 Dependency analysis

As outlined earlier, power system inertia could be estimated from system frequency by exploiting the dependency relation between the two variables - frequency and inertia. In order to establish the strongest dependency structure where the inertia can be more accurately estimated from frequency measurements, the correlation coefficients have been examined and compared among every potential combination of these two variables in their various states (e.g. rate of change of frequency/inertia).

A total of 25 combinations were examined, including frequency/inertia, changes of frequency/inertia, second derivatives of the changes of frequency/inertia, moving variances of frequency/inertia and moving variances of the changes of frequency/inertia. It should be noted here that the change of frequency data has been derived by summing the frequency increments averaging over the measurements taken at Glasgow, Manchester and London (on a 20 ms resolution) throughout the 5-minute interval instead of taking the two values at the two ends of each interval as

shown in (4-6). This is due to the fact that the unknown dynamics of system inertia within the 5-minute interval could lead to estimation errors if an exceptional generation disconnection/connection occurs in between. In contrast, the averaged value over the 5-minute interval provides a better learning of the dynamics, as well as highlighting the impact of inertia change on the frequency variations on a system level.

$$\Delta f = \sum_{t=t_0}^{t_0+5mins} \frac{1}{3} \left| \Delta f_{GL\_20ms} + \Delta f_{MN\_20ms} + \Delta f_{LN\_20ms} \right| \quad (4\text{-}6)$$

where,

Δf_{GL_20ms} is the frequency change at Glasgow on a 20 ms basis
Δf_{MN_20ms} is the frequency change at Manchester on a 20 ms basis
Δf_{LN_20ms} is the frequency change at London on a 20 ms basis
Δf is the sum of frequency increments (on a 20 ms resolution) over the 5-minute period
t_0 is the initial counting time from when the frequency measurements start to be summed up

Given the 28,800 training pairs, the histograms which reflect the degree of dependency in each combination were plotted as in Appendix E. Small correlation coefficients lower than 0.3 [144] are generally seen through all the 25 combinations. The four (of a possible 25) strongest dependent variable combinations are presented in Figure 4-9, namely:

- $\Delta H \; vs. \Delta f$
- $\Delta(dH/dt) \; vs. \Delta f$
- $\Delta(dH/dt) \; vs. \Delta(df/dt)$
- $var(\Delta H) \; vs. var(\Delta f)$

where,

ΔH is the change of system inertia on a 5-minute basis, defined as $\Delta H = H_{t_0+5min} - H_{t_0}$ with H_{t_0} and H_{t_0+5min} specified as the system inertia constants at time t_0 and 5 minutes after t_0
$\Delta(dH/dt)$ is the change in the rate of change of inertia on a 5-minute basis
$\Delta(df/dt)$ is the sum of increments in the rate of change of system frequency on a 20 ms basis over 5-minute period
‘ var ’ is a moving window filtering the variances of two consecutive inertia/frequency measurements

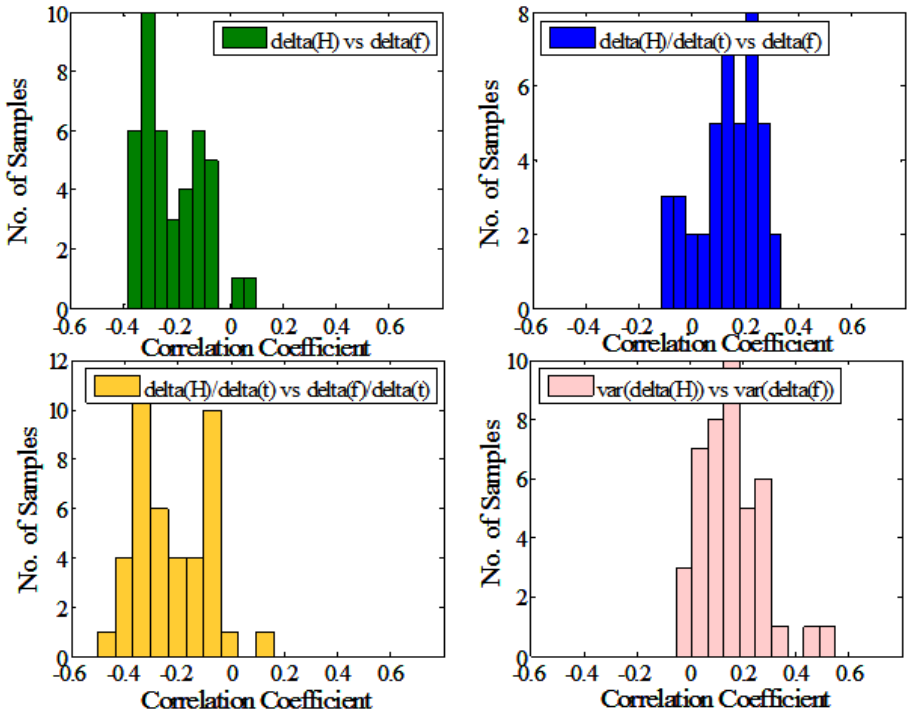

Figure 4-9 Histograms of the four strongest correlation pairs

A cumulative error exists when approximating lower order derivatives from the integration of higher order derivatives. Such errors are adversely affected by the step length taken for the approximation [145]. Inaccuracies caused by such cumulative errors are inherent in the second and third combinations listed above which upset the performance of proposed model, especially with a 5-minute data resolution. Therefore, these two dependency pairs (i.e. $\Delta(dH/dt)$ vs. $\Delta(df/dt)$ and $var(\Delta H)\ vs.\ var(\Delta f)$) that estimate inertia from the second derivative of the change of frequency were omitted. Moreover, the employment of moving frequency variances is also error prone owing to the absence of an integrating constant when attempting to derive the inertia constants from the variances. The same accuracy issue is apparent when generating inertia estimates from the second derivative of frequency but, in this case, caused by their variances. The averaged mean of the correlation coefficient between Δf and ΔH, which generally varies between -0.3 to 0.3, is higher than other groups. As such, Δf and ΔH was selected as the most dependent pair to formulate the joint distribution. The computation of prevailing system inertia is, thereby, defined as the sum of estimated change of system inertia and the inertia constant derived at the latest known state:

$$H_{est\_t} = H_0 + \sum_{t=1}^{k} \Delta H_{est\_t|\Delta f} \quad (4\text{-}7)$$

where,

H_0 is the latest observed system inertia

$\Delta H_{est\_t|\Delta f}$ is the estimated change of system inertia conditional on an observed system summed frequency variation average Δf on a 5-minute basis

H_{est_t} is the estimated system inertia at time t

The fact that the correlations among the assessed pairs are far below 1 also gives a reasonable justification of utilising the mixture model as such probability distribution is capable of accommodating the noise existing in the data set associated with weaker relations as in this case.

4.4.2 Selection of Gaussian components

In addition to the BIC expression, the type of Gaussian covariance matrix also plays an important role in the GMM cardinality. It will not only affect the number of Gaussian components but also the accuracy of representing observations with Gaussian mixtures. There are three typical types of Gaussian covariance matrices: spherical (independent variables with a common variance), diagonal (independent variables with different variances in the diagonal of the matrix) and full (linear dependence). A graphic example is shown in Figure 4-10. For the same group of data, the representations (highlighted in red) using different covariance matrices vary from each other with the one of full covariance matrix, in this case, expressed in more adequacy. In turn, it also affects the mixture number of Gaussians with growing size to compensate for the coarse representation from spherical, to diagonal, to full.

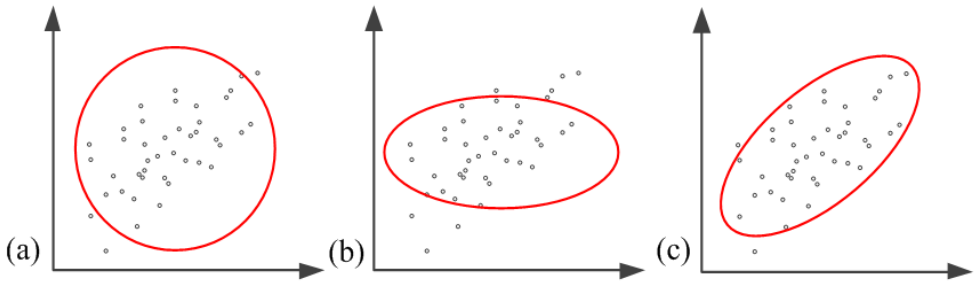

Figure 4-10: Graphic example of the Gaussian covariance matrix: (a) spherical, (b) diagonal, (c) full.

Conducted with the historical training data set, main figures identifying the performance of various covariance matrices are presented in Table 4-2. The first three indexes (i.e. precision, computation efficiency and covariance matrix) are the inherent characteristics of each covariance type itself. Therefore, they will not play deterministic roles independently from the number of Gaussian components which are derived from the targeted dependency structure in the light of the minimum BIC. Component of the mixture model refers to the number of Gaussians used to represent the overall distribution which, on the other hand, indicates the complexity of the model itself. Taking the GB system as an example, over 50 components are requested if expressing the given historical training data set with a spherical matrix, while this number would be reduced to 27 for a diagonal type and 21 for a full type.

Table 4-2: Comparison of various forms of covariance matrices [146]

	Spherical	Diagonal	Full
Precision	Low	Medium	High
Computation	High	Medium	Low
Covariance matrix	$\begin{bmatrix} \sigma^2 & 0 \\ 0 & \sigma^2 \end{bmatrix}$	$\begin{bmatrix} {\sigma_t}^2 & 0 \\ 0 & {\sigma_{t-1}}^2 \end{bmatrix}$	$\begin{bmatrix} {\sigma_t}^2 & \sigma_t\sigma_{t-1} \\ \sigma_{t-1}\sigma_t & {\sigma_{t-1}}^2 \end{bmatrix}$
No. of Gaussian Component	>50	27	21

It should be stated that the training of GMM is performed off-line. Thereby, the computational efficiency is not as important as the precision of capturing more observation information and the complexity given by the number of mixture components. Therefore, the 21-component GMM was selected in this case, to designate the historical dependency relation between the change of frequency and the change of inertia as its full covariance matrix provides the most comprehensive expression in nature while in less complexity than the other two.

An example of 21-component GMM is shown in Figure 4-11 using the historical training data set of the GB system. The contribution of each Gaussian giving an estimate is presented in the 2-D scatter plot in Figure 4-11 (a). Contribution of each Gaussian to form the mixture model is shown in Figure 4-11 (b). Each colour represents one Gaussian distribution with its unique mean and variance.

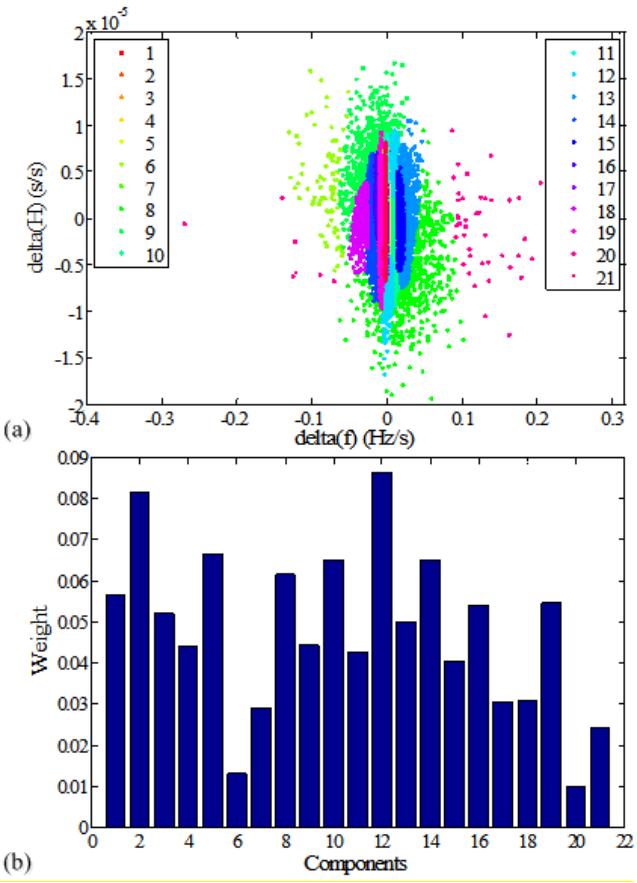

Figure 4-11: Example of a 21-component GMM: (a) labelling of the 21 Gaussians, (b) weight distribution of each Gaussian component.

4.4.3 Inertia estimates from slice sampling

By learning through the historical training data set, the 21-component GMM has now been formulated where a unique conditional probability distribution will be generated for a given frequency observation. Figure 4-12 illustrates an example of the joint distribution (Figure 4-12 (a)) of the learnt frequency change observations given the potential values of inertia change. The conditional probability aggregated from the 21 Gaussians for a selected -0.2 Hz frequency variation is extracted in Figure 4-12 (b). It follows a non-Gaussian distribution within the investigation range, linearly combined and weighted from the 21 individual Gaussians.

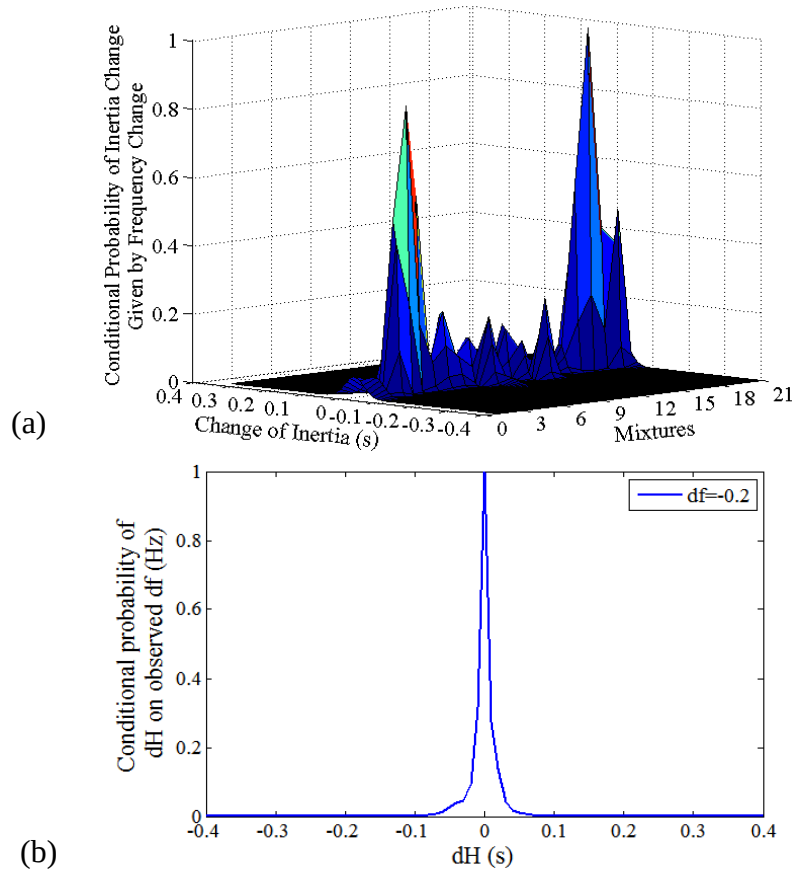

Figure 4-12: Probability distribution of inertia variations: (a) 3-D conditional distribution; (b) 2-D extracted conditional distribution on an observed frequency variation (df =−0.2 Hz)

As stated earlier, the final estimate will be taken from the samples drawn from such a conditional distribution while which one to select needs to be justified. Theoretically, the number of samples taken has an impact on estimation accuracy - the larger size will give more accurate indication whilst it takes a longer time to compute. In this case, a series of sample size from 200 to 2000 has been compared in steps of 200 where a size of 1000 slices was selected as a trade-off between accuracy and efficiency. This is due to the increment in the processing time where an extra 9% processing time will be added for every 200 more samples. The estimation accuracy (indicated by MSE) of each sample size is illustrated in Figure 4-13 where the results shown are averages through repeated 50 runs for each sample size. A local minimum of MSE is reached when the number of sampled slices equals to 1000. A significant reduction of around 5% up to 37% can be observed against other sample sizes within the investigated range.

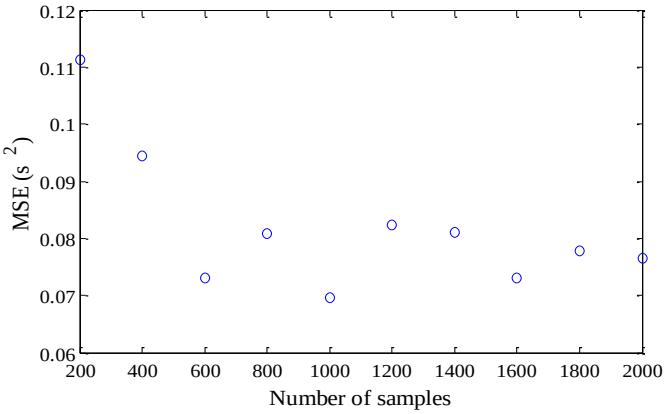

Figure 4-13: Impact of slice sampling size to the accuracy of estimation

As all the slices are randomly generated within the given range, such a large sample size creates extra difficulty in terms of which one should be selected from the total 1000 samples. To solve this problem, two sample selection strategies were thereby proposed for testing:

1) Averaging over the entire sample slices
2) Randomly select from the sample slices

Thus far, the procedure for training the GMM has been presented. The following section focuses on assessing the hypothesis that the estimation accuracy of formulated GMM can be improved if coupled with Markov Chain coupled with comparisons on the approaches of selecting from samples.

4.5 Off-line Performance Test

4.5.1 On-line calibration cycle

The estimates generated from the profiled joint distribution are the variations of inertia which is not the variable of interest in this research. To derive the inertia estimates, (4-7) will need to be used where the estimates of inertia variations are continuously aggregated to the last known system inertia constant on a 5-minute interval. This indirect deduction approach although approved through dependency analysis, inevitably introduces a certain degree of errors. Eventually, the accumulated

errors would deviate inertia estimates significantly from the actual inertia constants as shown in Figure 4-14. This, if unaware or unregulated, would leave advanced system functionalities that are designed to be activated by the real-time inertia estimates or taken the real-time inertia estimates as references in extremely high risk of malfunction.

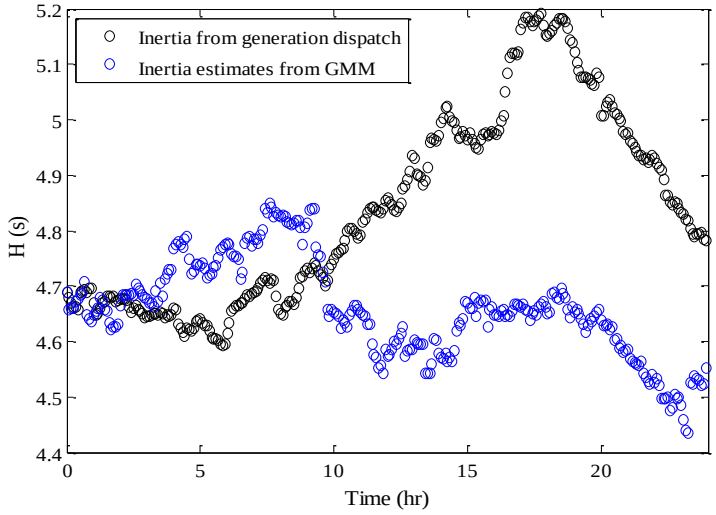

Figure 4-14: An example of accumulated errors

In order to cope with the anticipated induced errors, OCC is introduced. It refers to a certain period of time after which the estimated inertia constant will be corrected against an equivalent reference inertia constant derived from (2-3) using current generation dispatch data in the GB system. Such information is available every thirty minutes on [116] which gives the minimum OCC of half an hour.

The time scale of the estimation procedure is shown in Figure 4-15 with an example given for a half-hourly OCC. The left part presents the off-line model training and it is conducted with historical data on a 5-minute resolution. The right part shows the on-line operation sequence where the estimates are generated every 5 minutes using averaged real-time frequency measurements. The introduced OCC is identified in pink where the initial point of the following cycle is started with the calibrated value other than the estimated one.

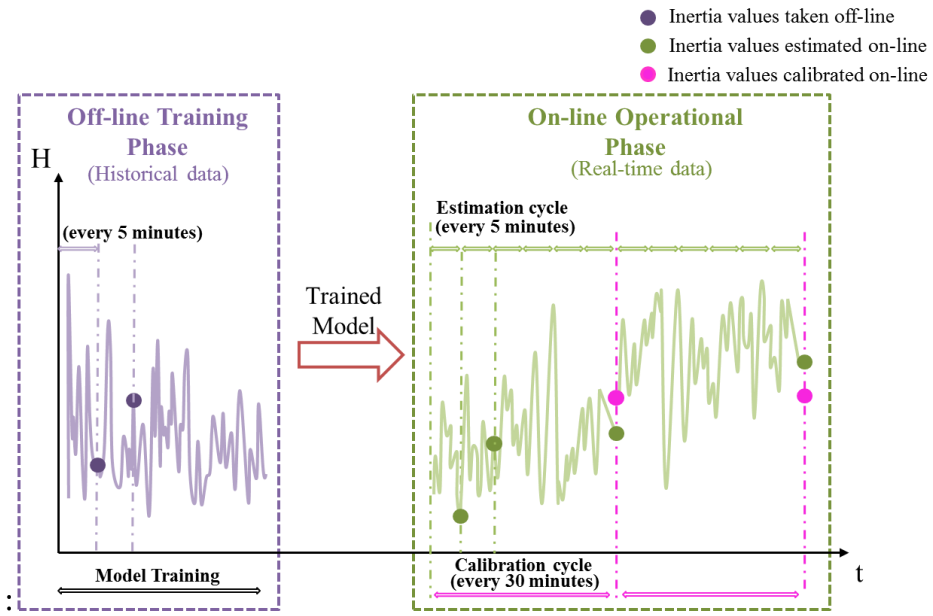

Figure 4-15: The graphic procedure of the model with a half-hourly OCC

4.5.2 Encoding with switching Markov dynamics

The proposed model should be able to cope with different system conditions and remain accurate when subjected to system disturbances. Although the flexibility can be provided by adjusting the mixing weights of individual Gaussian, its accuracy is suspended as it only captures the dependency between paired frequency and inertia variations which are formulated accordingly in a bivariate space. The potential time-series dependency between every two (or even more) consecutive frequency-inertia dependency pairs is hardly learnt and therefore cannot be revealed if it exists. Such a time spatial indication can be perceived by encoding with Markov Chain which captures the underlying temporal features and profiles current states from a single or multiple prior states. In this research work, the stepwise function in MATLAB Statistics Toolbox (Appendix D.3) was used to assess the past states in frequency measurements that are regressive to the current state.

Given the 28,800 historical training data set, the temporal analysis observed a strong regression between the current state and its prior 2^{nd}, 3^{rd}, 4^{th} and 5^{th} states (subscripted as $t_{k-2}, t_{k-3}, t_{k-4}, t_{k-5}$), returning a fourth-order SMGM. It should be noted that the full covariance matrix was no longer valid for formulating the fourth-

order SMGM. This could be caused by the extra sparseness and higher dimension that have been introduced when formulating the probability curve with additional temporal dependency of a greater variety of co-behaviours. Therefore, the diagonal type was applied instead as its simplicity and precision is second only to the full covariance matrix. Accordingly, the optimal component number in the mixture model has changed. As shown in Table 4-3, the newly formulated SMGM is exhibited by 13 Gaussians coupled with a regressive dependency articulated from its past four states. The zero-order SMGM refers to the original GMM without Markov dynamics.

Table 4-3: Comparisons among different forms of SMGM

	Zero-order SMGM	Fourth-order SMGM
No. of Gaussian Component	21	13
Covariance Matrix	Full	Diagonal
Dimensions	2	5
Skip Transition State	t_k	$t_k, t_{k-2}, t_{k-3}, t_{k-4}, t_{k-5}$

4.5.3 Assessing the performance of SMGMs by MSE

As previously discussed, performance of the SMGM should be compared off-line among the four combinations of sample selection approaches and the forms of SMGM for the most accurate on-line estimation model. The accuracy evaluated by MSEs individually is presented in Table 4-4 and Table 4-5 with the training data set being formulated and sampled into 1000 slices. A total of 500 runs have been taken for a generic result. The MSEs are given in the form of their maximum values among the 1000 samples and the mean values averaging through the 1000 samples over the 500 runs. The length of OCC from half an hour to 24 hours has also been assessed, taking into account the impact from daily demand that varies throughout the course of a day. The one which gives best performance will be applied for the final model.

Table 4-4 lists the maximum MSEs of the zero-order/fourth-order SMGM with regards to various lengths of OCC and the random/averaged sample selection

approach. For the growing length of the OCC, the increase in maximum MSEs are observed for all the four combinations.

Table 4-4: Max MSEs for different forms of SMGM

OCC (hours)	MSE for Zero-order SMGM (s^2)	MSE for Fourth-order SMGM (s^2)
Random Slice		
0.5	0.1372	0.1285
1	0.2103	0.1732
3	0.6291	0.6999
12	1.3640	1.1320
24	2.5148	2.1953
Averaged Slice		
0.5	0.0601	0.0588
1	0.0635	0.0604
3	0.3175	0.3072
12	0.4001	0.3652
24	0.6989	0.6810

Comparisons for the approach of sample selection and the order of SMGM are depicted in Figure 4-16 (a) and (b) respectively in the light of Table 4-4 and they are expressed in percentage of MSE reduction. In Figure 4-16 (a), the percentage value is calculated by dividing the difference between the maximum MSEs in the random approach (stated as 'R') and averaged approach (stated as 'A'). The resultant positive percentage values in (a) indicates that choosing randomly from the sliced samples gives a marginally higher error in contrast to the averaged slice values for both zero-order and fourth-order SMGMs. Such a percentage reduction experiences a minimum of 49.5% and 56.1% for the zero-order SMGM and fourth-order SMGM respectively when the length of OCC reaches three hours. Figure 4-16 (b) presents the influence of encoding the Markov Chain to the reduction of MSEs where the zero-order SMGM is stated by 'Z' and the fourth-order SMGM is stated by 'F'. The max MSEs entailed by the random sample selection approach are generally higher when employing the zero-order SMGM. However, the zero-order SMGM results in a higher MSE reduction with an OCC equal to three hours where negative value is observed. Stagnation in the percentage reduction of MSE is seen for both zero-order and fourth-order SMGMs for OCC longer than 12 hours.

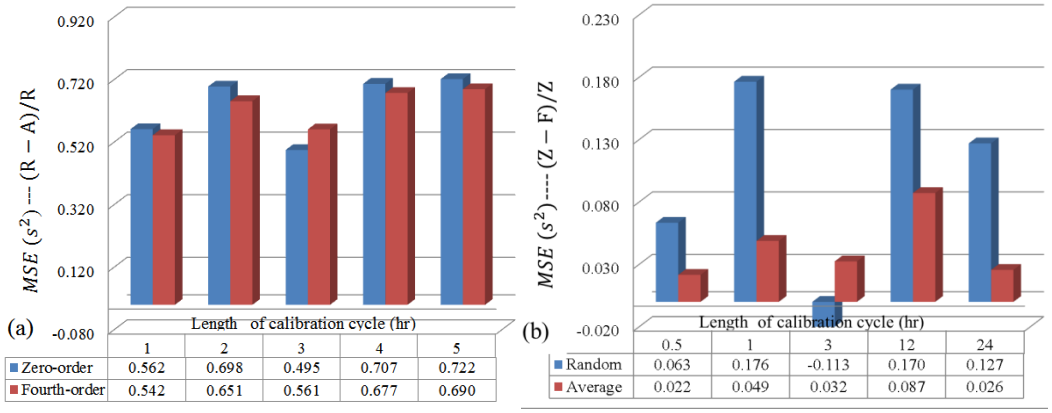

Figure 4-16: Max MSEs comparison for (a) sample selection approach, (b) order of SMGM.

Table 4-5 summarises the mean MSEs for the four combinations being calibrated at different resolutions. The same as the above analysis, the comparisons between sample selection approach and SMGM order are shown in Figure 4-17 but using the mean MSEs instead.

Table 4-5: Mean MSEs for different forms of SMGM

OCC (hours)	MSE for Zero-order SMGM (s^2)	MSE for Fourth-order SMGM (s^2)
Random Slice		
0.5	0.0632	0.0597
1	0.0823	0.0751
3	0.4143	0.3379
12	0.6493	0.5123
24	0.9857	0.9132
Averaged Slice		
0.5	0.0023	0.0020
1	0.0071	0.0059
3	0.0298	0.0243
12	0.0901	0.0779
24	0.1703	0.1600

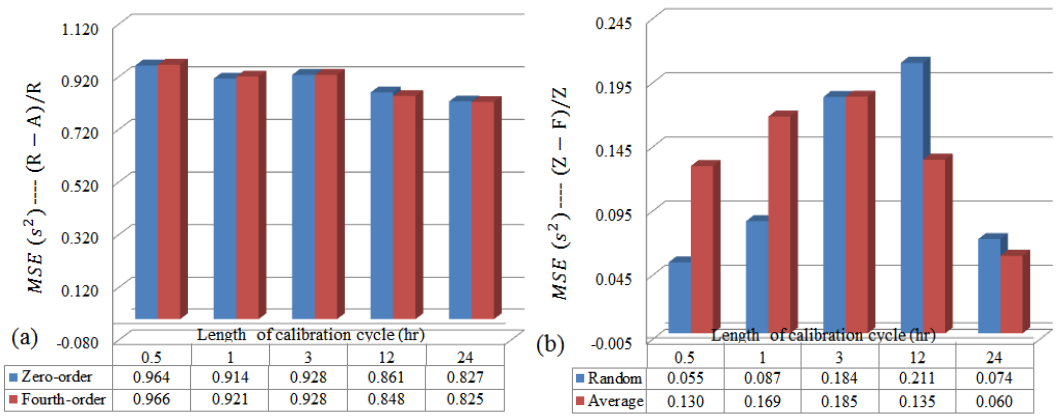

Figure 4-17: Mean MSEs comparison for (a) sample selection approach, (b) order of SMGM.

In Figure 4-17 (a), a small percentage drop (0.3%~0.8% difference) of the mean MSE is witnessed for both SMGMs if the averaged selection approach is applied. The improvement of averaged sample selection over an OCC of half an hour up to 24 hours decreases by approximately 14%. The advantages of applying fourth-order SMGM can also be confirmed from the increased estimation accuracy in Figure 4-17 (b), reflected from all the positive values by subtracting the mean MSEs of fourth-order SMGM from zero-order SMGM ones. However, the averaged selection approach has more accurate performance when OCC is lower than three hours while the random selection approach will claim the benefits for OCC longer than three hours.

From the above analysis, the following conclusions can be made:

- The averaged sample selection approach generally preserves a lower max MSE for both SMGMs. It reduces the max MSEs by an average of 63.7% for the zero-order SMGM and 62.4% for the fourth-order SMGM. It also decreases the mean MSEs by around 90% for both SMGMs.
- The introduction of Markov Chain improves the estimation accuracy. It reduces the max MSE by 8.5% for the random sample selection approach and 4.3% for the averaged sample selection approach. The mean MSEs also decrease by 12.2% for the random sample selection approach and 13.6% for the averaged sample selection approach.

- MSEs increase in line with the growing length of OCC, regardless of the sample selection approach and the order of SMGM. Such an increase has a critical point at three hours where the improvements can be seen in both the averaged sample selection approach and the fourth-order SMGM stagnated. Especially as shown in Table 4-5, the mean MSEs increase in an order of magnitude and the slope of MSE increment is steeper for shorter OCC while more gentle for longer OCC.

4.5.4 Assessing the performance of SMGMs by estimation trajectory

In addition to the comparisons made based on the MSEs, the estimation performance of the formulated SMGMs for the GB system will be presented in this section for a more comprehensive assessment.

Two examples are given in Figure 4-18 where the estimation trajectories are depicted throughout a randomly selected date outside of the training data set. In this case, the inertia constants on the 2nd of January 2013 are presented. There are three groups of data presented in each figure, namely the estimates generated from zero-order SMGM, fourth-order SMGM and the corresponding actual system inertia constants referenced from generation dispatch. Comparisons are also made for the sample selection approach and the length of OCC.

The estimates in Figure 4-18 (a) and (b) were calibrated on a half-hourly basis while a three-hour OCC was applied to estimates in Figure 4-18 (c) and (d) which has been seen as a critical point in Figure 4-16 and Figure 4-17. With the increase in OCC, the estimates are seen scattered further away from the reference values, which on the other hand, indicates that the errors are increased. Therefore, the visualisation of estimation performance again verifies that half an hour is the most desirable calibration resolution to maintain sensitive and accurate inertia estimation.

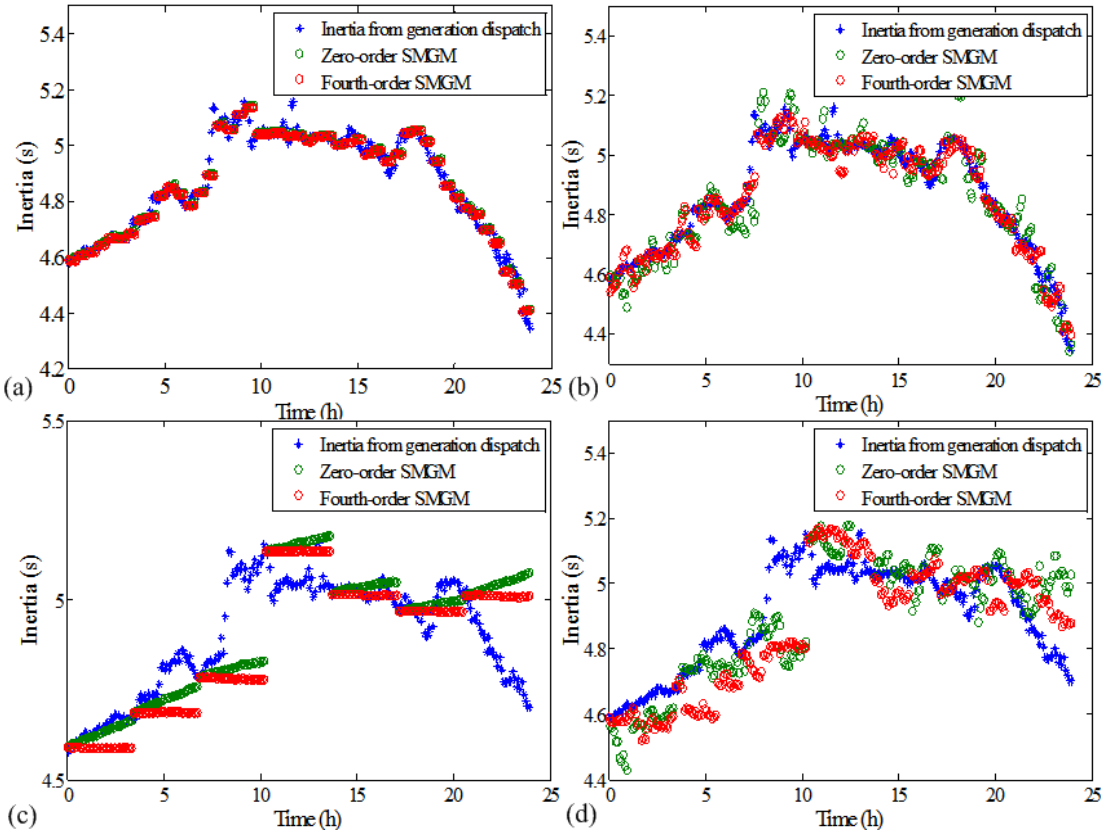

Figure 4-18: Performance of SMGM algorithm on the 2nd of January 2013 with (a) half-hourly OCC with averaged samples, (b) half-hourly OCC with random samples, (c) three-hour OCC with averaged samples, (d) three-hour OCC with random samples.

The estimates in Figure 4-18 (a) and (c) were taken from the average sample selection approach while the ones shown in Figure 4-18 (b) and (d) were randomly selected from the 1000 samples. The impact of selection approach cannot be clearly observed for a half-hourly OCC as they all oscillate closely around the actual inertia constants. However, with an OCC of three hours, the performances using averaged slice sample could fail to trace the features of inertia variation as a result of the over-smoothing of individual variations, given the estimates lined up within each OCC over the course of one day. Therefore, further investigation would be required, for example defining additional comparison metrics, to make a better judgement about the estimation accuracy for a longer OCC.

Examples of estimation performance using two different OCCs are extracted from Figure 4-18 and illustrated in Figure 4-19. A greater feasibility in tracking system

inertia variations and the changing trend in the system can be observed, especially for a half-hourly OCC as it is of less estimation errors. This can also be verified statistically with a MSE of 0.07 s^2 for a half-hourly OCC and a 0.4 s^2 for a three-hour OCC for the presented day. Moreover, it shows that the fourth-order SMGM preserves a relatively higher consistency with the reference curve.

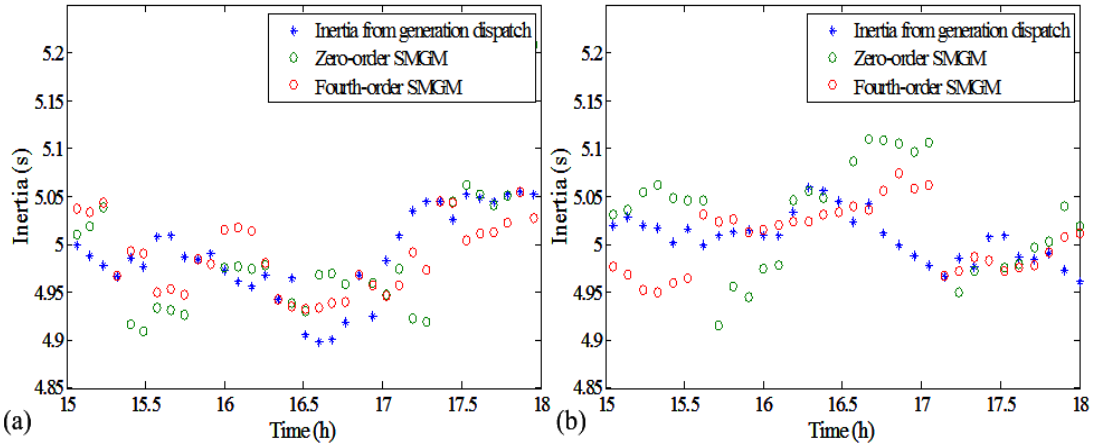

Figure 4-19: Examples of enlarged figure of SMGM performance from (a) Figure 4-18 (b), (b) Figure 4-18 (d).

Conducted with the 28,800 randomly selected historical data set, the introduction of mixed-order Markov Chain contributes to express the underlying frequency-inertia dependency in a greater temporal detail and has been verified effective to reduce the errors of inertia estimation than GMM in this research. Following the criteria that the model of minimum MSE gives the most representative estimation performance in line with the estimation performance, the fourth-order SMGM coupled with average sample selection approach and a half-hourly OCC is therefore concluded as the most accurate real-time inertia estimation model for the GB system.

4.6 Validating the performance of SMGM on Real-time Inertia Estimation

In addition to continuous monitoring the system inertia level, the estimated inertia constant can also act as a potential enabler or participant to achieve some designed

system functionalities, such as advanced control or adaptive protection. Therefore, the accuracy of delivering such pro-active actions based on estimated inertia constants plays an important role to mitigate the negative impact from system anomalies, where, under no circumstances, would provide invalid estimates.

To verify the validity of the proposed methodology, the real-time performance of the fourth-order SMGM formulated for the GB power system will be evaluated against three recorded daily operation data, including two historical events occurred in the GB system. The data sets used for validation are all excluded from the model training data set. The reliability and robustness of the proposed model will also be tested for its feasibility of providing accurate inertia estimates during loss of frequency observations and in the presence of system noise.

4.6.1 Estimating system inertia using historical data during normal system operation

Figure 4-20 shows the inertia estimates of the GB system on the 20th of May 2013 and the corresponding daily system frequency performance using the proposed SMGMs. This is to test the performance of the SMGMs against normal system operation which was recorded but not included in the historical training data set.

Both of the SMGMs were assessed adopting the average sample selection approach with a half-hourly OCC. Given no severe disturbance but observed normal frequency oscillations due to dynamic system operation, 95% of the maximum MSEs were limited to within 0.03 s^2 for both SMGMs throughout the day with the fourth-order SMGM further lower the maximum MSE by 0.01 s^2. The estimated inertia constants center around the referenced inertia constants derived from generation dispatch within a range of ±0.17 s. In contrast, such a variation will range from -0.32 s to +0.32 s (a maximum MSE of 0.1 s^2) for a three-hour OCC which is nearly twice higher than the model with a half-hourly OCC. Therefore, the fourth-order SMGM with a half-hourly OCC as stated earlier, gives a more accurate estimation performance.

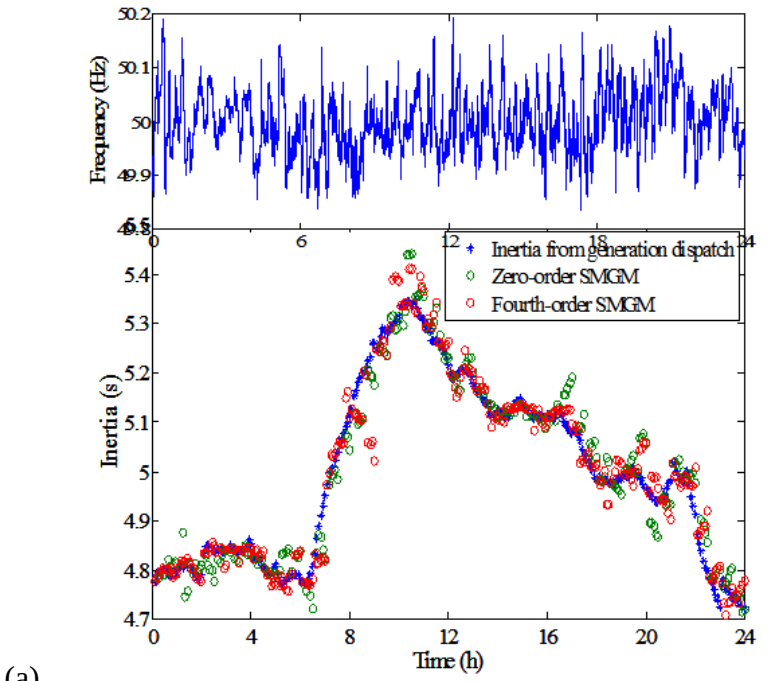

(a)

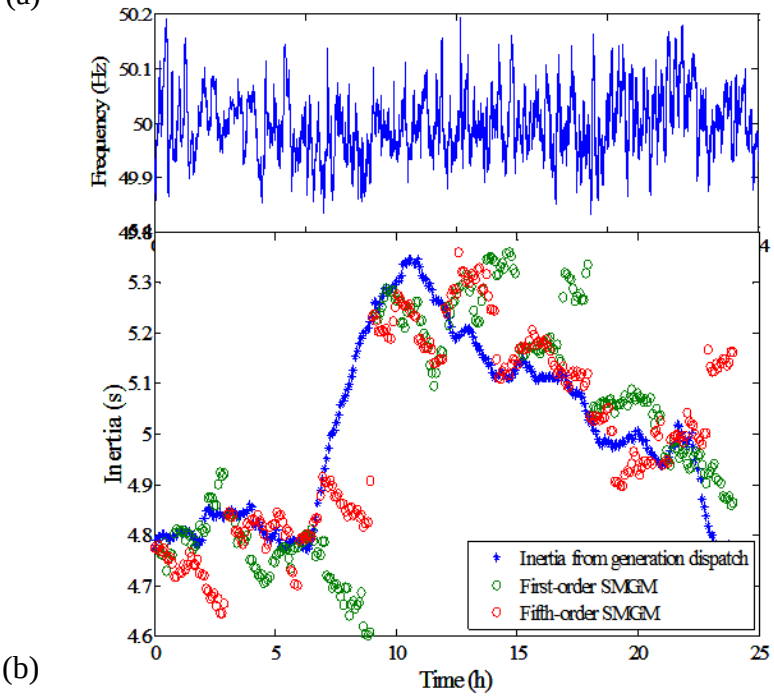

(b)

Figure 4-20: Validation using data on the 20th of May 2013 (a) half-hourly OCC, (b) three-hour OCC.

The fact that the MSEs of the SMGM estimating system inertia outside of the training data set still stay within the ranges identified in Table 4-5 verifies that the proposed model is feasible to accurately estimate system inertia during normal system operation.

4.6.2 Estimating pre-event system inertia for recorded system disturbance

The data for this historical event used relates to the loss of the UK/France interconnector on the 30th of September 2012 at around 14:03 UTC [147]. Upon the occurrence of the approximate 695 MW interconnector loss, the total generation in the GB system was around 33,000 MW and an average of 0.113 Hz/s frequency change was observed across the GB system.

The system inertia level should theoretically stay the same prior to and just after the event, owing to the fact that it was a loss of HVDC link (which has no inertia). Therefore, the inertia constant estimated pre-disturbance using the proposed model can be compared with the inertia constant calculated from the Swing Equation. As shown in the zoom-in window in Figure 4-21, the inertia estimate generated from the zero-order SMGM is 4.43 s and 4.44 s from the fourth-order SMGM. The transient system data during the loss, according to (2-1), gives a system inertia of 4.66 s. These assign to differences of 5.0% and 4.7% respectively to the value derived from Swing Equation which indicates an accurate estimation in system transient state.

The errors in inertia constant (0.23 s for zero-order SMGM and 0.22 s for fourth-order SMGM) corresponds to MSEs of 0.054 s^2 and 0.048 s^2. Since the errors of both SMGMs stay within the mean MSE in Table 4-5, which gives the generic MSE values over a large sample size, the proposed model is therefore verified to be capable of estimating system inertia prior to a system event and thus could provide effective reference data for designed proactive control and protection functions. Moreover, the fourth-order SMGM with a half-hourly OCC gives a more accurate estimation performance.

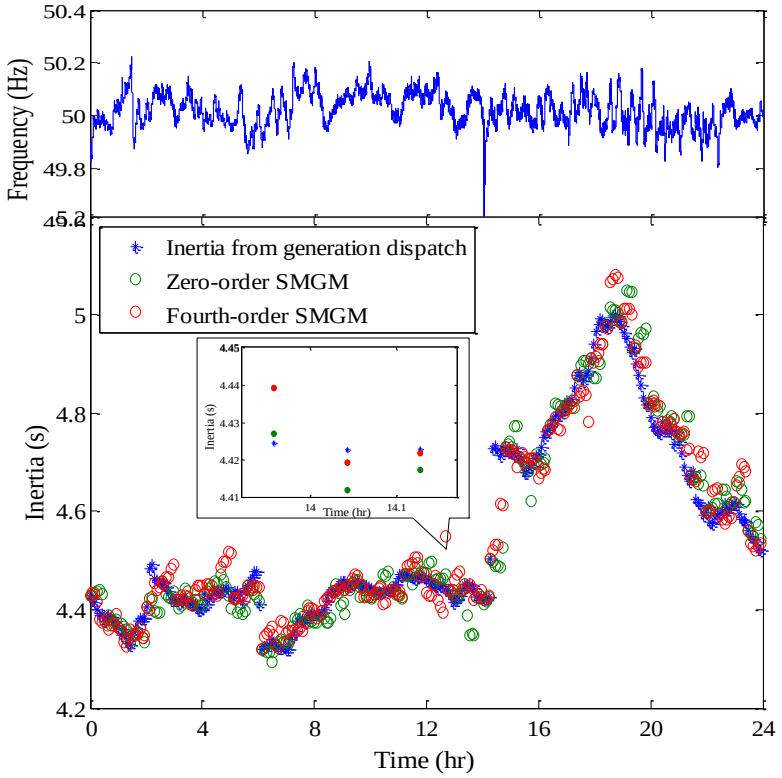

Figure 4-21: Inertia estimation for the loss of the UK/France interconnector on the 30th of September 2012

4.6.3 Estimating post-event system inertia for recorded system disturbance

The second historical event occurred on the 19th of April 2011 where a large generation plant around 1 GW in the north was lost at around 6:36 UTC. The total system generation prior to the loss was 39,286 MW and the averaged RoCoF values from PMU recordings is -0.11 Hz/s.

Figure 4-22 shows the estimation of system inertia with a zoom-in figure after the loss. The estimates generated from zero-order and fourth-order SMGMs just after the disturbance are 6.02 s and 6.06 s respectively, given by the MSEs of 0.078 s^2 and 0.058 s^2. Both of the SMGMs with a half-hourly OCC limit 90% of the maximum MSEs within 0.05 s^2. However, compared with the mean MSEs listed in Table 4-5, the fourth-order SMGM shows a higher accuracy as it stays below the 0.0659

average value for the half-hourly OCC while the zero-order SMGM is beyond its average. In contrast to a system inertia of 6.3 s derived from the Swing Equation in (2-1), a 4.4%/3.8% lower value is estimated using SMGM.

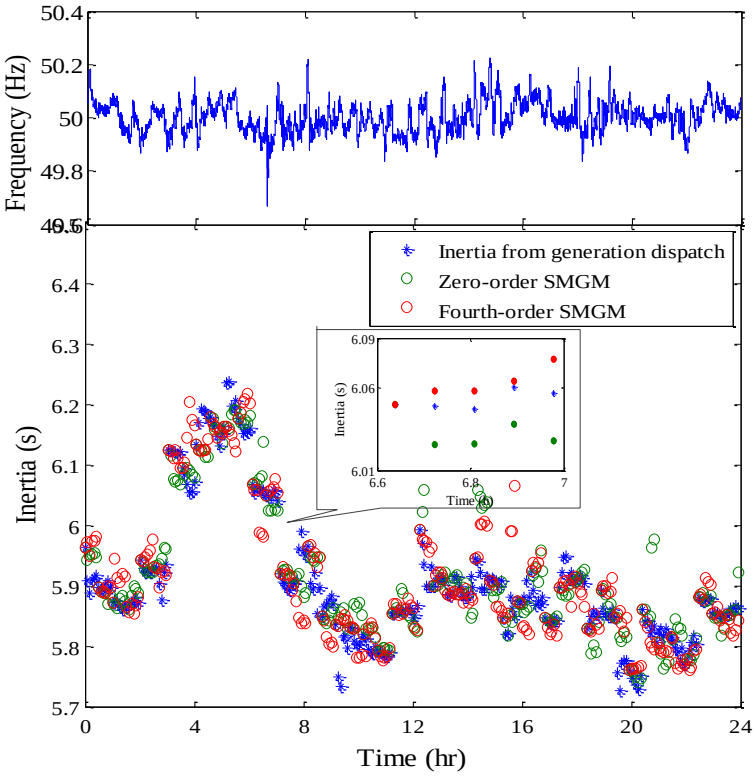

Figure 4-22: Validation using the data on the 19th of April 2011

As such, it can be concluded that the proposed SMGM is able to more accurately estimate system inertia post-disturbance. The fourth-order SMGM with a half-hourly OCC gives a more accurate estimation performance for the system inertia drop due to the loss of synchronous generation plant.

4.7 Robustness of SMGM against loss of data infeed

Considering the feasibility of implementing the SMGM into an actual power system, the proposed algorithm, taking system frequency measurements as input, should be able to resist any loss of frequency observations, at least for a period of time. In practice, such loss of observation could occur anywhere and anytime as a result of

failure in software communication or hardware, such as the frequency measurement devices.

Assessment of the suitable fail-safe strategy has been carried out for the loss of frequency observation from one estimation cycle (5 minutes) up to 60 cycles (5 hours) following the rules:

- A frequency change value of zero shall be input into SMGM
- A constant frequency change equals to the last valid measurement shall be input into SMGM

on detection of the loss of frequency observations until the successful delivery of the next valid frequency measurement.

An example is given in Figure 4-23 where the simulated data loss was taken on the 20th of May 2013 and assumed to occur at 1:00 UTC. The two fail-safe strategies were applied independently with the significance of the impact quantified by the most likely MSE (this refers to the MSE value of the highest probability that generated from the 1000 sample slices).

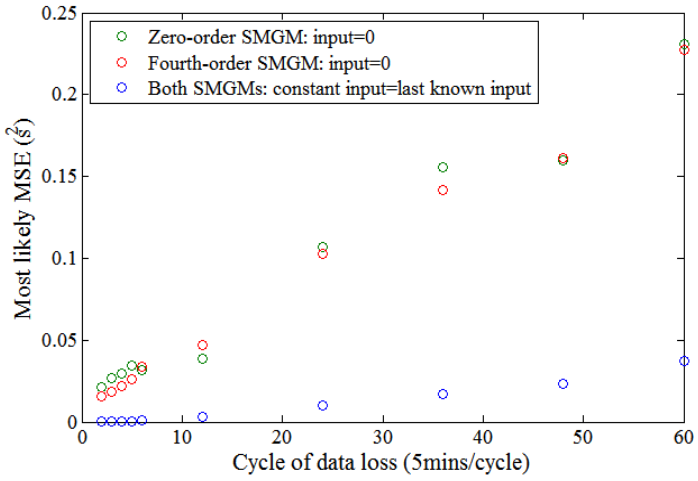

Figure 4-23: Most likely MSEs for various durations of data loss on May 20th 2013 applying different fail-safe strategies

An almost linear increase of MSE is observed for both SMGMs with the increasing duration of data loss if inputting zero as frequency measurements into SMGM upon the loss. In contrast, a slower exponential increase is seen for a constant same as last valid measurement where the MSE is limited within 0.05 s^2 which in general gives a

more accurate estimation. Therefore, the fail-safe plan for the real-time deployment of the proposed SMGM should maintain the last valid measurement as a constant input into SMGM until the successful delivery of the next valid frequency measurement. Moreover, the proposed model is considered robust against loss of frequency measurements up to two hours at which point an error of 10% for the actual system inertia level would be obtained. However, greater differences could be witnessed for the relatively large inertia variations in future networks, therefore these two fail-safe strategies may need to be re-examined.

4.8 Reliability of SMGM against system noise

Power system noise is defined as undesirable electrical signals that distort or interfere with an original (or desired) signal [148]. Due to the existence of such noise (e.g. switching of electronic elements, system harmonics), measured signals are inevitably distorted, indicating a degradation on the accuracy of the measurements.

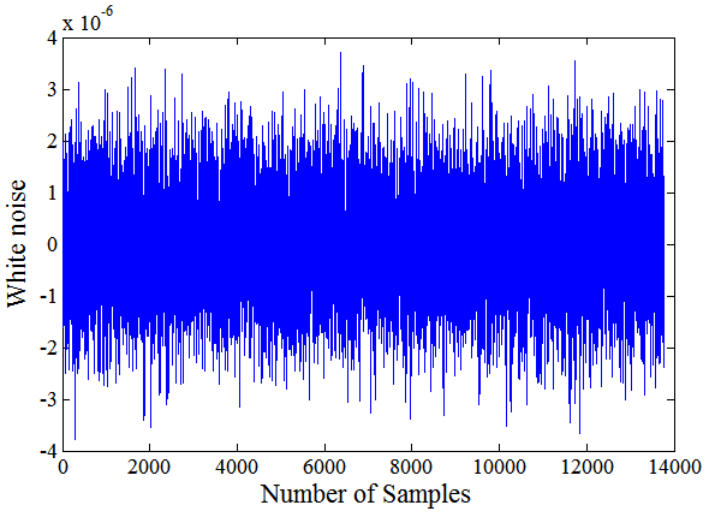

Figure 4-24: White noise injected into the measurements

This section, therefore, is devoted to verifying the reliability of the proposed SMGM in facing undesirable noise in the system which commonly exists in the original frequency measurement instants. A Gaussian white noise, as demonstrated in Figure 4-24, was added to the frequency measurements on the 20th of May 2013 to simulate the presence of system noise. The noise was generated in a power of -6 as the order

of magnitude of frequency variations (on 20 ms resolution) is around -5, giving a signal-to-noise ratio (SNR) of around 10 dB (the worst case for a frequency shift channel [149]).

Table 4-6: 95% confidence interval (upper boundary) of MSEs

MSE (s^2) \ OCC (hours)	0.5	1	3	24
Zero-order SMGM	0.0047	0.010	0.033	0.31
Fourth-order SMGM	0.0045	0.0096	0.031	0.27
Zero-order SMGM + noise	0.0058	0.011	0.035	0.35
Fourth-order SMGM + noise	0.0050	0.010	0.032	0.28
Increase for the zero-order SMGM (%)	23	10	6	13
Increase for the fourth-order SMGM (%)	11	4	3	4

The 95% confident intervals generated for the MSEs (calculating from the 1000 sampled slices) with and without the Gaussian white noise are listed in Table 4-6. Comparing the boundary value of the interval, an increment in MSEs is generally observed for the ones with noise injected. Such an increment reaches the maximum for both of the SMGMs with a half-hourly OCC while experiencing local minimum for a three-hour OCC. For the recommended fourth-order SMGM with a half-hourly OCC, its MSE grows by 11% in the presence of system noise. However, the resulted MSE of 0.005 s^2, as converted into the value of inertia variation, gives a magnitude of 0.07 s which only contributes to 2.3% of the error on the basis of a 3 s system inertia. Therefore, the fourth-order SMGM is still capable of providing reasonably accurate inertia estimates in the presence of system noise with a SNR ratio of 10.

4.9 Discussion on the Accuracy of SMGM

The previous section demonstrated that the hidden dependency between system inertia and frequency can be expressed by the proposed continuous real-time inertia estimation model and such has been validated through implementing the model on the GB system. One of the major advantages of this algorithm is its independence of system transient disturbance for the inertia estimation. However, there are still

factors that need to be addressed with regards to the existing errors during the estimation process and its practical implementation in future networks.

4.9.1 Selection of the algorithm parameter values

The type of conditional distribution covariance matrix, the number of components in the Gaussian mixture and the order of Markov dynamics are three parameters that largely affect the representability of the statistical model built through off-line training. In this research, a 21-component GMM with full covariance matrix was formulated at the beginning to express the dependency between frequency and inertia variations in the GB system. However, the number of GMM has been reduced to 13 with the encoding of the Markov Chains, giving a 6.4% reduction in the max MSEs and 12.9% in the mean MSEs. Although complexity of the model increases in line with the introduction of the Markov Chains, the estimation accuracy is also increased. In addition, the covariance matrix has been changed to the diagonal type, attributing to the fact that the full type has been verified no longer able to accommodate the extra complexity introduced by such a three-dimensional distribution. Due to the fact that the selection of these three parameter values is processed off-line, there is no need to concern the extra time consumed on such training as introduced by the increasing order of Markov Chains.

However, the consecutive time on the basis of an accurate performance will need to be carefully considered when selecting the parameter values which are involved in the real-time estimation. Such parameters include the sampler size in the slice sampling process, the approach to select estimates from samples. The number of sampled slices and selection of samples have great impact on obtaining an accurate estimate. A sample size of 1000 was selected through comparisons made on the MSE for the sample sizes from 200 to 2000. Significant reductions in MSE, ranging from 5% to 37%, were observed for a sample size of 1000 while consuming reasonable time to sample. The averaging approach in most cases produces smaller estimation error and would, therefore, be a preferred method to use in practice, especially with shorter calibration periods such as 30 minutes. However, the performance of applying the average selection approach does not preserve satisfactory result for

longer calibration periods and further investigation would be required, for example defining additional comparison metrics, to make a better judgement about the estimation accuracy.

An almost linear increase in MSE has been seen for the growing length of OCC. This attributes to the designated real-time inertia calculation equation (defined as (4-7) in the light of the unveiled frequency-inertia dependency) where estimation errors are accumulated for every subsequent computation until the next calibration. A critical point has been identified at two hours above which the mean MSE increases in an order of magnitude. In practical implementation, the half-hourly OCC is recommended due to its lowest MSE and the data for the calibration is also available on a minimum of half-hourly basis. However, a training data set of finer resolution or the introduction of extra system variable (e.g. rate of change of demand) could all assist to reduce the reliance on OCC to improve estimation accuracy.

The generic nature of SMGM makes it readily applicable to various power systems for which it can be trained or current system with a new window of recorded data to be re-trained to cope with any changes or upgrades (e.g. changes that emerge in generation mix and inverter based renewable penetration). The employment of correlation, EM, BIC and stepwise regression as described in this thesis provides robust justifications for identifying the methods' parameters, such as the optimal numbers of Gaussian components and Markov orders. Widespread implementation of this approach is thus supported, whereby the SMGM is trained off-line and then utilised on-line through exposure to frequency measurements and regular calibration with dispatch data. Moreover, the accuracy and time consumption should be defined in line with the intended system operators in keeping with the specifics of the inertia estimation's application. For example, the allowed error for monitoring, control or protection applications would likely be different from each other.

4.9.2 Sources of errors in the proposed model

The first error is inherent in the real-time inertia calculation (4-7). This equation is generated from the dependency analysis where the current system inertia is derived

from summing the inertia variation estimates (given by frequency observations) to a previous known system inertia constant. Errors are inevitably produced and accumulated every time the estimate is drawn from the conditional distribution. As the concept of OCC is introduced, magnitude of such error depends on the length of designed OCC where the increasing OCC indicates a longer time for error accumulation thereby resulting larger errors.

The second error could occur as an under/over-estimation of real system inertia. This is due to the fact that system inertia constants for model training and as reference for model performance assessment, in this research, were derived both from generation dispatch data on ELEXON using typical values for each generation fuel type. The published data reflects only large generation plants in the system and mainly on transmission level. Therefore, there are uncertainties lying under the contribution from small generators, very small DGs and motor loads which are connected at distribution level or the synthetic inertia injected from the control system which cannot be directly monitored over time. Features of these generation units are missing in the model learning as there is no such inertia data fed into the training data set but included in the frequency observations. As a result, the corresponding real-time estimates generated from the trained model cannot cover inertia variations contributed from them. Moreover, the inertia constants taken for each generation type were assumed with their typical values which are varying from one to another even with the same generation fuel type in the real system. However, such an accuracy issue could be mitigated with training data set of a higher and reachable time resolution or adding other statistical models formulated to represent these mismatch. More detailed system information, including the estimated proportion of demand served by generation units at the distribution level, if can be formulated as statistical model, could also contribute to the reduction of errors. However, this will not be investigated in this research but will be included in future work.

The third error could be the over-sized sampling period where both the training data and the on-line estimation are limited to a 5-minute resolution. This could miss the inertia variation feature that interrelates with system frequency variation during the

interval that leads to estimation error. A finer resolution of less than 5 minutes, if achievable, can be used to compare and address such a potential error.

In addition, the criteria applied to populate SMGM with optimal parameter values are based on the minimum error when continuously fitting observations with candidate models. Inherent in such performance assessment algorithms, is the imperfection of not fully expressing the entire data set but key features.

4.9.3 Effectiveness of frequency observations

The use of frequency data collected from PMU recordings in this work demonstrates the value of such frequency data to the application of the proposed continuous real-time inertia estimation model, and thus their value in inferring system conditions. The form of frequency data associated with the number and locations of PMUs have at the same time been investigated.

While the approach relies upon three PMUs and the averages over the three frequency measurements, it is recognised that (i) single sources of data may present reliability concerns, and (ii) the location of a single measurement point on the system will dictate the nature of the variations (and swings) of the frequency observed. A table of MSE with only frequency data at University of Strathclyde is provided in Table 4-7. In comparison with the results generated from the averaged frequency data across the three accessible locations in Table 4-4 and Table 4-5, a general reduction of 4% can be seen for both max and averaged MSE. It evidences the fact that using data from multiple PMUs can effectively reduce the estimation error. Consequently this work makes use of one frequency value which has been averaged from three measurements, giving better reflections of true system-level conditions.

Due to the fact that system frequency variations are strongly correlated during normal operating conditions but coupled with local variations, the impact of a greater number of PMUs or the exact locations of each PMU would affect the estimation accuracy. However, the frequency observations available in this research are from

University of Strathclyde, University of Manchester and Imperial College London which firstly considers geographical distribution; secondly are representative for diverse local generation and load structures: more generation and particularly from renewable resources than the demand (i.e. University of Strathclyde), more synchronous units (i.e. University of Manchester), higher demand than the generation (i.e. Imperial College London). Therefore, the averages are considered effective to smooth out the local impacts and provide valid frequency observations to reflect system level inertia variations.

Table 4-7: Max and averaged MSEs for different forms of SMGM with only frequency data at University of Strathclyde

OCC (hours)	MSE for Zero-order SMGM (s^2)		MSE for Fourth-order SMGM (s^2)	
Random Slice				
	Max	Averaged	Max	Averaged
0.5	0.1399	0.0679	0.1386	0.0659
1	0.2241	0.0854	0.1867	0.0811
3	0.6404	0.4212	0.701	0.3479
12	1.3659	0.6752	1.186	0.5418
24	2.6186	0.9931	2.217	0.9534
Averaged Slice				
	Max	Averaged	Max	Averaged
0.5	0.0609	0.0025	0.0631	0.0022
1	0.0674	0.0076	0.0652	0.0065
3	0.3428	0.0318	0.3090	0.0266
12	0.4017	0.0919	0.3753	0.0808
24	0.7078	0.1712	0.6870	0.1664

Although this work is not dependent on the data being sourced from PMUs but more as a valid means of obtaining the frequency data, they do provide a convenient and promising source of system frequency data from laboratories or utility data networks. The practicalities of using PMUs to source the frequency measurements for implementing the proposed continuous real-time inertia estimation model in future networks can be supported by learning from projects such as EFCC [78] and VISOR [79]. It is recognised that frequency measurements might be equally-well sourced elsewhere.

4.10 The Role of the proposed Continuous Real-time Inertia Estimation Model in Future System

Future system, which will not only experience the gradual reduction of system inertia, but also more frequent and magnified inertia variations over time, could benefit considerably if the system inertia estimation can be realised in real time. The potential fields it can contribute to include:

- System health diagnosis/prognostics [150]
- Proactive adaption of protection settings [151]
- Synthetic inertia control and management [152]
- Ancillary reserve planning [153]

The proposed continuous real-time inertia estimation model could assist in identifying and quantifying system stability issues and risks in real time based on the awareness of current system inertia. A relatively low inertia constant indicates an increase in system dynamic oscillation when a high percentage of renewable resources is integrated in the system and vice versa. The most cost-benefit amount of renewable output with which the system stability can be secured would also be planned for real-time demand referencing from the inertia estimates.

The real-time inertia estimates generated from the proposed continuous real-time inertia estimation model can provide reference inputs to activate designated functionalities prior to any disturbance taking place, such as changing the setting of protection relays or the control and management strategy. From the system conditions identified, such proactive actions can be carried on from frequency behaviour in response to hypothetical disturbances to the amount of synthetic inertia that are necessitated to maintain desired inertial frequency. With system parameters fine tuned to prevailing system inertia conditions, deterioration on its operational performance can be mitigated in the presence of any oncoming disturbance. Taking adaptive protection as an example (which will be revised in the next chapter), protection settings (for those operated by or affected by inertia level) are de-

sensitised for a falling system inertia to de-risk potential protection mal-operation, thereby, maintaining system stability.

In addition to the enhancement on system stability, the continuous real-time inertia estimation model can also facilitate to achieve operational economics through, for example, more informed ancillary reserve planning using knowledge of prevailing system inertia constant and stability margins. Financial incentives and system optimisation, such as electricity price, the cost to schedule balancing mechanisms, can be applied for a more economic approach.

As a promising enabler of some proactive actions, a supervisory system should be introduced when implementing the continuous real-time inertia estimation model into future systems. It can continuously monitor the performance (suitability and accuracy) of the model during its commissioning. Re-training of the model is necessitated in situations where the trained model can no longer cope with the changes entailed by system development (reflected as, for example, a continuous large estimation error beyond the designated acceptable constraints). An example is given in [154] where ABB COM600 computer is implemented in an advanced substation automation system taking the supervisor role.

4.11 Chapter Summary

In response to the discussions on issues brought by system inertia reduction and the necessity of providing real-time inertia information to mitigate their impact in the previous chapter, this chapter presented a novel statistical model to realise real-time inertia estimation. The proposed model is formulated as GMM with temporal dependence encoded as a Markov Chains. It operates through optimising the joint likelihood of the underlying frequency-inertia dependency to formulate a multivariate distribution, where samples are drawn accordingly for given real-time frequency observations. By assuming multiple underlying operating regimes, the proposed continuous real-time inertia estimation model is able to accommodate the complex stochastic and dependency structure inherent in the system. Unlike the

methods using Swing Equation or other existing methodologies, this approach is capable of extracting and learning the hidden variables/states that exist but cannot be directly measured in dynamic system operations, thereby no longer relying on the occurrence of system disturbances to estimate inertia.

This chapter reviewed existing practices of inertia estimation which depend on the occurrence of system disturbances that can not achieve continuous estimation of system inertia in real time. Challenges to establish the designed frequency-inertia dependency were analysed from the non-stationary and non-linear system dynamics to the feasibility of using model hypothesis to extract and express these uncertainties. With the analysis narrowed down to the statistical approach, SMGM was hypothesized as an effective and explicit expression to achieve this goal. Relevant terminologies and statistical methods for data analysis were reviewed for further incorporation to formulate the SMGM.

Feasibility and reliability of SMGM on real-time inertia estimation have been verified throughout its implementing on the GB system and a fourth-order SMGM was finalised as the one best profiling frequency-inertia dependency in the GB system. A two-phase algorithm was designed to formulate the model, including off-line model training and on-line estimation. A series of rigid statistical analysis criteria, including EM, BIC and MSE, were applied to extract features hidden in the multivariate distribution and populate the model with the most representative parameter values. Factors, which affect the accuracy of estimation, were discussed explicitly from the selection of model parameter values and the design/configuration of the algorithm respectively.

The step-by-step training and performance improvement procedure shows that a fourth-order SMGM coupled with average sample selection and a half-hourly OCC is the best mixture model to profile the frequency-inertia dependency in the GB system. A significant reduction of around 5% to 37% in MSE was firstly observed when sampling with 1000 slices in the range of 200 to 2000. The mean MSE was brought further down by 12.9% (6.4% for the max MSE) by introducing Markov dynamics on originated GMM where the temporal dependency between each investigated

frequency-inertia pair was articulated. The average sample selection approach produces lower MSE than another tested randomly selection approach. However, as the ability of tracking the inertia variation trend is not evident over a long-term estimation, further investigation would be required, for example defining additional comparison metrics, to make a better judgement about the estimation accuracy. Moreover, OCC was introduced to reduce the error inherent in the defined real-time inertia calculation equation and the induced error aggregated for each estimate. With the increase of the OCC, the MSE maintained an almost linear growth. Therefore, half an hour was selected as attributing to the highest accuracy. However, future research is required to reduce the reliance on OCC to improve estimation accuracy for more practical application. Comparison was also made between a single frequency measurement and multiple where a 4% lower MSE was seen for the frequency input taken as the average over multiple frequency measurements.

The proposed model has been validated against historical events from which its capability of providing credible estimates pre/post-disturbance were both verified. Moreover, the model has been proved robust through observation interruptions of up to a period of two hours if remaining the same frequency input as the last valid measurement. The practicability of SMGM to cope with the existing noise in actual system has also been examined where 95% of MSEs would stay within 0.01 s^2 for a SNR ratio of 10.

Analysis on the model itself has provided evidence that a finer resolution and comprehensive system dynamic information are beneficial to provide more accurate estimation in future. The formulated model can be re-trained to capture any upgrades in the applied system or for a new system with a new window of recorded data. Integrating this within an overarching application management system would maintain estimation accuracy over longer term use in the practical implementation.

5. A Zonal Adaptive Scheme to Improve the Performance of RoCoF-based LoM Protection in Future System

5.1 Chapter Overview

Inherent in adaptive protection scheme is the flexibility that is required by future protection system. This is to accommodate more frequent and magnified system dynamics that are increasingly exhibited from generation mix. Following on the demonstration of protection mal-operation issues in Chapter 3.6.1, the hypothesis of applying adaptive solution will be examined in this chapter using the RoCoF-based DG anti-islanding protection.

Firstly, this chapter states the need to implement zonal adaptive settings in future power networks. To facilitate the integration of the adaptive functionality on conventional protection schemes, a three-layer architecture has been designed based on previous work. Functionalities of each layer are presented in details where the proposed continuous real-time inertia estimation model and the zonal adaptive protection setting algorithm should be allocated respectively.

Verification of the hypothesis has been taken through assessing the stability and sensitivity of the DG anti-islanding protection scheme with/without adaptive feature. The stability of a proposed zonal adaptive protection scheme (Z-APS) is tested against loss of large infeed scenarios and the presence of system faults. The non-detection risk in real LoM events is evaluated to assess the sensitivity of the proposed zonal adaptive DG anti-islanding protection scheme.

Discussions are presented at the end including how and when to adapt the protection settings, the configuration of the settings, the benefits of being zonal adaptive, the

fail-safe strategy for any communication failure as well as the challenges of its wide implementation.

The main contributions of this chapter are:

- Proposal of a zonal adaptive DG anti-islanding protection scheme which incorporates the proposed continuous real-time inertia estimation model in Chapter 4.
- Verification of the improved protection stability and sensitivity by incorporating the proposed Z-APS on conventional RoCoF-based DG anti-islanding protection against future low inertia scenarios.
- Assessment of the zonal risk of non-detection.

5.2 Driving towards Zonal Adaptive Settings

As stated in Chapter 2.4, the GB power system is moving towards a renewable-dominated future. In the face of these system changes, protection systems, whether during planned reinforcement or unplanned outages, should always follow the operational criteria of being stable, sensitive, coordinated and discriminative. However, the added strength from more flexible system operation has pushed the present-day power system to operate closer to its operational limits where the challenges to achieve desired performance of protection schemes have been incurred.

Chapter 3.6.1 had identified protection mal-operation issues for the conventional RoCoF-based DG anti-islanding protection system and UFLS scheme in a low inertia system. Their protection performances were jeopardised by the magnified frequency excursions that occurred under high renewable penetration during normal system operation. Conventional protection schemes are of fixed settings that are unable to actively speed up or delay the operation of protection relays to effectively avoid such deterioration. Therefore, a more flexible protection system that operates in the light of prevailing system conditions is more desirable to maintain a reliable power supply.

Moreover, protection mis-coordination issues induced by the integration of DGs are comprehensively addressed in [155, 156] where the performance of the conventional protection system is deteriorated. It is not only observed among primary protection devices but various protection functions among the primary and the backup protection devices. For example, the increased fault current downstream of a connected DG leads to an under-rating issue of the overcurrent (OC) relays upstream. When a fault occurs under this circumstance, the upstream OC relay could trip before the downstream relays that breaks the grading among all the OC relays. If adaptive settings were applied, the DG and load downstream of the false tripped relay could all be saved. As such, a protection system of wider observability and higher flexibility could assist to mitigate such protection mal-operation.

Evaluation in Chapter 3.5 also reveals that the frequency response in the initial few seconds after the disturbance and the maximum RoCoF values experienced in each zone are different from each other. In current practice of the GB power system, fixed thresholds are generally applied for the frequency-based protections despite the fact that the GB grid experiences less severe fluctuation in the midlands during disturbances than in the north and south ends. Therefore, protection sensitivity of the conventional protection system is potentially deteriorated due to improper settings in the course of the system development, where the dynamic local features that are different from each other cannot be taken into account. To cope with such zonal variations, the protection threshold should be set up based on the local frequency performance where desensitised settings shall be applied for zones that have higher renewable penetration level while the settings should be lowered for zones have higher percentage of frequency-responsive synchronous units. As such, the ability to dynamically adjust protection settings based on zones could further stand to keep a reasonably low threshold, giving them a higher protection sensitivity.

To this end, a zonal adaptive protection scheme could be a promising solution to better fulfil the operational criteria of frequency-based protections as well as improve the performance of these protection schemes in future low inertia networks.

5.3 Design of the Adaptive Protection Scheme

5.3.1 The three-layer architecture

In order to test the hypothesis that adaptive protection will effectively improve the performance of frequency-based protections in future scenarios, valid adaptive architecture should be developed encompassing the designed protection functions. Configuration and contextual interpretation of each partitioned hierarchy, functions of grading and the interactions among them should all be clearly mapped to the architecture.

A three-layer adaptive architecture designed for implementing the proposed Z-APS is depicted in Figure 5-1 with each layer assigned to specific functionality. It is based on the three-layer architecture firstly proposed in [20] while further developed in [21] where more detailed constituent functions, clarification on each functional blocks under further considerations of the practical implementation were presented. With focuses placed on the system-level frequency response in this research project, this architecture is further detailed with the proposed continuous real-time inertia estimation model at the top management layer and the protection setting adaption achieved by the joint efforts of the coordination layer and the execution layer.

The execution layer lies at the bottom of the adaptive hierarchy. It incorporates control and protection intelligent electronic devices (IEDs) at the secondary side of the primary circuit. With measurements of the primary network taken at this layer, protection settings and the status of relays are collected and transferred to the coordination and management layers to achieve certain design functions.

The role that coordination layer plays can be classified into three parts: monitoring primary and secondary systems and collecting selective system information, sending selective system information to the management layer and receiving system-level configuration information from the management layer, verifying/sending/confirming protection settings at the execution layer.

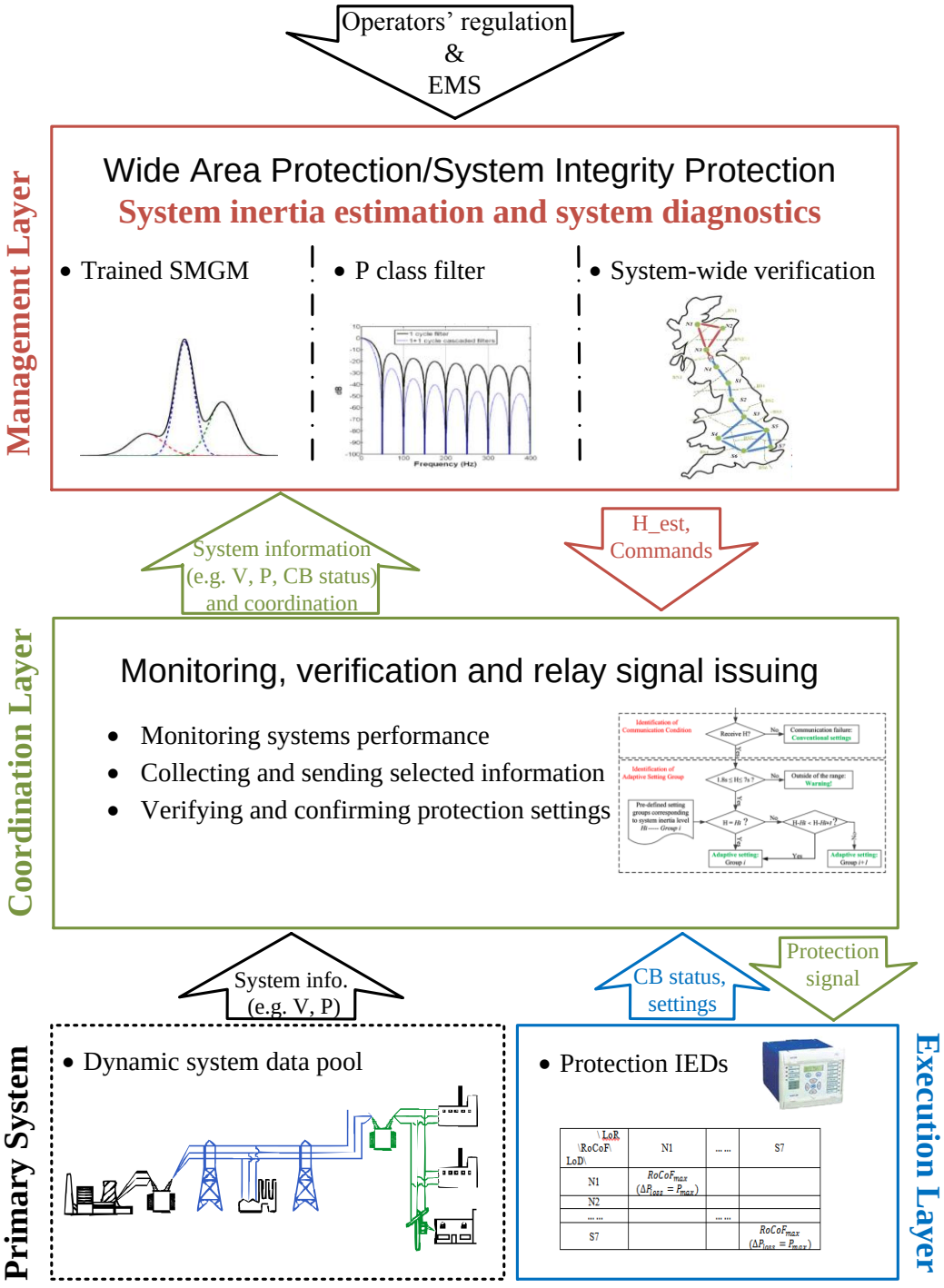

Figure 5-1: Graphic view of the designed adaptive protection scheme

The top management layer consecutively monitors and evaluates overall protection system performance. Other than coordination layer which has limited observation, the top layer is capable of visualising system-level dynamics and assessing the suitability of protection settings in an integrated way. By grading and identifying the

locations where unsuitable protection settings are applied, corresponding adaption of the protection settings will be issued. In addition, system operators can also participate in adjusting protection settings by giving instructions from the EMS.

In this case, estimated values of system inertia are continuously drawn from the trained continuous real-time inertia estimation model – SMGM in the management layer, using system frequency data collected from PMUs in real time. Combined with the evaluation of protection performance from both local area (coordination layer) and system wide (management layer), protection settings will be selected from the pre-defined look-up table in line with the estimated prevailing system inertia level. The look-up table is designed to be generated from off-line studies where the maximum RoCoFs in each zone are evaluated from a range of system operating conditions, including different sizes of infeed loss, different locations of the loss, different system inertia constants and different renewable dispatch scenarios. If during this process the system inertia level has changed, the zonal protection settings should be re-selected from the look-up table and replaced with appropriate values. Further details for such an adaptive process will be presented in the following sections.

5.3.2 Strategy of active protection setting adjustment

System inertia, affected by the penetration level of renewable resources, profoundly influences the magnitude of the maximum frequency drop, the magnitude and speed of the frequency deviation during the inertial period of events. The adaptive protection settings that are inherently tuned based on prevailing system conditions, are thereby selected on the basis of system inertia. This facilitates a more flexible and sensitive protection performance, especially more effective in dealing with the stability issues brought by the integration of renewable resources.

The incorporation of Z-APS in the coordination layer is presented in Figure 5-2 where the signal of setting change is issued and sent to the execution layer. To ensure

the flexibility and reliability during its commissioning, the proposed Z-APS has two configurable stages:

- Selection of relay mode
- Selection of relay settings

The first stage is to identify the health condition of the communication system where the relay mode alters between the conventional settings and the proposed Z-APS. The adaptive functionality is normally enabled, while disabled and switched to the conventional settings as a fail-safe strategy in case of failure in receiving inertia estimates from the management layer. Such failures can be as a result of a complete breakdown of the communication channel, a long-time delay or a severe interference in the channel.

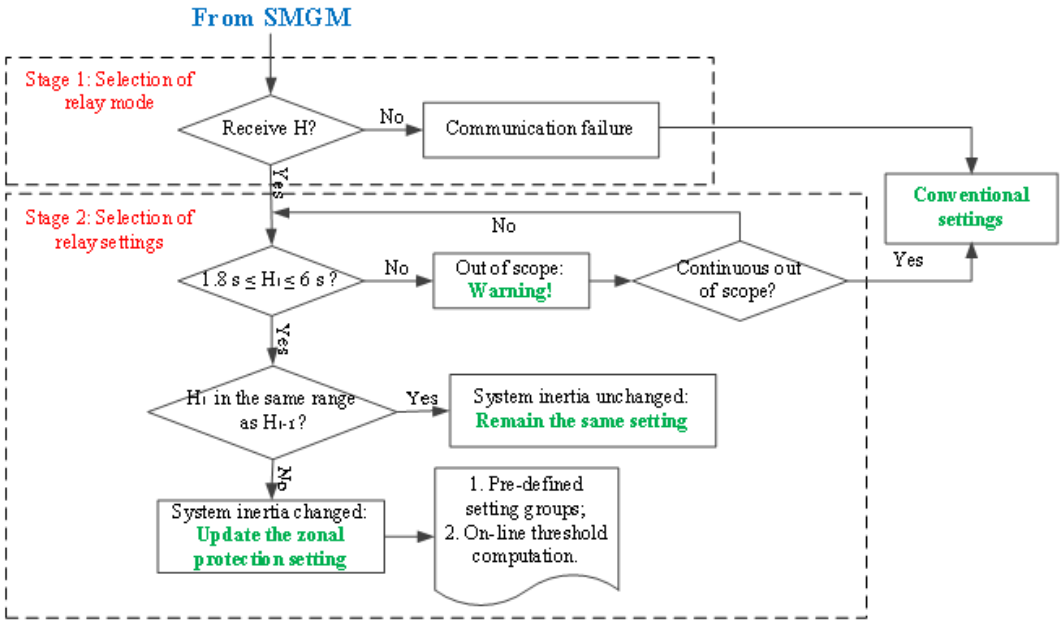

Figure 5-2: Strategy of proposed Z-APS

The second stage is to adjust relay settings. The setting group is selected referencing the inertia estimates generated from the SMGM in the management layer. If the inertia estimates stay within the range between, in this case, 1.8 s to 6 s, which indicate renewable contributions from 70% to 0% of the total demand [2, 92], the system will be treated valid to operate in adaptive protection mode. Otherwise, an out of scope warning will be issued to both the supervisor system of the SMGM and the

system operators, requesting for an inspection of the accuracy of the proposed continuous real-time inertia estimation model and the prevailing power system conditions. If the warning continuously appears for a certain period of time (depends on the application and specifics from system operators), the settings would be switched back to the conventional model. In the case of a valid inertia estimate, the current system inertia estimate (H_t) is then compared to the equivalent inertia values representing the range of renewable penetration. The settings will be updated if the system inertia no longer stays in the same range as pervious estimate (H_{t-1}). Such an adaptation could either be applied in the form of groups of pre-defined values from off-line studies such as in [157, 158] or values calculated on-line through techniques like fuzzy logic and artificial neural network [96, 159]. In this thesis, pre-defined setting groups will be used to achieve the adaptive functionality and will be discussed in details later.

5.3.3 Software environment for the implementation

The proposed Z-APS has been tested through the interface between MATLAB and PSCAD/EMTDC. The GB network model built in PSCAD/EMTDC includes functionalities equivalent to the coordination layer and the execution layer. The frequency measurements are taken from the terminal bus in each zone where the protection relays are also placed. The coordination layer was assumed to be integrated at the boundary of each zone as a local centre. The measured dynamic frequency variations in the GB system in PSCAD/EMTDC due to dynamic generation and load change were assumed synchronously transferred to MATLAB which takes the role of management layer. The proposed continuous real-time inertia estimation model has been programmed in MATLAB where the generated inertia estimates in real time are then transferred back to the reduced model in PSCAD/EMTDC. The relay settings located in each zone in the reduced model are then updated based on which inertia range the estimated value sits.

A schematic diagram is shown in Figure 5-3. The system variables communicating between these two software are real-time frequency measurements and its

conditional inertia estimates. It was assumed that both software use the same initial network conditions and hence a closed-loop process was constructed in between them.

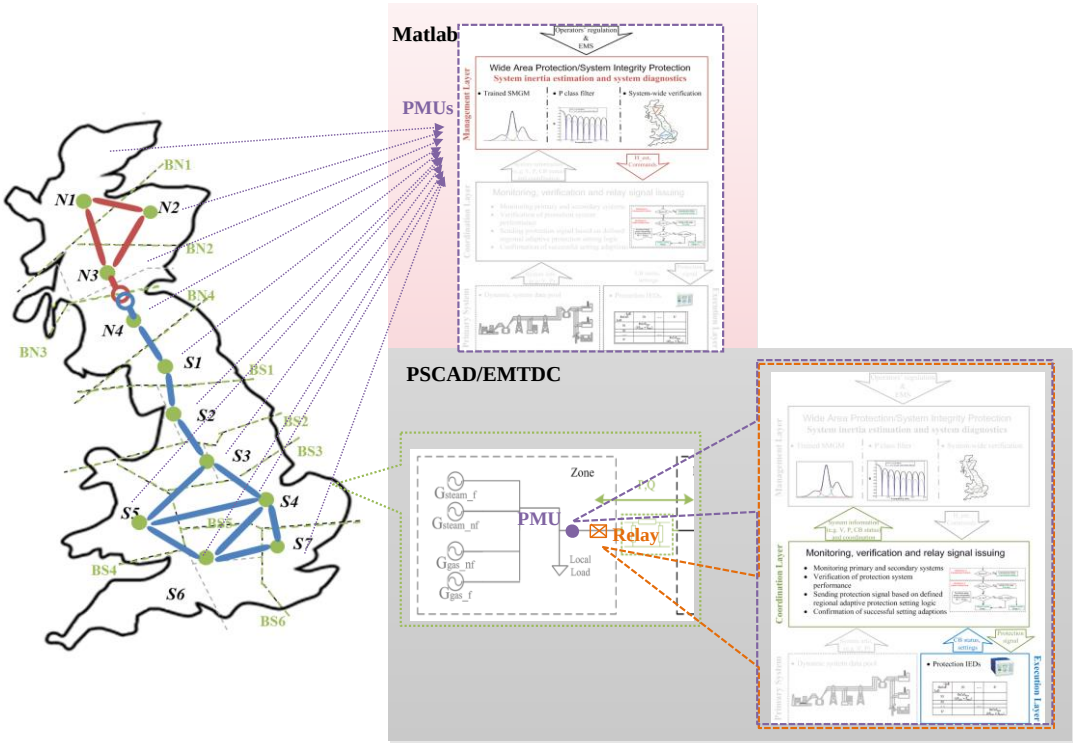

Figure 5-3: Interfacing between MATLAB and PSCAD-EMTDC

5.4 Performance Analysis for the Verification of the Developed Z-APS

This section will verify the benefits the Z-APS presenting to the protection performance by introducing it to the RoCoF-based DG anti-islanding protection scheme. Protection stability will be evaluated through the sudden loss of large infeed events and the fault-ride-through scenarios, where the RoCoF-based DG anti-islanding protection scheme should not operate. Real LoM events will also be assessed to quantify the improvement of protection sensitivity brought by the developed Z-APS.

5.4.1 Implementing Z-APS with setting groups

The designated adaptive functionality, in this research, has been realised through changing among multiple setting groups. According to the maximum RoCoF values concluded in Appendix B, a total of three adaptive setting groups were applied and they are listed in Table 5-1 based on the worst case scenario among all assessed case of the same system conditions but various locations of the loss. These setting groups were proposed to mitigate the mal-operation of the local DGs when subjected to large infeed loss under normal operating conditions. The setting groups were chosen in the light of the renewable penetration levels from a typical 30% to a deemed 70% in steps of 20% given equivalent system inertia constant accordingly. A ratio of 1.2 was multiplied on top of the maximum zonal RoCoF values in each specific scenario to tolerate the existence of the communication delay, the time for relay reset, the measurement noise and the errors of transformers (due to spike, etc.) in practical commissioning.

Table 5-1: Recommended zonal adaptive settings under various renewable penetration levels

Penetration Level / Inertia ` Zone RoCoF (Hz/s)	0%~30% (6 s ~ 4.2 s)	30%~50% (4.2 s ~ 3 s)	50%~70% (3 s ~ 1.8 s)
N1	0.34	0.50	0.86
N2	0.34	0.50	0.85
N3	0.34	0.50	0.84
N4	0.32	0.47	0.76
S1	0.29	0.40	0.67
S2	0.23	0.38	1.03
S3	0.20	0.35	0.88
S4	0.25	0.47	1.27
S5	0.22	0.41	1.25
S6	0.24	0.49	1.40
S7	0.23	0.40	1.30
Name of Setting Group	Z-APS_G1	Z-APS_G2	Z-APS_G3

There is no doubt that a rigorous analysis of the system performance can be achieved by a larger number of setting groups in line with finer step changes of the renewable penetration level. However, the uncertainties in future system dynamics would place concerns of diminishing the value of using setting groups if changing protection settings too often. Moreover, it is likely to end up with an unlimited number of setting groups for the finer resolution that leaves burden for protection system to accurately distinguish the renewable penetration level as well as issuing correct signals to change the protection settings in time.

The setting groups in this case also took into account the errors generated from the inertia estimation model. This is to avoid the undesired operation of the proposed Z-APS in the presence of the estimation errors. If the recommended fourth-order SMGM with a half-hourly OCC and average sample selection approach was utilised, the maximum error that could be possibly accumulated through this period would be 1.8 s ($5\sqrt{0.1285}$ from Table 4-4). Although such a large estimation error is most unlikely to happen, it was still taken as the worst case scenario. Since the worst case inertia estimation error equals to an inertia variation of an approximate 20% renewable penetration, the setting groups in this research, were thereby identified in a grade of 20% renewable penetration.

5.4.2 Stability evaluation: Loss of large infeed event

Stability of the DG anti-islanding protection scheme will be tested in this section against loss of large infeed events with and without integrating the developed Z-APS. The performance of the protection schemes will be compared for the impact brought by the Z-APS.

The worst case identified in Chapter 3 is the loss of a 1800 MW infeed in zone S6 in Case 1 scenario under 70% renewable penetration. In this scenario, the maximum RoCoF values in zone S4 to S7 exceed the permitted 1 Hz/s protection setting. Accordingly the setting group Z-APS_G3 will be applied prior to the loss in the case where the adaptive functionality is enabled.

Figure 5-4 and Figure 5-5 show the frequency performance with the Z-APS disabled/enabled for the above addressed system contingency. When the Z-APS is disabled, 1 Hz/s protection setting threshold was assumed. DGs in zone S4 to S7, which are equipped with the RoCoF-based LoM protection, will be disconnected after the 1800 MW infeed loss. The GB system is, therefore, subjected to a subsequent frequency degradation due to the unexpected tripping of these DGs which eventually leads to system frequency collapse. This corresponds to the concerns raised in Chapter 3.6.2 where a potential cascading system deterioration was addressed. In contrast, these DGs remain connected in the system when the Z-APS is enabled. The subsequent frequency degradation is avoided as the minimum frequency system experienced is 48.88 Hz which is above the threshold of the first stage UFLS. As such, by mitigating the unexpected trip of DGs, the proposed zonal adaptive DG anti-islanding protection scheme is able to maintain higher system stability in a sudden loss of large infeed event, which to some extent also reduces the potential interruptions to the customers.

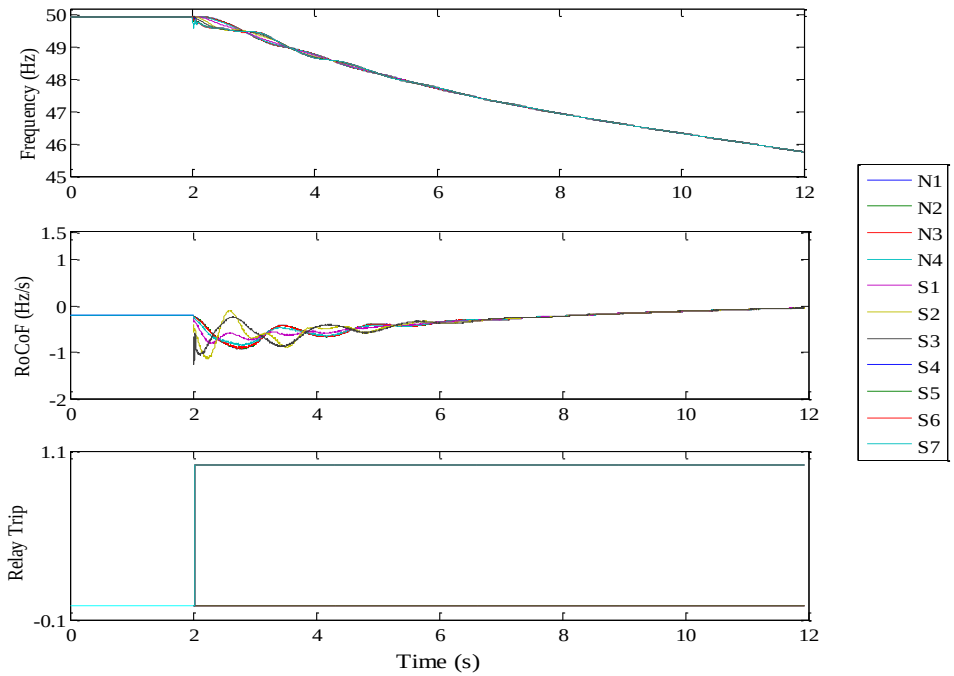

Figure 5-4: Frequency performance with Z-APS disabled

In this case, 7.2 GW DGs were simulated for the subsequent disconnection and assumed equally distributed in these four zones, reflected as the result of the spurious

tripping of RoCoF-based LoM protection relays. This amount was derived based on the installed capacity of the DGs in Gone Green scenario in year 2020 [81], assuming 35% of the total installed capacity of DGs will be equipped with the RoCoF-based protection relay. The 35% was referenced from the figures in year 2012 given a maximum of 4.35 GW DGs were equipped with RoCoF-based protection relay[160].

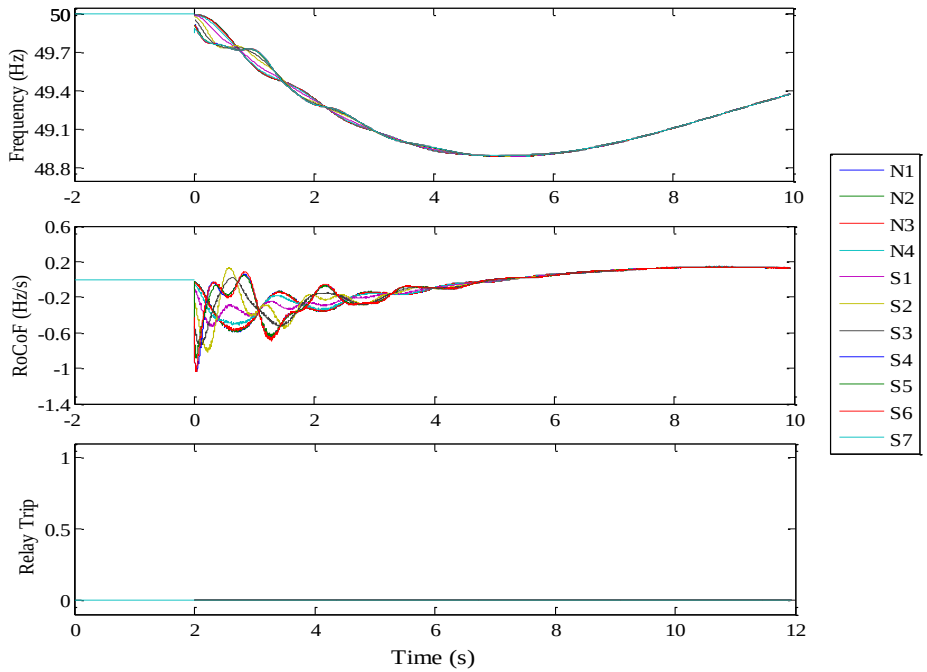

Figure 5-5: Frequency performance with Z-APS enabled

5.4.3 Stability evaluation: Fault ride-through

It is a critical feature for the proposed Z-APS to maintain desired performance when subjected to transient faults. This attributes to the fact that practical system experiences transient faults quite frequently (especially the single-phase faults [161]) and the fluctuations on system frequency observed by the proposed continuous real-time inertia estimation model could generate false inertia estimate that issues wrong signal for changing protection settings.

In this case, both single-phase ground fault and three-phase ground fault were included in this assessment. Faults were placed between N1 and N2, S1 and S2, S6 and S7, referring to as in the north, midlands and south of the GB power system. This

case study still took the worst case that the system is operating under 70% renewable penetration with all the renewable resources output from the south region while with the Z-APS is enabled.

The performance of designed protection scheme in facing these transient faults is shown in Figure 5-6 to Figure 5-11. In general, the observed oscillations in the frequency and RoCoF values are more severe when subjected to a single-phase ground fault than a three-phase ground fault. Due to the fact that the estimates generated from the continuous real-time inertia estimation model are on a 5-minute basis, the frequency fluctuations during the fault, as in a magnitude of 10^{-2}, are smoothed out when taken by the continuous real-time inertia estimation model to profile the real-time inertia values. Therefore, the impact of fault ride-through on system inertia estimates is negligible, giving that the protection settings regulated by the Z-APS would not change during the transient fault. As the RoCoF values are generally seen less than 0.05 Hz/s, the RoCoF-based DG LoM protection relay, thereby, would not trip. As such, the proposed zonal adaptive DG anti-islanding protection scheme is proven robust in the presence of transient faults.

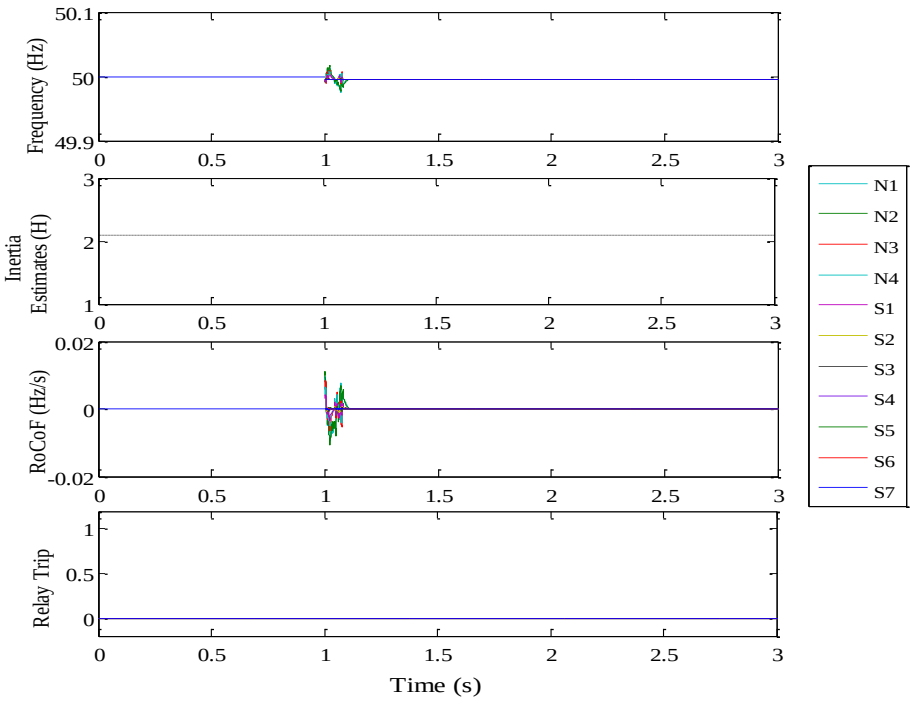

Figure 5-6: Single-phase ground fault on line between N1 and N2

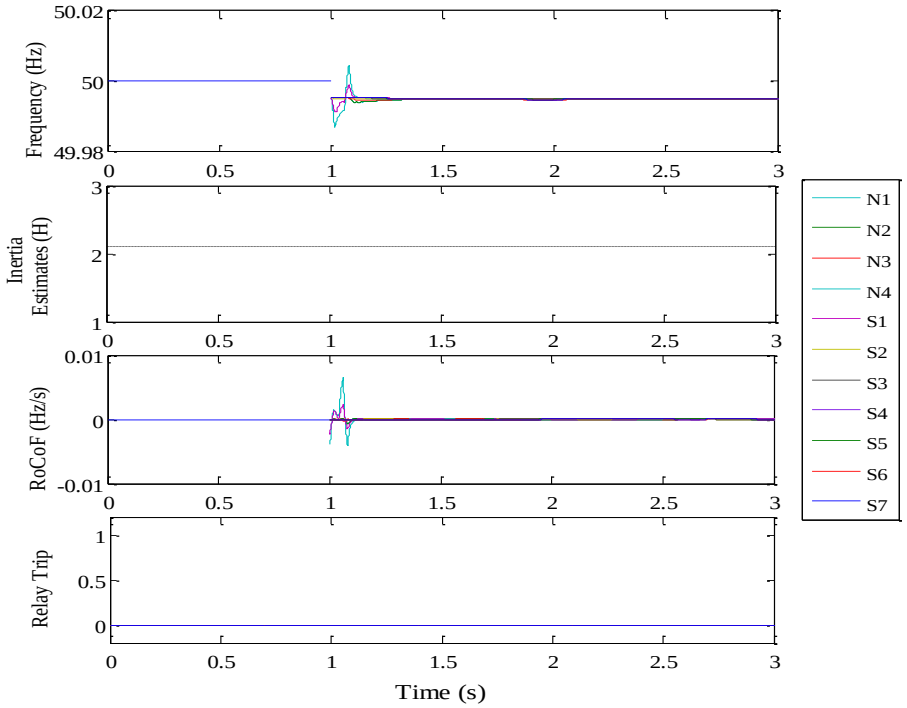

Figure 5-7: Three-phase ground fault on line between N1 and N2

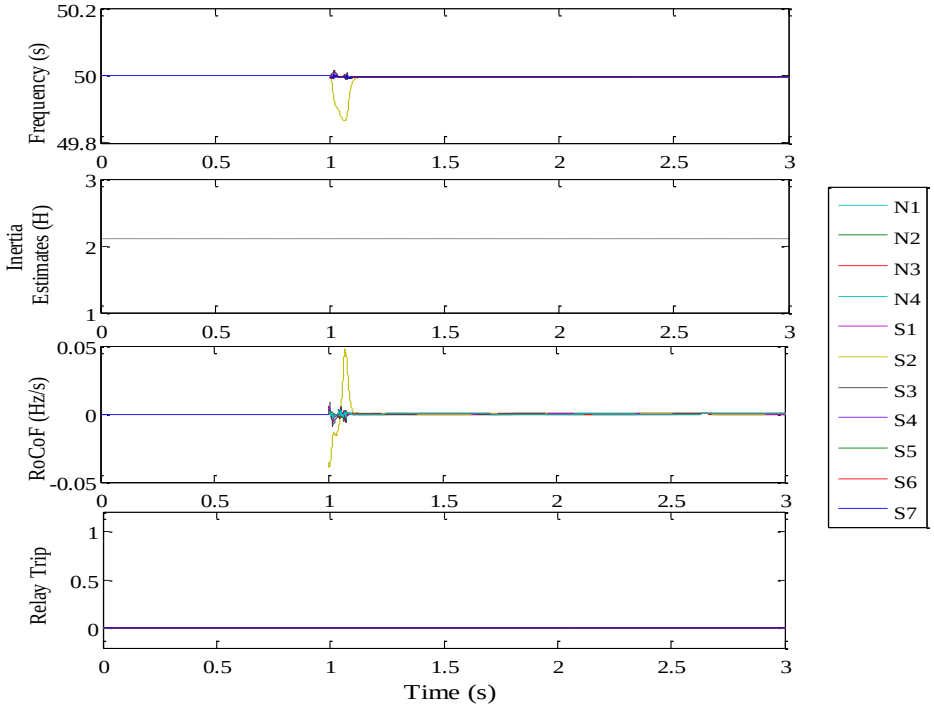

Figure 5-8: Single-phase ground fault on line between S1 and S2

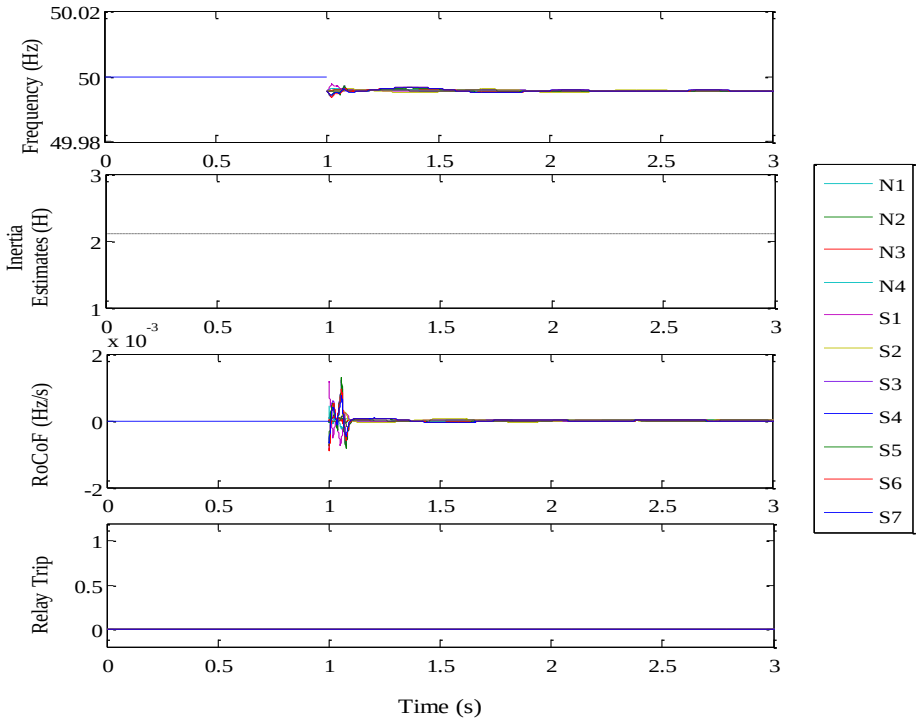

Figure 5-9: Three-phase ground fault on line between S1 and S2

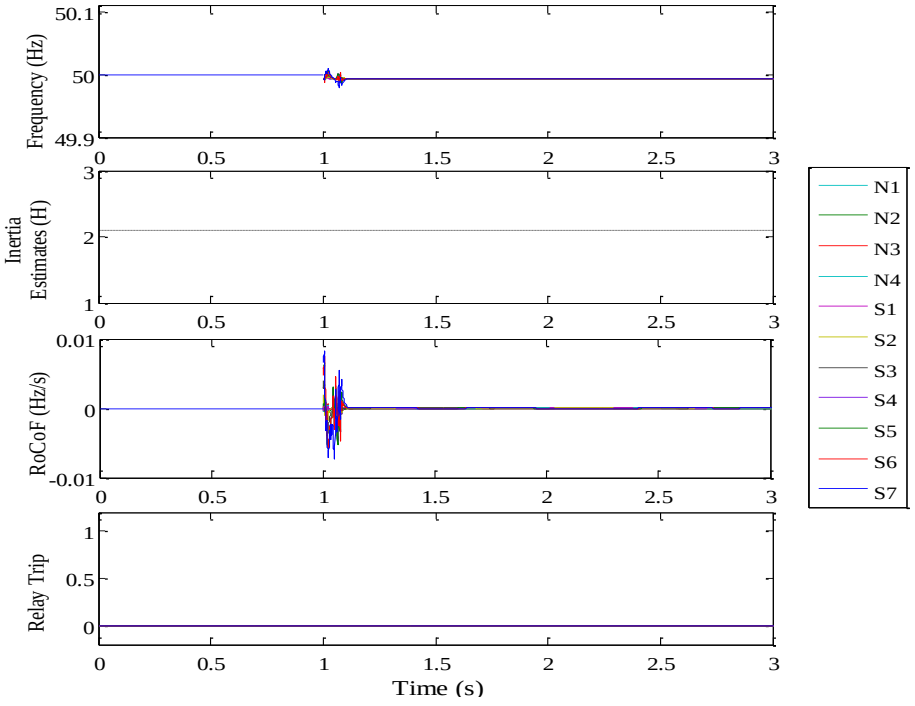

Figure 5-10: Single-phase ground fault on line between S6 and S7

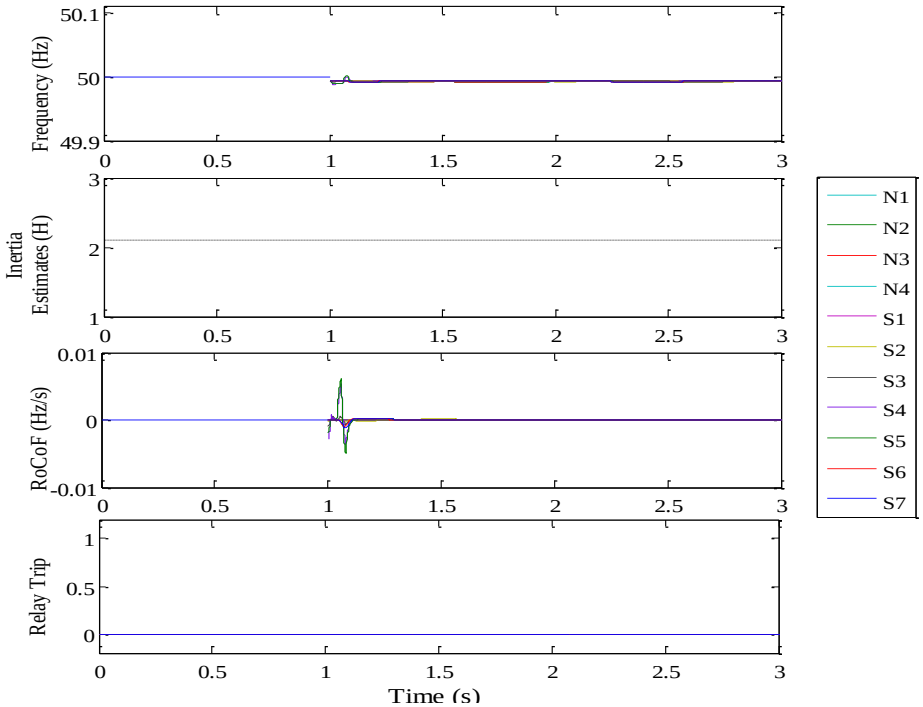

Figure 5-11: Three-phase ground fault on line between S6 and S7

5.4.4 Sensitivity evaluation: Real LoM event

An enhanced protection performance has been verified for the proposed zonal adaptive DG anti-islanding protection scheme against a large infeed loss in previous section. However, the developed Z-APS should also function properly to detect the real islanding events. With the more localised and flexible protection settings, an improved protection sensitivity is expected to be achieved, reducing the risk of protection system fail to operate in real islanding events.

To assess the sensitivity of the proposed zonal adaptive DG anti-islanding protection scheme, the concept of non-detection risk (NDR) was applied to quantify its performance. Non-detection occurs when the real power between the local demand and the DG outputs are very close (surplus or deficit) prior to the occurence of an islanding and this makes it hard to be detected. The percentage of the power mis-match to the DG rating is defined as non-detection zone. The probability of the power mismatch occurring in this zone is the NDR [162].

Assessment in this research referenced the risk of undetected islanding of an individual generator in [18] while additionally, taking the zonal variations into account. The zonal variations include the number of DGs in each zone and the proposed zonal settings. The probability of non-detection calculated in [18] was used to derive the probability of non-detection of each individual DG. It takes the width of the non-detection zone evaluated through laboratory testing where eight industrial load profiles and an incremental output from DGs were assessed in an iterative approach.

In this case, the worst case scenario among the three valid cases in [18] was taken for the evaluation presented in this research work. This is owing to the sufficiently high time resolution that these three were recorded with a more representative load dynamics while the worst case can give more extreme comparison results. Following assumptions were made:

- The investigation was undertaken for DGs with installed capacity ranging between 5 MW and 50 MW and it was assumed that DGs lower than this boundary currently cannot be directly controlled from the control centre where the management layer of the adaptive protection scheme locates.
- A total number of 183 DGs were considered in the GB system which are synchronous generators only according to the accessible data given in [160].
- All synchronous generators mentioned in previous assumption were equipped with RoCoF-based protection relay. This was used to investigate the worst case scenario.
- The number of synchronous DGs in each defined study zone was depicted in Table F-1 (in Appendix F) based on the data in [160] and the regions each distribution operator is responsible for [163].
- The expected annual number of LoM occurrences in a single substation was 0.0375 [18] and this was assumed to be the same across the GB grid.
- The assessment was taken on synchronous DGs with P-V control technique only as the P-pf controlled DGs are of nearly no risk of non-detection [18].

Assuming the risk of non-detection is proportional to the number of generators, the NDR in Table 5-2 is given for each zone with various protection settings. It should be noted that no time delay was considered when calculating zonal risk at this stage and the values under the settings of 1 Hz/s+500 ms listed in the table are for comparison purposes only.

Table 5-2: Zonal risk of undetected islanding event from [18]

Threshold (Hz/s) + Time delay (ms)		0.125 + 0	1 + 0	1 + 500
Study Zone	N1	4.27E-08	8.52E-07	9.48E-07
	N2	3.2E-08	6.39E-07	7.11E-07
	N3	3.2E-08	6.39E-07	7.11E-07
	N4	1.49E-07	2.98E-06	3.32E-06
	S1	2.24E-07	4.47E-06	4.98E-06
	S2	2.24E-07	4.47E-06	4.98E-06
	S3	1.92E-07	3.83E-06	4.27E-06
	S4	1.71E-07	3.41E-06	3.79E-06
	S5	2.88E-07	5.75E-06	6.40E-06
	S6	5.44E-07	1.09E-05	1.21E-05
	S7	1.07E-07	2.13E-06	2.37E-06

However, the strategy in [18] follows a nationwide fixed threshold regardless of the local system configuration, where the proposed zonal adaptive settings as shown in Table 5-1 are excluded from the evaluated four settings in [18]. In order to derive the zonal NDR when applying the proposed adaptive settings, curve fitting technique was applied. Few different curve types have been initially considered such as polynomial, exponential and power. Taking zone N1 as an example as depicted in Figure 5-12, the 2^{nd}-order and 3^{rd}-order polynomials are much closer to the original data points, indicated as higher values of the R-squared indices (0.9997 and 1 respectively given in the bracket in legend). However, the uncertainty in the 3^{rd}-order polynomial, which has two critical points, may result in undesired "saturation" of the curve for settings beyond 1 Hz/s. Therefore, the 2^{nd}-order polynomial interpolation was selected as the best option for establishing the relation between RoCoF settings and the zonal NDR (as long as the setting is not significantly higher than 1 Hz/s).

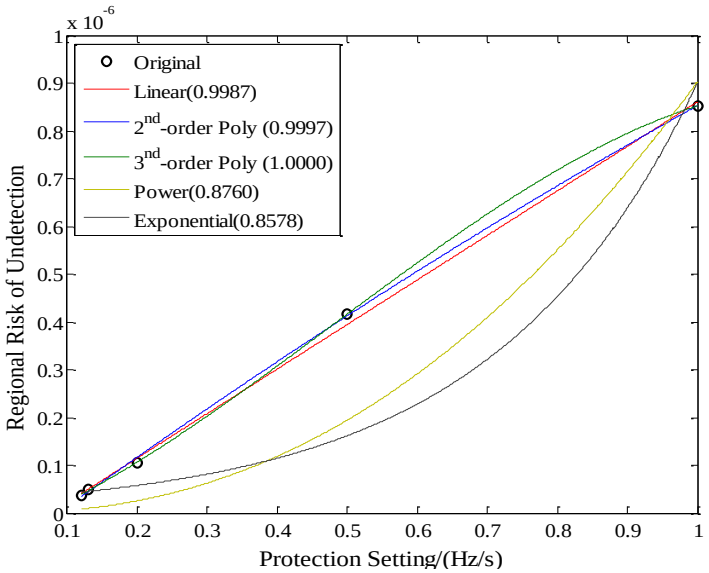

Figure 5-12: Curve fitting for the probability of undetected LoM with various settings in zone N1

Using the 2nd-order polynomial fitting in combination with the proposed zonal adaptive settings, the NDR under various penetration levels of renewable resources is able to be calculated from a zonal approach. The derived results are presented in Table 5-3 using the curve fitting equations given in Appendix F Table F-3 where x is the specific protection setting. For a growing renewable penetration from 30% to 70%, the zonal NDR generally experiences an increase in an order of magnitude.

Table 5-3: Zonal NDR using adaptive settings under various penetration levels of renewable resources – worst case scenario

Renewable Level / (System Inertia Constant)		0%~30% (6 s ~ 4.2 s)	30%~50% (4.2 s ~ 3 s)	50%~70% (3 s ~ 1.8 s)
Study Zone	N1	2.54E-07	4.17E-07	7.40E-07
	N2	1.90E-07	3.12E-07	5.47E-07
	N3	1.90E-07	3.12E-07	5.39E-07
	N4	8.49E-07	1.34E-06	2.26E-06
	S1	1.08E-06	1.64E-06	3.00E-06
	S2	7.61E-07	1.58E-06	4.61E-06
	S3	5.43E-07	1.19E-06	3.37E-06
	S4	6.77E-07	1.53E-06	4.26E-06
	S5	8.98E-07	2.19E-06	7.05E-06
	S6	2.00E-06	5.16E-06	1.49E-05
	S7	3.63E-07	7.82E-07	2.70E-06

A quantitive comparison is presented in Table 5-4 in the form of the NDR reduction by applying the zonal adaptive settings against the present fixed settings with and without time delay. The percentage values given in line with the renewable penetration levels were calculated by dividing the difference of NDRs between the adaptive and the fixed setting approaches over the NDR of fixed settings. It refers to an improved sensitivity of islanding detection for a positive value while degraded performance for a negative value.

Table 5-4: Reductions of NDR comparing the proposed zonal adaptive settings with the 1Hz/s+0ms and 1Hz/s+500ms protection settings

Settings		Adaptive *vs.* 1Hz+0ms			Adaptive *vs.* 1Hz+500ms		
Renewable Level / (System Inertia Constant)		0%~30% (6 s ~ 4.2 s)	30%~50% (4.2 s ~ 3 s)	50%~70% (3 s ~ 1.8 s)	0%~30% (6 s ~ 4.2 s)	30%~50% (4.2 s ~ 3 s)	50%~70% (3 s ~ 1.8 s)
Study Zone	N1	0.70	0.51	0.13	0.73	0.56	0.22
	N2	0.70	0.51	0.14	0.73	0.56	0.23
	N3	0.70	0.51	0.16	0.73	0.56	0.24
	N4	0.72	0.55	0.24	0.74	0.60	0.32
	S1	0.76	0.63	0.33	0.78	0.67	0.40
	S2	0.83	0.65	-0.03	0.85	0.68	0.07
	S3	0.86	0.69	0.12	0.87	0.72	0.21
	S4	0.80	0.55	-0.25	0.82	0.60	-0.12
	S5	0.84	0.62	-0.23	0.86	0.66	-0.10
	S6	0.82	0.53	-0.37	0.83	0.57	-0.23
	S7	0.83	0.63	-0.27	0.85	0.67	-0.14
National Average		0.78	0.58	0.00	0.80	0.62	0.10

In general, significant reduction of the NDR is observed by applying zonal adaptive settings across the entire GB network (as the ratios are generally positive), except for few under 70% renewable penetration. The improvements are reflected from two aspects: the flexibility in setting thresholds and the unemployment of time delay. Moreover, the percentage of NDR reduction decreases inversely in proportion to the penetration level of renewable resources. For a 30% renewable penetration, the zonal NDR can be reduced by an average of 78% while there is no reduction for a 70%

renewable penetration. The impact of introducing time delay to the protection setting on NDR is shown in Figure 5-13. On average, a further 5% reduction is achieved comparing settings with the 500 ms delay with no delay. Moreover, the negative penalty imposed by time delay is seen more severe for the growing renewable penetration level, which further increases the risk of non-detection.

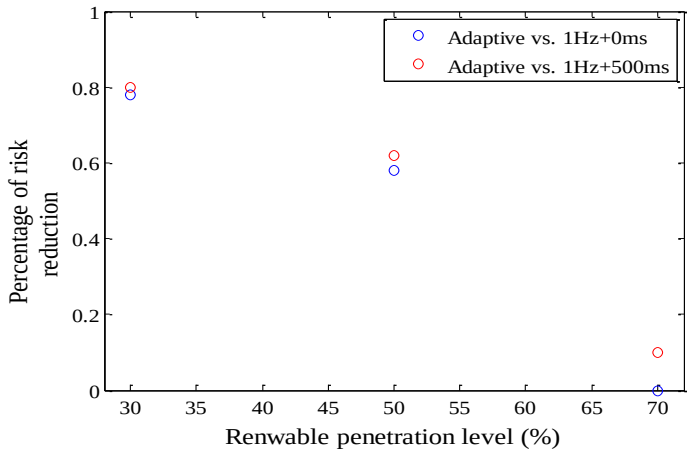

Figure 5-13: Reduction of NDR in graphic view

As a conclusion, the proposed zonal adaptive protection setting groups, compared with the current RoCoF relay setting, are more sensitive to real islanding events. The NDR can be effectively reduced by a national average of around 80% which drops exponentially to 10% for renewable penetration level increased from 30% to 70%. An average of 5% lower NDR will be achieved with the zonal adaptive settings without time delay feature.

For comparison purposes only, the case which uses the mean NDR value of the three valid cases is provided in Appendix F Table F-4. Comparing with the results derived from using the worst case scenario, the NDRs are further reduced by 3% for the fixed 1 Hz/s + 0 ms setting under 70% wind penetration while an average of 6.8% NDR reduction for the remaining scenarios. As such, the worst case scenario gives a more conservative and sensible comparison.

5.5 Discussions on the Implementation and Verification of the Z-APS

It has been verified in extensive scenarios that the proposed Z-APS could improve the performance of the RoCoF-based DG anti-islanding protection scheme. This has been demonstrated through the mitigation of the protection mal-operation when subjected to sudden infeed losses, reduced NDRs in the presence of real islanding events and its fault ride-through ability to maintain a reliable dynamic operation. However, realisation of such an improvement relies on choosing the right protection settings and making corresponding adjustments accurately and sensibly. Challenges, thereby, are imposed by dynamic system operation and the uncertainties brought with it. As such, this section will discuss the justifications of the proposed Z-APS, associated with the implementation and practical issues for the future employment of the scheme.

5.5.1 Benefits of setting groups over on-line computation

In reference to Table 5-1, protection settings are designed to be actively switched among three groups of zonal settings pre-calculated off-line in the light of renewable penetration level. However, as oppose to it, there is another option of computing protection settings in real time. The reasons will be discussed here explaining why the later one was not adopted in this research work.

The reliability Z-APS askes for is not only limited to deliver more flexible and suitable protection settings but also to accomplish the adaption in a permissible short period of time. With regards to the on-line computation approach, the latency introduced from processing measurement data to generate well coordinated protection settings, could delay the operation of relays, leading to the failure of islanding detection. Moreover, the greater flexibility that the on-line computation provides (as more tuned to system dynamics), on the other hand, could increase the risk of system instability as leaving protection thresholds active and unpredictable. This would be more observable and frequent in future systems, where severe system

inertia changes would occur more often. Furthermore, there are no standardisation among relay manufacturers and system operators to sharing the same strategy of RoCoF measurements and real-time setup of adaptive protection thresholds. This could incur spurious tripping as a result of mismatched agreements. To this end, the approach of applying pre-defined setting groups is selected as it satisfies the requirements of protection flexibility with the need for reliability.

5.5.2 The number of setting groups

The setting groups previously identified in Table 5-1 are chosen in the light of renewable penetration level coupled with the concerns of estimation error drawn from the continuous real-time inertia estimation model. These off-line settings are restricted to be chosen from a limited number of three groups and will only be switched to adapt to the confirmed prevailing system operating conditions when system inertia changes.

Theoretically, a finer resolution of the penetration level would provide a more sensitive and dedicated protection to cope with every single change in the inertia estimates. However, this would end up with numerous groups of settings that loses the objective of being simple while effective by embracing pre-calculated setting groups. The dynamic uncertainties hidden in system operations also place barriers to clearly distinguish and have sufficient time to take actions for every single system change (most of them are caused by daily load and/or generation variations). Moreover, the errors in estimating the real-time inertia constant from the model would also lead to false protection operation if the thresholds fall in the possible error range. Given a 1.8 s worst case inertia estimation error, an approximate 20% renewable penetration will mitigate the spurious changes of the protection settings due to the estimation error.

In future power systems, the growing unpredictability in system dynamics may will ask for a revision of the proposed zonal adaptive DG anti-islanding protection setting groups for a more concrete look-up table to cover all the uncertainties in flexible

system operation. To apply the proposed Z-APS in practical systems, restrictions posed by the number of setting groups should take into account the type of protection and the desired accuracy and flexibility that are expected to be achieved in system operation.

5.5.3 Benefits of being zonal and adaptive

As to the argument of whether the protection settings need to follow both zonal and adaptive criteria or only one of them and in what manner they should be applied, comparisons and justifications are presented here from all possible combinations formed from these two elements. The following discussions will centre on the adaptive feature first and then turn to the zonal character.

Conducted with the RoCoF-based DG anti-islanding protection, the proposed Z-APS has shown great improvement on system frequency response in the presence of a large infeed loss and the reduction of NDR in real islanding events. However, there is an argument of whether it is necessary to apply Z-APS across the entire system. Such an argument is open to implement Z-APS for the part which has the largest improvement of protection performance while leaving the rest still equipped with conventional protection settings or the adaptive protection settings will only be applied under certain conditions (e.g. the renewable penetration level higher than 50%). However, there are few constraints that limit these alternatives. Firstly, the line of distinguishing the boundary of protection being active or inactive is hardly drawn due to lack of concrete justifications. Secondly, the protection sensitivity in the system where conventional protection settings are applied will inevitably be compromised to a certain degree due to a lack of flexibility. Thirdly, a potential loss of coordination could occur at the boundaries between non-adaptive and adaptive parts or during the transition of switching between adaptive and non-adaptive strategies (if the discrimination is carried on through dynamic operation). Although the costs of implementing Z-APS in the system can be saved without applying any changes to the protection systems, future system, where more DGs, micro-generators

and frequency-responsive demand will be integrated, still see the need in order to deliver more stable while flexible system protection.

The thresholds set up in the proposed Z-APS provide a more accurate and sensitive protection by taking into account the local diversity. As previously verified in Chapter 3, the impact of local generation dispatch has on the performance of frequency response results in various RoCoF values from one place to another. The fixed threshold in conventional protection schemes would thereby desensitise the operation of the relays. In contrast, such risk can be effectively reduced if applying zonal settings because of the verified reduction in NDRs.

As a conclusion, being zonal adaptive provides the flexibility and sensitivity RoCoF-based DG anti-islanding protection needs to cope with the growing system dynamics while maintaining its stability against sudden large infeed losses in future low inertia networks.

5.5.4 Communication failure

The achievement of adaptive functionality relies on the communication channel to transfer data/signal among each function block. Therefore, any failure in communication would potentially lead to mal-function of these function blocks or a complete failure of the protection schemes. In this research project, there are two places where communication is employed to enable the Z-APS function properly: frequency measurements input to the SMGM for real-time inertia estimation; system inertia estimates to activate the switching among protection setting groups.

The failure in delivering frequency measurements to the continuous real-time inertia estimation model at the management layer has been evaluated in Chapter 4.7 where the estimation performance of the proposed SMGM is acceptable for frequency measurement interruptions of up to a period of two hours. Therefore, if the coordination layer fails to receive inertia estimates over two hours, the proposed Z-APS should be disabled and switched to the conventional settings instead. Although

the fixed settings to a certain extent compromise protection sensitivity, the entire system remains secured without leaving part of system unprotected or protected with inadequate settings (lower than it should be). The adaptive protection scheme will be switched back on-line until the next successful delivery of valid inertia estimate.

In practice, there is always a redundant communication channel installed in the system following the regulation standards or protocols like IEC61850 [164]. Therefore, proper protection operation should be maintained on the occurrence of communication failure in generally occasions.

5.5.5 Challenges on the wide implementation of the Z-APS

The realisation of real-time inertia estimation could provide valid reference inputs to proactive control and protection systems. System stability would be enhanced as well as achieving operational economics through, for example, more informed ancillary reserve planning using knowledge of prevailing system conditions and stability margins. However, the integration of Z-APS into future power networks should not only consider the benefits of it to the performance of protection schemes, but also the side effects it brings to the system operation. Such challenges will be discussed in this section from the following aspects.

To implement the proposed Z-APS in the network, current protection schemes need to be upgraded, including the expansion of the communication infrastructures and the replacement of relays with the ones have built-in adaptive functionalities. Frequency measurements from multiple locations across the network need to be gathered for the SMGM to estimate real-time inertia where sufficient communication channels are necessitated for taking these measurements. Moreover, the coordination among localised adaptive relays and the signals of changing protection setting groups also rely on the dual-communication between the execution and coordination layers. In addition, the expanded communication channels if can be realised would introduce extra challenges, such as hidden failures, noise or signaling latency [165], that could also contribute to the failures of adaptive protection schemes. Considering the fact

that the protection relays currently commissioning in the system are unable to change the settings automatically, this inevitably requires high investment and intensive manual work, more importantly the time to replace them all. Besides, the potential issues incurred by the maintenance and decommissioning of the relays will also need to be considered.

The commitment of the Z-APS cannot be fully achieved without a standardised procedure to regulate its functioning in future networks. It should operate without compromising the coordination among protection relays or disrupting the performance of existing protection schemes. Currently, there is no such policy to specify the acceptable errors that can be generically applied on specific protection functions or in different networks but the manufacturers themselves. Therefore, the reliance on the discretion of the manufacturers may lead to the failure of Z-APS. Moreover, a fail-safe strategy needs to be applied to ensure the system will not be left unprotected during the switching among adaptive protection setting groups or the transition between adaptive and conventional schemes. Such a strategy is dependent on the protection schemes and its application. In this case, the conventional settings should be applied for the RoCoF-based DG anti-islanding protection on the failure of the Z-APS.

5.6 Chapter Summary

Following on from Chapter 3 of identifying protection performance issues that stem from the lower inertia and more dynamic operation in future power systems, the hypothesis of adaptive protection as a flexible means to mitigate system deterioration from these issues has been examined in this chapter.

An enhanced protection performance of the RoCoF-based DG anti-islanding protection has been presented as an example given to verify the benefits of embracing the proposed zonal adaptive protection settings. The Z-APS was implemented on a three-layer adaptive architecture, originally designed in [20] and complemented in [21]. It was achieved through switching among three setting groups

which take into account the variations in zonal frequency response for an improved protection sensitivity. The continuous inertia estimates generated from the SMGM formulated in Chapter 4 was acting as the enabler to activate the Z-APS. A fail-safe strategy of switching back to conventional protection settings has been projected to cope with potential hardware failures or invalid inertia estimates from the continuous real-time inertia estimation model.

Through the stability analysis and risk assessment, the proposed zonal adaptive protection scheme has been verified to effectively mitigate the spurious tripping of DGs under large infeed loss scenarios in future low inertia networks. Moreover, compared with the 1 Hz/s + 500 ms setting that has been permitted to be applied in the GB system, the NDR of applying the Z-APS has been reduced from 10% (under 70% renewable penetration) up to 80% (under 30% renewable penetration) in the worst case scenario. Arguments on the configuration of adaptive protection settings, the benefits of being zonal adaptive, the strategy in facing communication failure and its challenges in future implementation have also been presented at the end of this chapter.

6. Conclusions and Future Work

The research work presented in this thesis has addressed the impact that high levels of renewable energy penetration (which results in reduced levels of overall inertia and significant variations in inertia as the generation profile changes) will have on the power system frequency stability in the future, and also on the performance of conventional frequency-based protection schemes, including loss of mains and under frequency protection. To mitigate the potential identified issues with frequency stability, a zonal, adaptive, anti-islanding protection scheme for DG has been proposed and tested which is enabled by the proposed continuous real-time inertia estimation model. Its performance in delivering enhanced protection functions has been verified under various renewable penetration and inertia scenarios using a reduced GB power network model. Without considerably compromising protection sensitivity, the designed scheme has been proven to be capable of maintaining the desired system frequency stability against sudden large infeed loss events in the future, under both low and variable system inertia conditions.

The following subsections outline the major conclusions arising from this research and explore issues that are worthy of being taken forward as future work in order to refine the implementation of the proposed methods in a practical applied system.

6.1 Conclusions

6.1.1 Evaluation of future system frequency response and the performance of conventional frequency-based protections

Based on the presented generic system modelling and validation process, an 11-node reduced GB dynamic power network model has been built and validated against historical system events to confirm its suitability for studying the impact of

reductions and more pronounced variations in system inertia and for ascertaining and quantifying the potential consequences for system frequency instability. The reduced model incorporates a mix of generation units including fossil/steam, gas and renewable resources. Values for the parameters of the control and governor systems were firstly set based on typical values and then fine-tuned to replicate the performance of actual recorded system events. The results show that the model exhibits a maximum of 0.25% difference in terms of the magnitude of the overall frequency drop across three recorded events and a 2.7% maximum difference between the measured and simulated initial RoCoF value. It can therefore be proposed as being representative of the dynamic system frequency response during a sudden loss of infeed scenario.

The impact of system inertia reduction and variation on system frequency response and frequency-based protections has been evaluated and quantified under a range of combined system conditions, including different locations and sizes of the sudden infeed loss, various penetration levels and distribution patterns of renewable resources (sourced from the National Grid 'Gone Green' scenario in the Future Energy Scenario document [47]). This provides a new and more comprehensive understanding of frequency response in the future UK grid. Frequency instability issue can be incurred due to the reduced system inertia and the increased size of the infeed loss. The studies were carried on with a minimum demand of 25.5 GW assumed for the worst case scenario. Simulations have shown that the 49.2 Hz minimum instantaneous frequency would be exceeded upon a 1800 MW sudden infeed loss if the overall system inertia is lower than 3.83 s. If the loss is at the southern end of the GB network, 1644 MW is the maximum loss for the system with 50% renewable penetration (given a inertia of 3 s on the basis of 25.5 GW generation) to maintain acceptable frequency response. The analysis of the simulations also showed that 55% of the RoCoF-protected DGs with a relay pickup of 1 Hz/s (which is the setting permitted to be implemented in the system [72]) will be unexpectively disconnected for a 1800 MW infeed loss under 70% renewable penetration. Furthermore, first stage automatic load disconnection with a threshold of 48.8 Hz would start if the system frequency prior to the 1800 MW infeed loss is lower than

49.84 Hz under 70% renewable penetration. Future system operation should take these boundary figures into account for the awareness of any potential frequency instability issues, as well as the future implementation of advanced control and protection strategies under certain operational scenarios.

It was shown through the simulations that the performance of the RoCoF-based DG anti-islanding protection (with proposed future settings of 1 Hz/s [72]) is in future largely desensitised. Although the initial frequency response in each zone is dependent nonlinearly on the location of the loss and the nature and inertia of the local generation, there are only few occasions in the simulation where the maximum RoCoF value exceeds 1 Hz/s. Therefore, the anticipated 1 Hz/s protection threshold should be reassessed incorporating more flexibility in the protection settings in order to improve protection sensitivity against real islanding events in future grids.

6.1.2 Formulation of the continuous real-time inertia estimation model

The continuous real-time estimation of power system inertia has been, for the first time, achieved during normal system operation using a Switching Markov Gaussian Model with real-time frequency measurements and less frequent generation dispatch data. The probability-based model can be trained to learn the features that inter-relate historical steady-state frequency and system inertia derived from generation dispatch. Using this model, the real-time system inertia can be estimated conditionally on the observed small-scale and "normal" frequency variations. Unlike other methods that use Swing Equation or recursive state estimation, this approach does not rely on the occurrence of a disturbance and is capable of formulating the hidden variables/states (such as the real-time system control and regulation mechanisms) that exist but cannot be directly measured over time in dynamic system operation.

A fourth-order 13-component Switching Markov Gaussian Model has been identified as the continuous real-time inertia estimation model for the GB power system and is capable of generating inertia estimates on a five-minutes' basis. Formulation of the

probability model using changes of frequency and changes of inertia was based on the correlation analysis using historical frequency data on a 20 ms reporting rate and inertia information derived from historical generation dispatch data on a 5 minutes resolution. A series of training processes have been carried out to choose the optimum constituent elements for the model to profile the relationship between the selected changes of frequency and changes of inertia that result in minimum estimation errors. The training data set included the frequency and generation dispatch data taken during normal operating conditions in the 100 days randomly selected from the past two consecutive years. The selection of the methods' parameters started with the number of Gaussian components where the full type covariance matrix has been chosen to minimise the errors comparing with the diagonal and spherical types. In order to further improve the representation of the trained model, Markov Chain has been introduced to the Gaussian Mixture Model where the mean squared error has been reduced by an average of 12.9%. There were two approaches proposed to draw inertia estimates from the sliced conditional distribution given by the real-time frequency variations: averaging over the entire sample slices and randomly selecting from the sample slices. The averaging approach in most cases produces smaller estimation error and would, therefore, be a preferred method to use in practice, especially with shorter calibration periods such as 30 minutes. However, the performance of applying the average selection approach does not preserve satisfactory result for longer calibration periods and further investigation would be required, for example defining additional comparison metrics, to make a better judgement about the estimation accuracy. With the robust justifications provided from the employment of statistical analysis criterion to select the methods' parameters, such as correlation, EM, BIC and stepwise regression, the frequency-inertia dependency can be expressed in greater detail and a more representative way.

Knowledge of the generation dispatch data increases the estimation accuracy over time. This is achieved through calibrating the real-time inertia estimates with the equivalent inertia constants derived from the generation dispatch. Due to the limited available data published on ELEXON, half an hour is the minimum time period

between updates of real-time generation dispatch data currently available, which defines the minimum calibration cycle for the developed model. This, however, reveals the value of the proposed continuous real-time inertia estimation model to provide visualisation of system inertia information and reference for the proactive control/protection actions, especially within the half an hour period. The simulation results show that the mean squared error can typically be maintained within 0.1 s^2 for 95% of the daily estimation if calibrated on a half-hourly basis (which has 21% less error compared with longer calibration cycles of up to 24 hours). Therefore, the proposed Switching Markov Gaussian Model is recommended to be calibrated every 30 minutes. However, further investigation is required to reduce the reliance on OCC to improve estimation accuracy, as well as introducing extra variables (e.g. rate of change of demand) for a more accurate representation of the dynamic relationship between frequency and inertia.

In the event of the input frequency measurements being lost, it is recommended to keep the input value to the proposed inertia estimation model the same as the last observed change of frequency until successful delivery of the next frequency data. Such a 'fail-safe' strategy gives a 6.5% lower mean squared error than inputting a change of frequency equal to zero. A maximum 10% variation from the system inertia level derived from generation dispatch data has been observed for a loss of input frequency measurements lasting for two hours.

The utilisation of averaged frequency variation from multiple PMU recordings located across the entire GB network has demonstrated the value over single frequency measurement to the application of the SMGM algorithm, and thus their value in inferring system conditions. It is recognised that: (i) single sources of data may present reliability concerns; (ii) the location of a single measurement point on the system will dictate the nature of the variations (and swings) of the frequency observed. Consequently, this work made use of frequency measurements averaged over three locations which reduces the estimation error by approximately 4% compared to using single frequency measurement. It is thereby considered that an averaged value better reflects true system-level conditions. Due to the fact that

system frequency variations are strongly correlated during normal operating conditions, the impact of a greater number of PMUs is not considered particularly significant for estimating system inertia constant during normal system operation while further investigation should be requested for the impact of the PMU positioning to the accuracy of the real-time inertia estimation. With the frequency data (on a 20 ms basis) input to the continuous real-time inertia estimation model being averaged over the 5-minute sample interval, the noise and latency effects are further minimised.

The proposed continuous real-time inertia estimation model can be trained to be applied in future power networks where the variations of system inertia would potentially pose system frequency stability issues. Such applications include early-stage system diagnostics, frequency-related protection, regulation of power reserve and synthetic inertia control and management. This attributes to the flexibility posed in its switching regimes coupled with the finite mixture model that allow the model to be able to accommodate the complexity and uncertainties in power system dynamics. Additionally, the model can be automatically re-trained and its performance (in terms of suitability and accuracy) could be continuously monitored by integrating within an overarching application management system in order to maintain estimation accuracy over longer term use.

6.1.3 Verification of the ability of adaptive protection schemes to enhance system stability and protection sensitivity

The hypothesis that adaptive protection schemes can enhance system stability and improve protection sensitivity has been tested and verified through simulations applying the proposed zonal, adaptive, DG anti-islanding protection scheme. It has been shown that by implementing the zonal adaptive protection settings, the sensitivity of RoCoF-based anti-islanding protection can be improved without increased risk of false tripping when subjected to large infeed loss. This is reflected

by an averaged 78% reduction in the non-detection risk of a real islanding event across the investigated GB network, in contrast to the fixed 1 Hz/s threshold proposed to be applied in the GB system. A further 5% reduction can be achieved if the time delay feature equipped with the fixed setting is disabled. Moreover, the robustness of the proposed adaptive DG anti-islanding protection has been proven to stay stable in fault ride through scenarios where phase-ground and phase–phase faults were tested at different locations. The non-detection risk calculated in this research work took into account of the zonal variations in frequency response and the proposed zonal adaptive settings, which presents more accurate risk analysis than previous work.

The proposed adaptive protection scheme is based on the use of three pre-defined settings groups that can be dynamically activated by the real-time inertia estimates generated from the proposed continuous real-time inertia estimation model. Each setting group has 11 zonal RoCoF settings that are derived from the off-line frequency response case studies where the relays in each zone adapt their settings in response to the real-time inertia estimates. This considers and highly reflects the differences in local frequency response as a result of the diversities in zonal generation and demand structure. Future power systems could benefit considerably from such adjustable protection settings for more enhanced network operation. The design that there are individual zonal setting sensitive to the variations in local frequency response in each adaptive protection setting group, is the first of its kind.

6.2 Future Work

The proposed continuous real-time inertia estimation model has been formulated based on the established dependency between steady state change of frequency and change of system inertia. However, as shown in the dependency analysis, the historical frequency and inertia (derived from generation dispatch) variations were not fully correlated. This raises a conjecture relating to whether or not there are some other variable(s) that affect the correlation. Moreover, the generation dispatch data used in the model training data set was restricted to the measurements taken at the

transmission level. With no visibility of the distribution level where embedded generation is ‘hidden’, the accuracy of the trained model to truly reflect system dynamics is limited. Therefore, the research can be extended to improve the estimation accuracy of the proposed continuous real-time inertia estimation model with multi-variable inputs rather than only frequency observations. Such variables may include the estimated amount of dynamic system loads with rotating mass (e.g. motors), demand side response (e.g. from electric vehicles), very small DGs that are embedded in distribution level, etc. Moreover, an equivalent system model should be used to explore various options and parameters for the proposed inertia estimation method. This way there is no limit to data availability and the true value of inertia is known so the other sources of error coming from the limited dispatch data can be ruled out.

This study only formulated a single model for the estimation of system inertia and used averaged values of frequency measurements taken at multiple locations. However, in a large system where zonal inertia variations could lead to different local frequency response, the zonal inertia can be a more appropriate index for advanced proactive actions, such as ancillary reserve planning and frequency-related adaptive protection schemes. Therefore, further investigation can be carried out on the estimation of zonal inertia with a single measurement taken for the estimation of system inertia given by variations in local frequency response.

In order to implement the proposed continuous real-time inertia estimation model and the adaptive protection scheme into practical power systems, standard of the schematic implementation, agreement on network protocols and data sharing among the system operators should all be developed and arranged. These could reduce the risk of undesired deterioration of system performance and the failure in realising the state-of-the-art system practices. Moreover, the specifics for this application, such as the data types that would need to be added to the utility probes and the devices that feature certain functions should also be taken into consideration.

References

[1] National Grid, "Future Energy Scenarios - UK gas and electricity transmission," July 2015.

[2] National Grid. *Electricity Ten Year Statement 2014*. Available: http://www2.nationalgrid.com/UK/Industry-information/Future-of-Energy/Electricity-Ten-Year-Statement/, last visit: 19/04/2016

[3] National Grid, "NETS Security and Quality of Supply Standard," 05 March 2012 2012.

[4] Charles River Associates, "Primer on demand side management: With an emphasis on price-responsive programs" 2005.

[5] D. P. Chassin, Z. Huang, M. K. Donnelly, C. Hassler, E. Ramirez, and C. Ray, "Estimation of WECC system inertia using observed frequency transients," *Power Systems, IEEE Transactions on*, vol. 20, pp. 1190-1192, 2005.

[6] P. Wall and V. Terzija, "Simultaneous Estimation of the Time of Disturbance and Inertia in Power Systems," *Power Delivery, IEEE Transactions on*, vol. PP, pp. 1-14, 2014.

[7] J. H. Chow, A. Chakrabortty, L. Vanfretti, and M. Arcak, "Estimation of Radial Power System Transfer Path Dynamic Parameters Using Synchronized Phasor Data," *Power Systems, IEEE Transactions on*, vol. 23, pp. 564-571, 2008.

[8] F. Lingling, M. Zhixin, and Y. Wehbe, "Application of Dynamic State and Parameter Estimation Techniques on Real-World Data," *Smart Grid, IEEE Transactions on*, vol. 4, pp. 1133-1141, 2013.

[9] X. Cao, I. Abdulhadi, A. Emhemed, C. Booth, and G. Burt, "Evaluation of the impact of variable system inertia on the performance of frequency based protection," presented at the DPSP, 2014.

[10] F. Gonzalez-Longatt, E. Chikuni, and E. Rashayi, "Effects of the Synthetic Inertia from wind power on the total system inertia after a frequency disturbance," in *Industrial Technology (ICIT), 2013 IEEE International Conference on*, 2013, pp. 826-832.

[11] Y. Jun, C. Liuchen, and C. Diduch, "A New Adaptive Logic Phase-Shift Algorithm for Anti-Islanding Protections in Inverter-Based DG Systems," in *Power Electronics Specialists Conference, 2005. PESC '05. IEEE 36th*, 2005, pp. 2482-2486.

[12] A. Saffarian and M. Sanaye-Pasand, "Enhancement of Power System Stability Using Adaptive Combinational Load Shedding Methods," *Power Systems, IEEE Transactions on*, vol. 26, pp. 1010-1020, 2011.

[13] H. Ying-Yi and C. Po-Hsuang, "Genetic-Based Underfrequency Load Shedding in a Stand-Alone Power System Considering Fuzzy Loads," *Power Delivery, IEEE Transactions on*, vol. 27, pp. 87-95, 2012.

[14] U. Rudez and R. Mihalic, "Monitoring the First Frequency Derivative to Improve Adaptive Underfrequency Load-Shedding Schemes," *Power Systems, IEEE Transactions on*, vol. 26, pp. 839-846, 2011.

[15] H. Samet and M. Rashidi, "Coordinated under frequency load and capacitor shedding for bulk power systems," *Generation, Transmission & Distribution, IET*, vol. 7, pp. 799-812, 2013.

[16] H. Ying-Yi and W. Shih-Fan, "Multiobjective Underfrequency Load Shedding in an Autonomous System Using Hierarchical Genetic Algorithms," *Power Delivery, IEEE Transactions on*, vol. 25, pp. 1355-1362, 2010.
[17] X.Cao, I. Abdulhadi, A. Emhemed, C. Booth, and G. Burt, "Evaluation of the impact of variable system inertia on the performance of frequency based protection," in *Developments in Power System Protection (DPSP 2014), 12th IET International Conference on*, 2014, pp. 1-6.
[18] A. Dyśko, I. Abdulhadi, X. Li, and D. C. Booth, "Technical Report : Assessment of Risks Resulting from the Adjustment of ROCOF Based Loss of Mains Protection Settings " University of Strathclyde2013.
[19] National Grid Working Groups, "Frequency Changes during large disturbance and their impact on the total system," 15 August 2013 2013.
[20] R. M. Tumilty, "A Study of Adaptive Protection Methods for Future Electricity Distribution Systems," Ph.D, University of Strathclyde, 2013.
[21] I. Abdulhadi, "Facilitating the Validation of Adaptive Power System Protection through Formal Scheme Modelling and Performance Verification," Ph.D, University of Strathclyde, Glasgow, 2013.
[22] P. Kundur, J. Paserba, V. Ajjarapu, G. Andersson, A. Bose, C. Canizares, *et al.*, "Definition and classification of power system stability IEEE/CIGRE joint task force on stability terms and definitions," *Power Systems, IEEE Transactions on*, vol. 19, pp. 1387-1401, 2004.
[23] "Large frequency disturbances: analysis and modelling needs," in *Power Engineering Society 1999 Winter Meeting, IEEE*, 1999, pp. 554-558 vol.1.
[24] J. Machowski, J. W. Bialek, and J. R. Bumby, *Power System Dynamics - Stability and Control*, Second ed.: John Wiley & Sons, Ltd, 2008.
[25] National Grid, "The Grid Code Issue 5 Revision 14," 26 August 2015.
[26] The Union for the Co-ordination of Transmission of Electricity (UCTE) (2004). *Continental Europe Operation Handbook - Policy1: Load-Frequency Control and Performance* Available: https://www.entsoe.eu/fileadmin/user_upload/_library/publications/entsoe/Operation_Handbook/Policy_1_final.pdf, last visit: 19/04/2016
[27] R. S. Pearmine, "Review of primary frequency control requirements on the GB power system against a background of increasing renewable generation," Brunel University 2006.
[28] D. P. Kothari, *Modern Power System Analysis*: McGraw-Hill Education (India) Pvt Limited, 2011.
[29] North American Electric Reliability Corporation (NERC), "Frequency Response Standard Background Document " Nov. 2012.
[30] P. Kundur, *Power System Stability and Control*: McGraw-Hill Inc., 1993.
[31] G. Shrinivasan, *Power System Analysis*: Technical Publications, 2009.
[32] J. Grainger and W. Stevenson, *Power System Analysis*: New York, 1994.
[33] P. Tielens and D. Van Hertem, "Grid Inertia and Frequency Control in Power Systems with High Penetration of Renewables," *status: published*, 2012.
[34] U. Rudez and R. Mihalic, "Analysis of Underfrequency Load Shedding Using a Frequency Gradient," *Power Delivery, IEEE Transactions on*, vol. 26, pp. 565-575, 2011.

[35] J. Undrill, "Power and Frequency Control as it Relates to Wind-Powered Generation," Dec. 2010.
[36] M. Peydayesh and R. Baldick, "The Effects of Very Fast Response to Frequency Fluctuation," in *USAEE/IAEE North American Conference*, Taxes, 2012.
[37] B. H. Chowdhury and S. Rahman, "A review of recent advances in economic dispatch," *Power Systems, IEEE Transactions on*, vol. 5, pp. 1248-1259, 1990.
[38] National Grid, "Ancillary Service Settlement Guide: Mandatory Frequency Response," 2009.
[39] National Grid. Available: http://www2.nationalgrid.com/uk/services/balancing-services/frequency-response/mandatory-frequency-response/, last visit: 19/04/2016
[40] National Grid Frequency Response Workshop, "Frequency Response - Workgroup Consultation," 2012.
[41] National Grid, "Operating the Electricity Transmission Networks in 2020 " June 2011.
[42] National Grid, "Firm Frequency Response Market Information," April 2012.
[43] G. Hathaway. *Frequency Response*. Available: https://www.nationalgrid.com/NR/rdonlyres/A7EF1F6C-A3E8-4687-85A8-179E57503EE2/36189/02FrequencyRespone.pdf, last visit: 19/04/2016
[44] KiWiPower Demand Management, *A closer look at Frequency Response*, March 4, 2014. Available: http://demandresponseblog.com/tag/frequency-response/, last visit: 19/04/2016
[45] National Grid. *Frequency control by demand management*. Available: http://www2.nationalgrid.com/uk/services/balancing-services/frequency-response/frequency-control-by-demand-management/, last visit: 19/04/2016
[46] KEMA. Inc, "System Services International Review - Market Update," Nov 2011.
[47] National Grid, "UK Future Energy Scenario 2014."
[48] L. Fangxing, Q. Wei, S. Hongbin, W. Hui, W. Jianhui, X. Yan, *et al.*, "Smart Transmission Grid: Vision and Framework," *Smart Grid, IEEE Transactions on*, vol. 1, pp. 168-177, 2010.
[49] Western Link Project Website Available: http://www.westernhvdclink.co.uk/, last visit: 19/04/2016
[50] Department of Energy and Climate Change, "Electricity System: Assessment of Future Challenges - Annex," 9 Aug 2012.
[51] Q. Hu and F. Li, "Hardware design of smart home energy management system with dynamic price response," *Smart Grid, IEEE Transactions on*, vol. 4, pp. 1878-1887, 2013.
[52] V. Terzija, G. Valverde, C. Deyu, P. Regulski, V. Madani, J. Fitch, *et al.*, "Wide-Area Monitoring, Protection, and Control of Future Electric Power Networks," *Proceedings of the IEEE*, vol. 99, pp. 80-93, 2011.
[53] D. Novosel, V. Madani, B. Bhargava, V. Khoi, and J. Cole, "Dawn of the grid synchronization," *Power and Energy Magazine, IEEE*, vol. 6, pp. 49-60, 2008.
[54] L. Ramesh, S. P. Chowdhury, and S. Chowdhury, "Wide area monitoring protection and control - A comprehensive application review," in

Developments in Power System Protection (DPSP 2010). Managing the Change, 10th IET International Conference on, 2010, pp. 1-4.

[55] J. De La Ree, V. Centeno, J. S. Thorp, and A. G. Phadke, "Synchronized Phasor Measurement Applications in Power Systems," *Smart Grid, IEEE Transactions on,* vol. 1, pp. 20-27, 2010.

[56] M. G. Adamiak, A. P. Apostolov, M. M. Begovic, C. F. Henville, K. E. Martin, G. L. Michel, *et al.*, "Wide Area Protection-Technology and Infrastructures," *Power Delivery, IEEE Transactions on,* vol. 21, pp. 601-609, 2006.

[57] E. Loukarakis, I. Margaris, and P. Moutis, "Frequency control support and participation methods provided by wind generation," in *Electrical Power & Energy Conference (EPEC), 2009 IEEE*, 2009, pp. 1-6.

[58] National Grid Frequency Response Workgroup, "GC022 - Frequency Response," 2013.

[59] M. Kayikci and J.V.Milanovic, "Dynamic Contribution of DFIG-Based Wind Plants to System Frequency Disturbances," *Power Systems, IEEE Transactions on,* vol. 24, pp. 859-867, 2009.

[60] G. Lalor, A. Mullane, and M. O'Malley, "Frequency control and wind turbine technologies," *Power Systems, IEEE Transactions on,* vol. 20, pp. 1905-1913, 2005.

[61] J. Morren, J. Pierik, and S. W. H. de Haan, "Inertial response of variable speed wind turbines," *Electric Power Systems Research,* vol. 76, pp. 980-987, 2006.

[62] R. Doherty, A. Mullane, G. Nolan, D. J. Burke, A. Bryson, and M. O'Malley, "An Assessment of the Impact of Wind Generation on System Frequency Control," *Power Systems, IEEE Transactions on,* vol. 25, pp. 452-460, 2010.

[63] H. D. Anca, I. Florin, B. Frede, and H. L. Lars, "Review of Contemporary Wind Turbine Concepts and their Market Penetration," *Journal of Wind Engineering & Industrial Aerodynamics,* vol. 28, pp. 247-263, 2004.

[64] B. Davito, H. Tai, and R. Uhlaner, "The smart grid and the promise of demand-side management," January 2010.

[65] L. Ning and D. J. Hammerstrom, "Design Considerations for Frequency Responsive Grid Friendly^{TM} Appliances," in *Transmission and Distribution Conference and Exhibition, 2005/2006 IEEE PES*, 2006, pp. 647-652.

[66] Y. Mu, J. Wu, J. Ekanayake, N. Jenkins, and H. Jia, "Primary Frequency Response From Electric Vehicles in the Great Britain Power System," *Smart Grid, IEEE Transactions on,* vol. 4, pp. 1142-1150, 2013.

[67] J. A. Lopes, F. J. Soares, and P. M. R. Almeida, "Integration of Electric Vehicles in the Electric Power System," *Proceedings of the IEEE,* vol. 99, pp. 168-183, 2011.

[68] K. Samarakoon, J. Ekanayake, and N. Jenkins, "Investigation of Domestic Load Control to Provide Primary Frequency Response Using Smart Meters," *Smart Grid, IEEE Transactions on,* vol. 3, pp. 282-292, 2012.

[69] R. A. Walling, R. Saint, R. C. Dugan, J. Burke, and L. A. Kojovic, "Summary of Distributed Resources Impact on Power Delivery Systems," *Power Delivery, IEEE Transactions on,* vol. 23, pp. 1636-1644, 2008.

[70] "IEEE Application Guide for IEEE Std 1547, IEEE Standard for Interconnecting Distributed Resources with Electric Power Systems," *IEEE Std 1547.2-2008*, pp. 1-207, 2009.
[71] A. Dyśko, G. Burt, and R. Bugdał, "Novel Protection Methods for Active Distribution Networks with High Penetrations of Distributed Generation Year II Report," 2006.
[72] Ofgem, "The distribution code and the guide to the distribution code of licensed distribution network operation of Great Britain," August 2014.
[73] "IEEE Guide for the Application of Protective Relays Used for Abnormal Frequency Load Shedding and Restoration," *IEEE Std C37.117-2007*, pp. 1-55, 2007.
[74] V. Terzija, "Adaptive underfrequency load shedding based on the magnitude of the disturbance estimation," *Power Systems, IEEE Transactions on*, vol. 21, pp. 1260-1266, 2006.
[75] J. F. Conroy and R. Watson, "Frequency Response Capability of Full Converter Wind Turbine Generators in Comparison to Conventional Generation," *Power Systems, IEEE Transactions on*, vol. 23, pp. 649-656, 2008.
[76] R. Pearmine, Y. H. Song, and A. Chebbo, "Influence of wind turbine behaviour on the primary frequency control of the British transmission grid," *Renewable Power Generation, IET*, vol. 1, pp. 142-150, 2007.
[77] S. Sharma, H. Shun-Hsien, and N. D. R. Sarma, "System Inertial Frequency Response estimation and impact of renewable resources in ERCOT interconnection," in *Power and Energy Society General Meeting, 2011 IEEE*, 2011, pp. 1-6.
[78] National Grid, *Enhanced Frequency Control Capability (EFCC) Project*. Available: http://www2.nationalgrid.com/Mediacentral/UK-Press-releases/2014/%C2%A312-6million-boost-for-two-innovative-National-Grid-projects/, last visit: 19/04/2016
[79] Scottish Power Energy Network, *Visualisation of Real Time System Dynamics using Enhanced Monitoring (VISOR) Project*. Available: http://www.spenergynetworks.co.uk/pages/visor.asp, last visit: 19/04/2016
[80] Ofgem, *Kent Active System Management (KASM)*. Available: https://www.ofgem.gov.uk/publications-and-updates/low-carbon-networks-fund-submission-uk-power-networks-%E2%80%93-kasm, last visit: 19/04/2016
[81] National Grid, "Electricity Ten Year Statement 2013," Nov. 2013.
[82] National Grid. *2011 National Electricity Transmission System (NETS) Seven Year Statement*.
[83] M. Nagpal, A. Moshref, G. K. Morison, and P. Kundur, "Experience with testing and modelling of gas turbines," in *Power Engineering Society Winter Meeting, 2001. IEEE*, 2001, pp. 652-656 vol.2.
[84] P. M. Anderson and M. Mirheydar, "A low-order system frequency response model," *Power Systems, IEEE Transactions on*, vol. 5, pp. 720-729, 1990.
[85] National Grid, "Report of the National Grid Investigation into the Frequency Deviation and Automatic Demand Disconnection that occurred on the 27th May 2008," February 2009.

[86] J. D. Glover, M. S. Sarma, and T. J. Overbye, *power system analysis and design*: Cengage Learning; 5th edition (January 3, 2011).
[87] X. Jun and A. Dysko, "UK transmission system modelling and validation for dynamic studies," in *Innovative Smart Grid Technologies Europe (ISGT EUROPE), 2013 4th IEEE/PES*, 2013, pp. 1-5.
[88] IEEE Task Force on Load Representation for Dynamic Performance, "Load representation for dynamic performance analysis [of power systems]," *Power Systems, IEEE Transactions on*, vol. 8, pp. 472-482, 1993.
[89] V. Terzija, P. Regulski, L. P. Kunjumuhammed, B. C. Pal, G. Burt, I. Abdulhadi, *et al.*, "FlexNet wide area monitoring system," in *Power and Energy Society General Meeting, 2011 IEEE*, 2011, pp. 1-7.
[90] Available: http://www.bmreports.com/, last visit: 19/04/2016
[91] National Grid, "Electricity Ten Year Statement 2012."
[92] S. K. Merz, "Growth scenarios for UK renewables generation and imlications for future developments and operation of electricity networks," BERR Publication URN 08/1021 June 2008 2008.
[93] The Union for the Co-ordination of Transmission of Electricity (UCTE), "P1 – Policy 1: Load-Frequency Control and Performance [C]," 2009.
[94] H. Motulsky and A. Christopoulos, *Fitting Models to Biological Data Using Linear and Nonlinear Regression: A Practical Guide to Curve Fitting*: Oxford University Press, USA, 2004.
[95] Z. Ying, K. Xiaoning, J. Zaibin, W. Zengchao, and S. Jiale, "A Novel Distance Protection Algorithm for the Phase-Ground Fault," *Power Delivery, IEEE Transactions on*, vol. 29, pp. 1718-1725, 2014.
[96] K. Seethalekshmi, S. N. Singh, and S. C. Srivastava, "Synchrophasor Assisted Adaptive Reach Setting of Distance Relays in Presence of UPFC," *Systems Journal, IEEE*, vol. 5, pp. 396-405, 2011.
[97] M. Jin and T. S. Sidhu, "Adaptive load encroachment prevention scheme for distance protection," *Electric Power Systems Research*, vol. 78, pp. 1693-1700, 2008.
[98] M. J. Reddy and D. K. Mohanta, "Adaptive-neuro-fuzzy inference system approach for transmission line fault classification and location incorporating effects of power swings," *Generation, Transmission & Distribution, IET*, vol. 2, pp. 235-244, 2008.
[99] H. Khorashadi Zadeh and Z. Li, "Adaptive load blinder for distance protection," *International Journal of Electrical Power & Energy Systems*, vol. 33, pp. 861-867, 2011.
[100] L. Xiangning, L. Zhengtian, K. Shuohao, and G. Yan, "Theoretical Fundamentals and Implementation of Novel Self-Adaptive Distance Protection Resistant to Power Swings," *Power Delivery, IEEE Transactions on*, vol. 25, pp. 1372-1383, 2010.
[101] S. M. Brahma and A. A. Girgis, "Development of adaptive protection scheme for distribution systems with high penetration of distributed generation," *Power Delivery, IEEE Transactions on*, vol. 19, pp. 56-63, 2004.
[102] P. H. Shah and B. R. Bhalja, "New adaptive digital relaying scheme to tackle recloser-fuse miscoordination during distributed generation interconnections," *Generation, Transmission & Distribution, IET*, vol. 8, pp. 682-688, 2014.

[103] J. C. M. Vieira, W. Freitas, X. Wilsun, and A. Morelato, "Efficient coordination of ROCOF and frequency relays for distributed generation protection by using the application region," *Power Delivery, IEEE Transactions on,* vol. 21, pp. 1878-1884, 2006.
[104] G. D. Rockefeller, C. L. Wagner, J. R. Linders, K. L. Hicks, and D. T. Rizy, "Adaptive transmission relaying concepts for improved performance," *Power Delivery, IEEE Transactions on,* vol. 3, pp. 1446-1458, 1988.
[105] S. H. Horowitz, A. G. Phadke, and J. S. Thorp, "Adaptive transmission system relaying," *Power Delivery, IEEE Transactions on,* vol. 3, pp. 1436-1445, 1988.
[106] S. Horowitz, D. Novosel, V. Madani, and M. Adamiak, "System-wide Protection," *Power and Energy Magazine, IEEE,* vol. 6, pp. 34-42, 2008.
[107] X.Cao, I. Abdulhadi, S. Bruce, C. Booth, and G. Burt, "Switching Markov Gaussian Models for Dynamic Power System Inertia Estimation," *IEEE Transactions on Power Systems,* vol. PP, pp. 1-10, Dec. 2015.
[108] P. M. Ashton, C. S. Saunders, G. A. Taylor, A. M. Carter, and M. E. Bradley, "Inertia Estimation of the GB Power System Using Synchrophasor Measurements," *IEEE Transactions on Power Systems,* vol. 30, pp. 701-709, Mar. 2015.
[109] P. M. Ashton, G. A. Taylor, A. M. Carter, M. E. Bradley, and W. Hung, "Application of phasor measurement units to estimate power system inertial frequency response," in *Power and Energy Society General Meeting (PES), 2013 IEEE,* 2013, pp. 1-5.
[110] P. Wall, F. Gonzalez-Longatt, and V. Terzija, "Estimation of generator inertia available during a disturbance," in *Power and Energy Society General Meeting, 2012 IEEE*, 2012, pp. 1-8.
[111] T. Inoue, H. Taniguchi, Y. Ikeguchi, and K. Yoshida, "Estimation of power system inertia constant and capacity of spinning-reserve support generators using measured frequency transients," *Power Systems, IEEE Transactions on,* vol. 12, pp. 136-143, 1997.
[112] G. Song and J. Bialek, "Synchronous machine inertia constants updating using Wide Area Measurements," in *Innovative Smart Grid Technologies (ISGT Europe), 2012 3rd IEEE PES International Conference and Exhibition on*, 2012, pp. 1-7.
[113] H. Zhenyu, D. Pengwei, D. N. Kosterev, and Y. Bo, "Application of extended Kalman filter techniques for dynamic model parameter calibration," in *Power & Energy Society General Meeting, 2009. PES '09. IEEE*, 2009, pp. 1-8.
[114] K. Kalsi, S. Yannan, H. Zhenyu, D. Pengwei, R. Diao, K. K. Anderson, *et al.*, "Calibrating multi-machine power system parameters with the extended Kalman filter," in *Power and Energy Society General Meeting, 2011 IEEE*, 2011, pp. 1-8.
[115] D. Curran-Everett, "Explorations in statistics: hypothesis tests and P values," *Advances in Physiology Education,* vol. 33, pp. 81-86, 2009.
[116] ELEXON. [Online]. Available: https://www.elexonportal.co.uk/article/view/7324?cachebust=p5bbmvxyui, last visit: 19/04/2016

[117] H. Xiaofei, C. Deng, S. Yuanlong, B. Hujun, and H. Jiawei, "Laplacian Regularized Gaussian Mixture Model for Data Clustering," *Knowledge and Data Engineering, IEEE Transactions on*, vol. 23, pp. 1406-1418, 2011.
[118] G. McLachlan and D. Peel, *Finite Mixture Models*: Wiley, 2004.
[119] J. B. Ekanayake, N. Jenkins, and G. Strbac. (2008) Frequency Response From Wind Turbines. *Wind Engineering*. 573-586. Available: http://multi-science.metapress.com/content/82v333372668x067/fulltext.pdf, last visit: 19/04/2016
[120] D. J. MacKay, *Information theory, inference and learning algorithms*: Cambridge university press, 2003.
[121] G. J. McLachlan and P. David, *Finite mixture models*: New York : Wiley, 2000.
[122] B. S. Everitt and G. Dunn, *Applied Multivariate Data Analysis*: Wiley, 2001.
[123] S. S. Venkatesh, *The Theory of Probability-Explorations and Applications*: Cambridge University Press, 2012.
[124] P. J. Brockwell and R. A. Davis, *Time Series: Theory and Methods*: Springer, 2009.
[125] J. Miles, *Applying regression & correlation : a guide for students and researchers*: London ; Thousand Oaks, Calif. : Sage Publications, 2001.
[126] N. Wermuth and D. R. Cox, "Statistical Dependence and Independence," in *Encyclopedia of Biostatistics*, ed: John Wiley & Sons, Ltd, 2005.
[127] C. M. Bishop. (2003). *Latent Variables, Mixture Models and EM*. Available: https://cw.fel.cvut.cz/wiki/_media/courses/a4b33rpz/2010.12.10-em-bishop.pdf
[128] D. Reynolds, *Encyclopedia of Biometric Recognition - Gaussian Mixture Models*: Springer, 2008.
[129] C. M. Bishop, *Pattern recognition and machine learning* vol. 1: springer, 2006.
[130] A. P. Dempster, N. M. Laird, and D. B. Rubin, "Maximum Likelihood from Incomplete Data via the EM Algorithm," *Journal of the Royal Statistical Society. Series B*, vol. 39, 1977.
[131] S. Konishi, *Information criteria and statistical modelling [internet resource]*: New York ; London : Springer, 2007.
[132] K. Hirose, S. Kawano, S. Konishi, and M. Ichikawa4, "Bayesian Information Criterion and Selection of the Number of Factors in Factor Analysis Models," *Journal of Data Science*, vol. 9, pp. 261-270, April 2011.
[133] R. E. Kass and A. E. Raftery, "Bayes factors," *Journal of the american statistical association*, vol. 90, pp. 773-795, 1995.
[134] V. c. Šmídl and A. Quinn, *The variational Bayes method in signal processing [internet resource]*: Berlin ; New York : Springer, 2006.
[135] I. Murray and R. P. Adams, "Slice sampling covariance hyperparameters of latent Gaussian models," in *Advances in Neural Information Processing Systems*, 2010, pp. 1732-1740.
[136] R. M. Neal, "Slice Sampling," *The Annals of Statistics*, vol. 31, pp. 705-767, 2003.
[137] L. Saul and F. Pereira, "Aggregate and mixed-order Markov models for statistical language processing," in *Proceedings of the Second Conference on Empirical Methods in Natural Language Processing* 1997, pp. 81-89.

[138] S. Fariaa and G. Soromenhob, "Fitting mixtures of linear regressions," *Journal of Statistical Computation and Simulation*, vol. 80, Feb. 2010.
[139] S. Frühwirth-Schnatter, *Finite mixture and Markov switching models*: New York : Springer, 2006.
[140] Pennsylvania State University. *Stepwise regression*. Available: https://onlinecourses.science.psu.edu/stat501/node/88
[141] D. van Dijk, T. Teräsvirta, and P. H. Franses, "Smooth Transition Autoregressive Models — a Survey of Recent Developments," *Econometric Reviews*, vol. 21, pp. 1-47, 2002/01/04 2002.
[142] A. Timmermann, "Moments of Markov switching models," *Journal of Econometrics*, vol. 96, pp. 75-111, 2000.
[143] National Institute of Sttandards and Technology/Semiconductor Manufacturing Technology, *Engineering Statistics Handbook* Available: http://www.itl.nist.gov/div898/handbook/prc/section2/prc242.htm, last visit: 19/04/2016
[144] J. Cohen, *Statistical Power Analysis for the Behavioral Sciences*: L. Erlbaum Associates, 1988.
[145] Universitetet I Oslo, *Numerical Differentiation and Integration*. Available: http://www.uio.no/studier/emner/matnat/math/MAT-INF1100/h08/kompendiet/diffint.pdf, last visit: 19/04/2016
[146] S. J. Prince, *Computer vision: models, learning, and inference*: Cambridge University Press, 2012.
[147] W. Hung, G. Ray, and G. Stein. (26 Oct. 2012). *Frequency Changes during Large Disturbances WG*. Available: http://www.nationalgrid.com/NR/rdonlyres/D07952E0-2B58-426F-B61F-C77A239D3964/57270/Meeting1Presentation.pdf, last visit: 19/04/2016
[148] G. Vijayaraghavan, M. Brown, and M. Barnes, "8 - Electrical noise and mitigation," in *Practical Grounding, Bonding, Shielding and Surge Protection*, G. V. B. Barnes, Ed., ed Oxford: Newnes, 2004, pp. 102-131.
[149] M. P. Sanders and R. E. Ray, "Power line carrier channel & application considerations for transmission line relaying," in *50th Protective Relay Conference, Georgia Tech, May*, 1996.
[150] I. M. Dudurych, "Statistical analysis of frequency response of island power system under increasing wind penetration," in *Power and Energy Society General Meeting, 2010 IEEE*, 2010, pp. 1-6.
[151] F. Gonzalez-Longatt, "Impact of synthetic inertia from wind power on the protection/control schemes of future power systems: Simulation study," in *Developments in Power Systems Protection, 2012. DPSP 2012. 11th International Conference on*, 2012, pp. 1-6.
[152] M. F. M. Arani and E. F. El-Saadany, "Implementing Virtual Inertia in DFIG-Based Wind Power Generation," *Power Systems, IEEE Transactions on*, vol. 28, pp. 1373-1384, 2013.
[153] L. Yutian and L. Changgang, "Impact of large-scale wind penetration on transient frequency stability," in *Power and Energy Society General Meeting, 2012 IEEE*, 2012, pp. 1-5.
[154] E. M. Davidson, M. J. Dolan, G. W. Ault, and S. D. J. McArthur, "AuRA-NMS: An autonomous regional active network management system for EDF

energy and SP energy networks," in *Power and Energy Society General Meeting, 2010 IEEE*, 2010, pp. 1-6.
[155] A. Girgis and S. Brahma, "Effect of distributed generation on protective device coordination in distribution system," in *Power Engineering, 2001. LESCOPE '01. 2001 Large Engineering Systems Conference on*, 2001, pp. 115-119.
[156] F. T. Dai, "Impacts of distributed generation on protection and autoreclosing of distribution networks," in *Developments in Power System Protection (DPSP 2010). Managing the Change, 10th IET International Conference on*, 2010, pp. 1-5.
[157] M. Sanaye-Pasand and P. Jafarian, "Adaptive Protection of Parallel Transmission Lines Using Combined Cross-Differential and Impedance-Based Techniques," *Power Delivery, IEEE Transactions on*, vol. 26, pp. 1829-1840, 2011.
[158] W. Hui, K. K. Li, and K. P. Wong, "An Adaptive Multiagent Approach to Protection Relay Coordination With Distributed Generators in Industrial Power Distribution System," *Industry Applications, IEEE Transactions on*, vol. 46, pp. 2118-2124, 2010.
[159] J. Upendar, C. P. Gupta, and G. K. Singh, "Comprehensive Adaptive Distance Relaying Scheme for Parallel Transmission Lines," *Power Delivery, IEEE Transactions on*, vol. 26, pp. 1039-1052, 2011.
[160] Distribution Code Review Panel, "Progress of Distributed Generators in changing frequency protection settings to comply with ER G59/2," vol. -Ref. DCRP_12_02_04, ed.
[161] J. Berdy, P. G. Brown, J. G. Andrichak, and S. B. Wilkinson, " High speed reclosing system and machine consideration," GE.
[162] Y. Zhihong, A. Kolwalkar, Y. Zhang, D. Pengwei, and R. Walling, "Evaluation of anti-islanding schemes based on nondetection zone concept," *Power Electronics, IEEE Transactions on*, vol. 19, pp. 1171-1176, 2004.
[163] Distribution Code Review Panel, Available: http://www.dcode.org.uk/, last visit: 19/04/2016
[164] IEC, "IEC 61850: Communication networks and systems in substations," ed, 2003.
[165] X.Cao, I. Abdulhadi, C. Booth, and G. Burt, "Defining the role of wide area adaptive protection in future networks," in *Universities Power Engineering Conference (UPEC), 2012 47th International*, 2012, pp. 1-6.

Appendix A. Reduced GB Dynamic Model Data

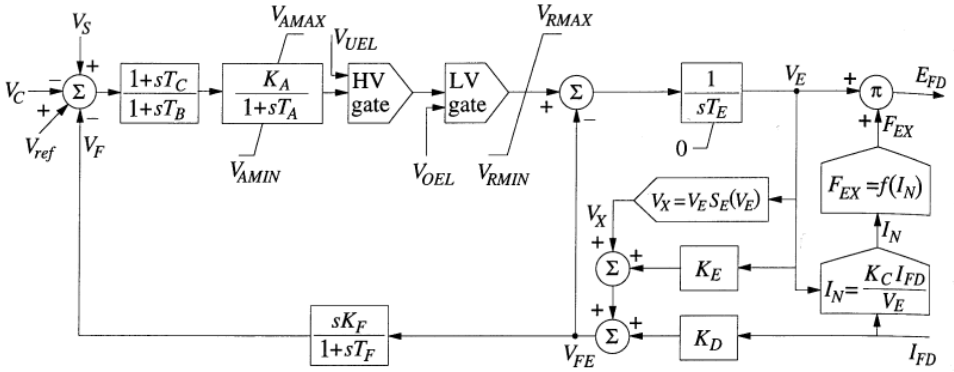

Figure A-1: IEEE standard AC1A exciter model [30]

Table A-1: IEEE type AC1A exciter and regulator data

Parameter	Representation	Value
K_a	Regulator gain	400
T_A	Regulator time constant [s]	0.02
T_B	Lag time constant [s]	0
T_C	Lead time constant [s]	0
K_F	Rate feedback gain	0.03
T_F	Rate feedback time constant [s]	1.0
K_E	Exciter constant related to field	1.0
T_E	Exciter time constant [s]	0.8
K_D	Demagnetizing factor	0.38

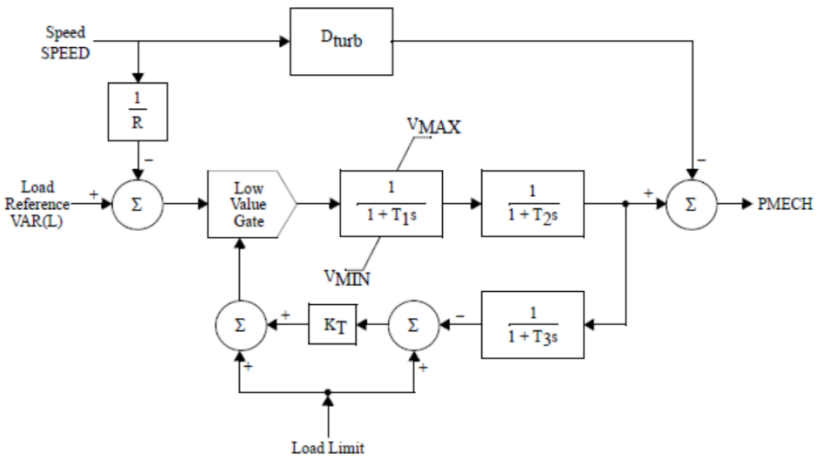

Figure A-2: GAST model [83]

Table A-2: Generic gas turbine and governing system data

Parameter	Representation	Value
R	Governor droop	0.084
T_1	Fuel system lag time constant 1 [s]	0.33
T_2	Fuel system lag time constant 2 [s]	2.0
T_3	Load limiter time constant [s]	2.0
K_T	Temperature control loop gain	2.0
V_{MAX}	Maximum value position	0.9
V_{MIN}	Minimum value position	0.2
D_{tur}	Turbine damping	0

Table A-3: Transformer Data

System parameter	Value
Transformer rating [MVA]	5000
Base operation frequency [Hz]	50
Positive sequence leakage reactance [pu]	0.0003
Copper losses [pu]	0.000001
Winding voltage [kV]	275/400

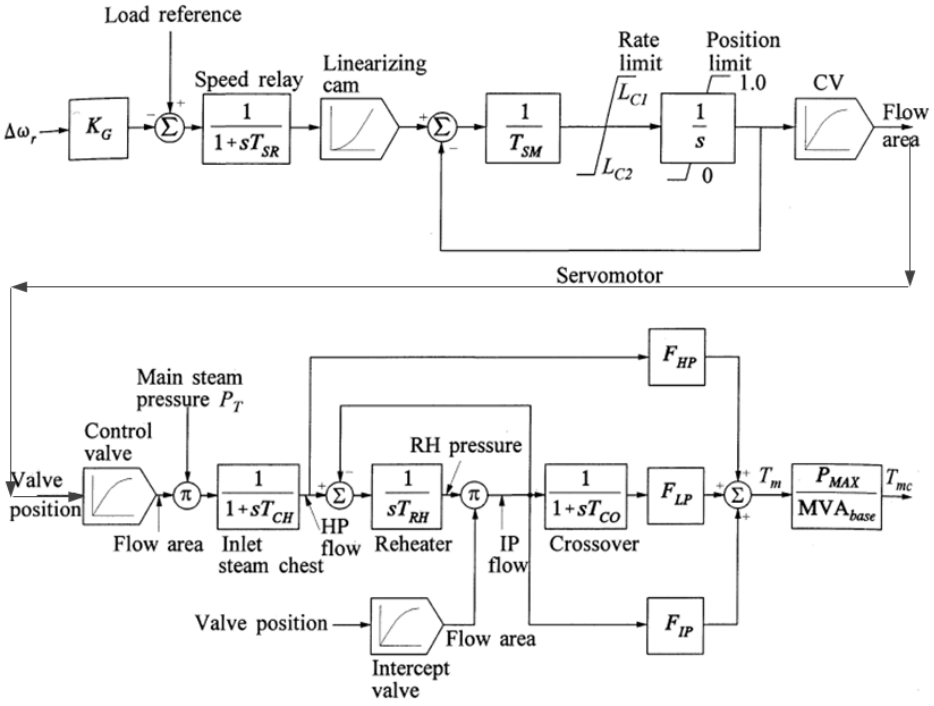

Figure A-3: Generic steam turbine and governing model [30]

Table A-4: Generic steam turbine and governing system data

Parameter	Representation	Value
K_G	Governor droop	0.035
T_{SR}	Speed relay time constant [s]	0.5
T_{SM}	Servomotor time constant [s]	0.2
L_{C1}	Opening rate limiter [pu/s]	0.1
L_{C2}	Closing rate limiter [pu/s]	-1.0
T_{CH}	Time Constant of Main Inlet Volumes and Steam Chest [s]	2.1
T_{RH}	Time Constant of Reheater [s]	7.5
T_{CO}	Time Constant of Crossover Piping and LP Inlet Volumes [s]	0.3
F_{HP}	Fraction of total turbine power generated by high pressure section	0.3
F_{IP}	Fraction of total turbine power generated by intermediate pressure section	0.2
F_{LP}	Fraction of total turbine power generated by low pressure section	0.5

Table A-5: Generator data

Parameter	Representation	Value
X_d	Synchronous Reactance	2.18
X_q		2.05
$X_d{}'$	Transient Reactance	0.329
$X_q{}'$		0.228
$X_d{}''$	Sub-transient Reactance	0.2420
$X_q{}''$		0.290
$T_{d0}{}'$	Transient OC Time Constant [s]	6.2286
$T_{q0}{}'$		0.85
$T_{d0}{}''$	Sub-transient OC Time Constant [s]	0.053
$T_{q0}{}''$		0.3304
X_l	Stator Leakage Inductance	0.130
R_a	Stator Resistance	0.002
K_C	Field Circuit Commutating Reactance	0.2
V_{RMAX}	Max Regulator Output	6.03
V_{RMIN}	Min Regulator Output	-5.43
V_{AMAX}	Max Regulator Internal Voltage	14.5
V_{AMIN}	Min Regulator Internal Voltage	-14.5
$SE(VE1)$	Saturation Voltage at VE1	0.1
$SE(VE2)$	Saturation Voltage at VE2	0.03

Table A-6: Equivalent transmission line data

Line Name	R (pu/m)	X_L (pu/m)	X_C (pu/m)
N1-N2	1.7E-06	2.2E-06	9.4E-05
N1-N3	5.8E-06	5.7E-06	1.1E-04
N2-N3	4.2E-06	3.4E-06	4.7E-04
N3-N4	3.3E-06	4.7E-06	7.7E-04
N4-S1	2.1E-06	6.1E-06	2.2E-03
S1-S2	1.5E-06	1.0E-05	3.9E-03
S2-S3	4.0E-07	4.3E-06	1.9E-03
S3-S4	2.4E-06	7.7E-06	1.6E-03
S3-S5	4.5E-06	1.2E-05	5.0E-04
S4-S5	2.1E-06	3.8E-06	2.4E-05
S4-S6	4.4E-06	6.8E-06	6.2E-05
S4-S7	1.5E-06	3.2E-06	5.7E-05
S5-S6	2.3E-06	3.0E-06	2.7E-05
S6-S7	2.9E-06	3.6E-06	2.9E-04

Appendix B. Maximum RoCoF Data for Case Studies in Chapter 3

Table B-1: RoCoF values for 1800MW loss in S2 under different system inertia constants

RoCoF (Hz/s) / H(s)	N1	N2	N3	N4	S1	S2	S3	S4	S5	S6	S7
7.00	0.10	0.10	0.10	0.09	0.08	0.08	0.08	0.08	0.08	0.09	0.09
6.50	0.11	0.11	0.11	0.10	0.08	0.09	0.09	0.09	0.09	0.10	0.10
6.00	0.12	0.12	0.12	0.11	0.09	0.10	0.09	0.10	0.10	0.11	0.11
5.50	0.13	0.13	0.13	0.12	0.10	0.11	0.10	0.11	0.11	0.12	0.12
5.00	0.15	0.15	0.15	0.13	0.11	0.12	0.11	0.12	0.12	0.13	0.13
4.50	0.17	0.17	0.17	0.15	0.12	0.14	0.13	0.14	0.14	0.15	0.15
4.00	0.20	0.19	0.19	0.17	0.14	0.16	0.15	0.16	0.16	0.17	0.17
3.50	0.23	0.23	0.22	0.20	0.16	0.19	0.17	0.19	0.18	0.20	0.20
3.00	0.28	0.27	0.27	0.23	0.19	0.22	0.20	0.22	0.22	0.24	0.24
2.50	0.34	0.34	0.33	0.29	0.24	0.28	0.25	0.28	0.27	0.30	0.30
2.00	0.44	0.44	0.43	0.37	0.30	0.39	0.32	0.36	0.35	0.39	0.39

Table B-2: RoCoF values for 1800MW loss in S6 under different system inertia constants

RoCoF (Hz/s) / H(s)	N1	N2	N3	N4	S1	S2	S3	S4	S5	S6	S7
7.00	0.16	0.16	0.16	0.15	0.13	0.10	0.09	0.10	0.10	0.10	0.10
6.50	0.17	0.17	0.17	0.16	0.14	0.11	0.10	0.11	0.11	0.11	0.11
6.00	0.19	0.19	0.19	0.18	0.16	0.12	0.11	0.12	0.12	0.12	0.12
5.50	0.21	0.21	0.20	0.19	0.17	0.13	0.12	0.13	0.13	0.13	0.13
5.00	0.23	0.23	0.23	0.22	0.19	0.15	0.13	0.14	0.14	0.15	0.15
4.50	0.26	0.26	0.26	0.24	0.21	0.17	0.15	0.17	0.16	0.17	0.16
4.00	0.30	0.30	0.30	0.28	0.24	0.19	0.17	0.20	0.18	0.19	0.19
3.50	0.35	0.35	0.35	0.33	0.28	0.23	0.19	0.24	0.21	0.23	0.22
3.00	0.42	0.42	0.42	0.39	0.33	0.27	0.23	0.30	0.25	0.30	0.26
2.50	0.52	0.52	0.52	0.48	0.41	0.33	0.29	0.39	0.34	0.40	0.33
2.00	0.68	0.68	0.67	0.62	0.52	0.43	0.37	0.51	0.47	0.54	0.47

Table B-3: RoCoF values for various size of infeed loss in S2 under 3 s system inertia

RoCoF (Hz/s) / ΔP	N1	N2	N3	N4	S1	S2	S3	S4	S5	S6	S7
300MW	0.04	0.04	0.04	0.04	0.03	0.03	0.03	0.04	0.04	0.04	0.04
500MW	0.07	0.07	0.07	0.06	0.05	0.06	0.05	0.06	0.06	0.07	0.07
800MW	0.12	0.12	0.12	0.10	0.08	0.09	0.08	0.10	0.10	0.11	0.11
1000MW	0.15	0.15	0.15	0.13	0.11	0.12	0.11	0.12	0.12	0.13	0.13
1320MW	0.20	0.20	0.20	0.17	0.14	0.16	0.14	0.17	0.16	0.18	0.18
1800MW	0.28	0.27	0.27	0.23	0.19	0.22	0.20	0.22	0.22	0.24	0.24

Table B-4: RoCoF values for various size of infeed loss in S6 under 3 s system inertia

RoCoF (Hz/s) / ΔP	N1	N2	N3	N4	S1	S2	S3	S4	S5	S6	S7
300MW	0.04	0.04	0.04	0.04	0.04	0.03	0.02	0.03	0.03	0.03	0.03
500MW	0.08	0.08	0.08	0.07	0.06	0.05	0.04	0.06	0.05	0.05	0.05
800MW	0.12	0.12	0.12	0.12	0.10	0.08	0.07	0.09	0.07	0.09	0.08
1000MW	0.16	0.16	0.16	0.15	0.13	0.10	0.09	0.11	0.10	0.11	0.10
1320MW	0.29	0.29	0.29	0.27	0.23	0.19	0.16	0.21	0.17	0.20	0.18
1800MW	0.42	0.42	0.42	0.39	0.33	0.27	0.23	0.30	0.25	0.30	0.26

Table B-5: RoCoF values for various renewable penetration scenarios for 1800MW infeed loss in S2

RoCoF (Hz/s)	N1	N2	N3	N4	S1	S2	S3	S4	S5	S6	S7
X_{PL}= 30%											
Case 1	0.16	0.15	0.15	0.14	0.13	0.16	0.14	0.16	0.15	0.17	0.17
Case 2	0.21	0.21	0.21	0.18	0.16	0.13	0.13	0.15	0.15	0.16	0.16
Case 3	0.20	0.20	0.20	0.20	0.18	0.15	0.13	0.16	0.16	0.17	0.17
X_{PL}= 40%											
Case 1	0.17	0.17	0.17	0.15	0.16	0.20	0.17	0.20	0.19	0.22	0.21
Case 2	0.24	0.24	0.23	0.21	0.17	0.17	0.16	0.18	0.18	0.19	0.19
Case 3	0.24	0.24	0.24	0.22	0.19	0.14	0.14	0.17	0.17	0.19	0.19
X_{PL}= 50%											
Case 1	0.20	0.20	0.19	0.19	0.21	0.28	0.23	0.26	0.25	0.28	0.28
Case 2	0.28	0.27	0.27	0.23	0.19	0.22	0.20	0.22	0.22	0.24	0.24
Case 3	0.30	0.30	0.30	0.29	0.28	0.22	0.19	0.24	0.23	0.26	0.26
X_{PL}= 60%											
Case 1	0.40	0.40	0.38	0.32	0.33	0.48	0.36	0.42	0.41	0.46	0.46
Case 2	0.39	0.39	0.38	0.32	0.33	0.48	0.35	0.36	0.35	0.39	0.39
Case 3	0.35	0.35	0.34	0.29	0.32	0.45	0.28	0.29	0.28	0.32	0.31
X_{PL}= 70%											
Case 1	0.40	0.40	0.40	0.40	0.44	0.86	0.58	0.63	0.61	0.70	0.70
Case 2	0.39	0.39	0.38	0.32	0.36	0.53	0.38	0.43	0.42	0.48	0.48
Case 3	0.53	0.53	0.53	0.53	0.51	0.43	0.34	0.43	0.42	0.47	0.47

Table B-6: RoCoF values for various renewable penetration scenarios for 1800MW infeed loss in S6

RoCoF (Hz/s)	N1	N2	N3	N4	S1	S2	S3	S4	S5	S6	S7
X_{PL}= 30%											
Case 1	0.27	0.27	0.27	0.25	0.21	0.19	0.17	0.21	0.17	0.20	0.17
Case 2	0.28	0.28	0.28	0.27	0.24	0.18	0.15	0.18	0.18	0.19	0.19
Case 3	0.21	0.21	0.21	0.21	0.21	0.19	0.15	0.17	0.17	0.18	0.17
X_{PL}= 40%											
Case 1	0.32	0.32	0.31	0.29	0.24	0.24	0.22	0.28	0.23	0.27	0.21
Case 2	0.34	0.34	0.34	0.32	0.28	0.22	0.18	0.23	0.21	0.22	0.22
Case 3	0.25	0.25	0.25	0.25	0.25	0.23	0.17	0.21	0.20	0.21	0.21
X_{PL}= 50%											
Case 1	0.38	0.38	0.37	0.34	0.28	0.32	0.29	0.39	0.34	0.41	0.33
Case 2	0.42	0.42	0.42	0.39	0.33	0.27	0.23	0.30	0.25	0.30	0.26
Case 3	0.31	0.31	0.31	0.31	0.31	0.29	0.21	0.26	0.25	0.27	0.26
X_{PL}= 60%											
Case 1	0.46	0.46	0.45	0.41	0.35	0.46	0.42	0.59	0.55	0.64	0.57
Case 2	0.54	0.54	0.53	0.49	0.40	0.36	0.32	0.43	0.38	0.45	0.38
Case 3	0.40	0.40	0.40	0.40	0.40	0.37	0.27	0.33	0.33	0.35	0.34
X_{PL}= 70%											
Case 1	0.58	0.58	0.57	0.50	0.52	0.80	0.73	1.06	1.04	1.17	1.08
Case 2	0.72	0.71	0.70	0.63	0.51	0.54	0.48	0.67	0.64	0.73	0.66
Case 3	0.56	0.56	0.56	0.56	0.56	0.52	0.37	0.48	0.46	0.51	0.48

Appendix C. GB Offshore Wind Farm Zones

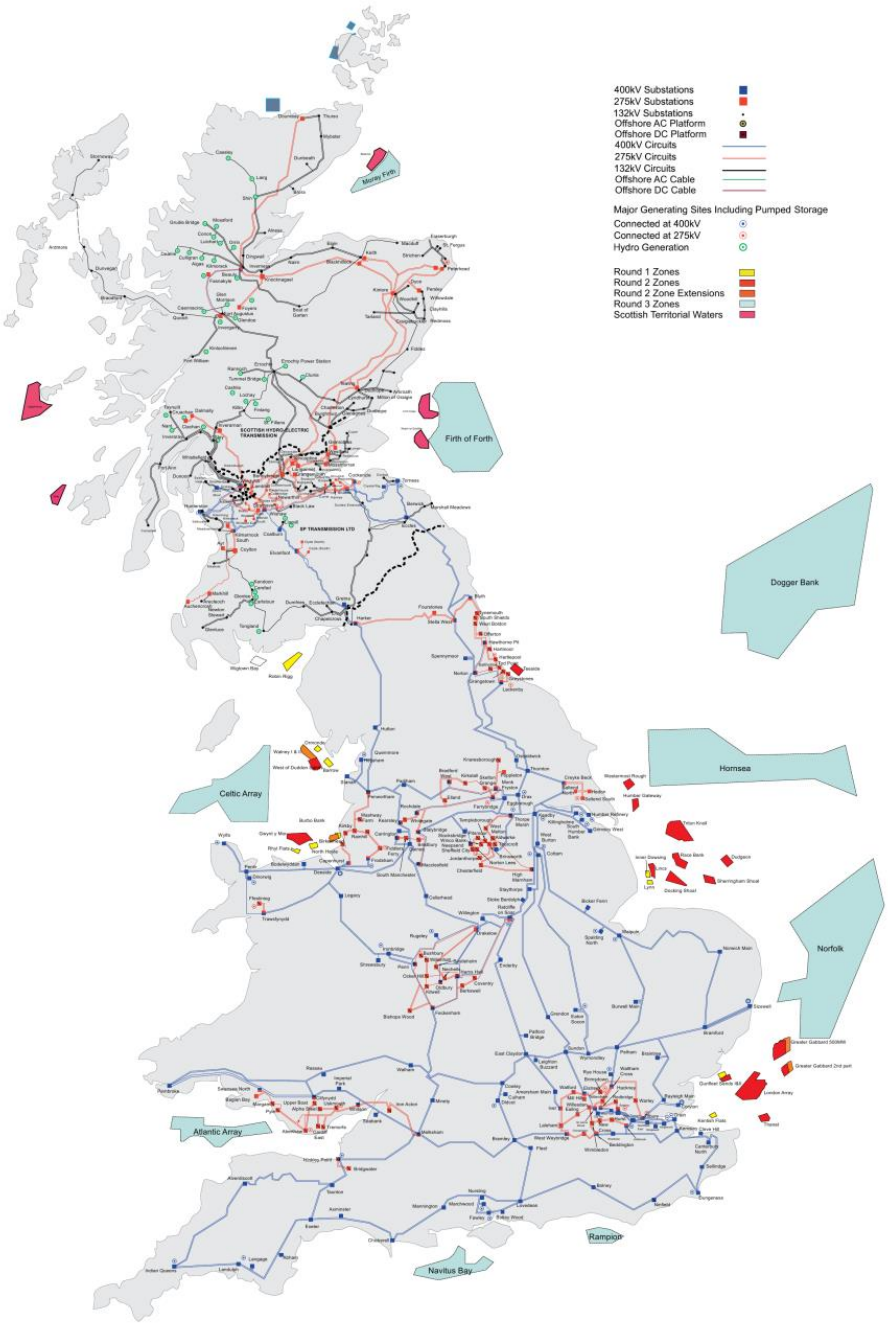

Figure C-1: GB offshore wind farm zones [2]

Appendix D. Statistics in SMGM

D.1 Covariance

$COV(f, H)$ is calculated as in equation below.

$$COV(f, H) = \frac{\sum_{i=1}^{n}[(f_i - f)(H_i - \bar{H})]}{(N-1)}$$

$$S_f = \sqrt{\frac{\sum_{i=1}^{N}(f_i - \bar{f})^2}{(N-1)}} \quad S_H = \sqrt{\frac{\sum_{i=1}^{N}(H_i - \bar{H})^2}{(N-1)}}$$

$\bar{f}/\bar{H}$ is the mean of the independent variable f$/H$,

N is the number of data points in the sample.

D.2 Bayesian Information Criterion

The following equation indicates that the optimal model for the data is selected as the one given minimum BIC value which also refers to the maximum likelihood. It is expressed as below where $p_i * log(n)$ stands for the penalty term introduced by BIC [132].

$$BIC = -2 * log(f_i(x_n|\widehat{\theta_i}) + p_i * log(n)$$

where

$f_i(x_n|\widehat{\theta_i})$ stands for the maximised likelihood of observation x_n given by the i^{th} candidate model

p_i stands for the number of free parameters to be estimated (e.g. p_i=3 for a 3-component GMM).

D.3 Stepwise selection criteria in MATLAB Statistics Toolbox

Table D-1 shows the default 'PEnter' and 'PRemove' values for different selection criteria where the proper model should have all the values allocate in between. SSE is sum squared error and AIC refers to the Akaike's Information Criterion. Rsquared is coefficient of determination. AdjRsquared is the modification of Rsquared that

adjusts for the number of explanatory terms in a model that increases only if the new term improves the model more than would be expected by chance. They all indicate how well the given data set fit a statistic model.

Table D-1: Stepwise selection criteria in MATLAB

Criterion	PEnter	PRemove	Compared against
SSE	0.05	<0.10	p-value for F-test
AIC	0	<0.01	Change in AIC
BIC	0	<0.01	Change in BIC
Rsquared	0.1	>0.05	Increase in R-squared
AdjRsquared	0	>-0.05	Increase in adjusted R-squared

Appendix E. Histograms of correlation coefficient between different forms of inertia and frequency

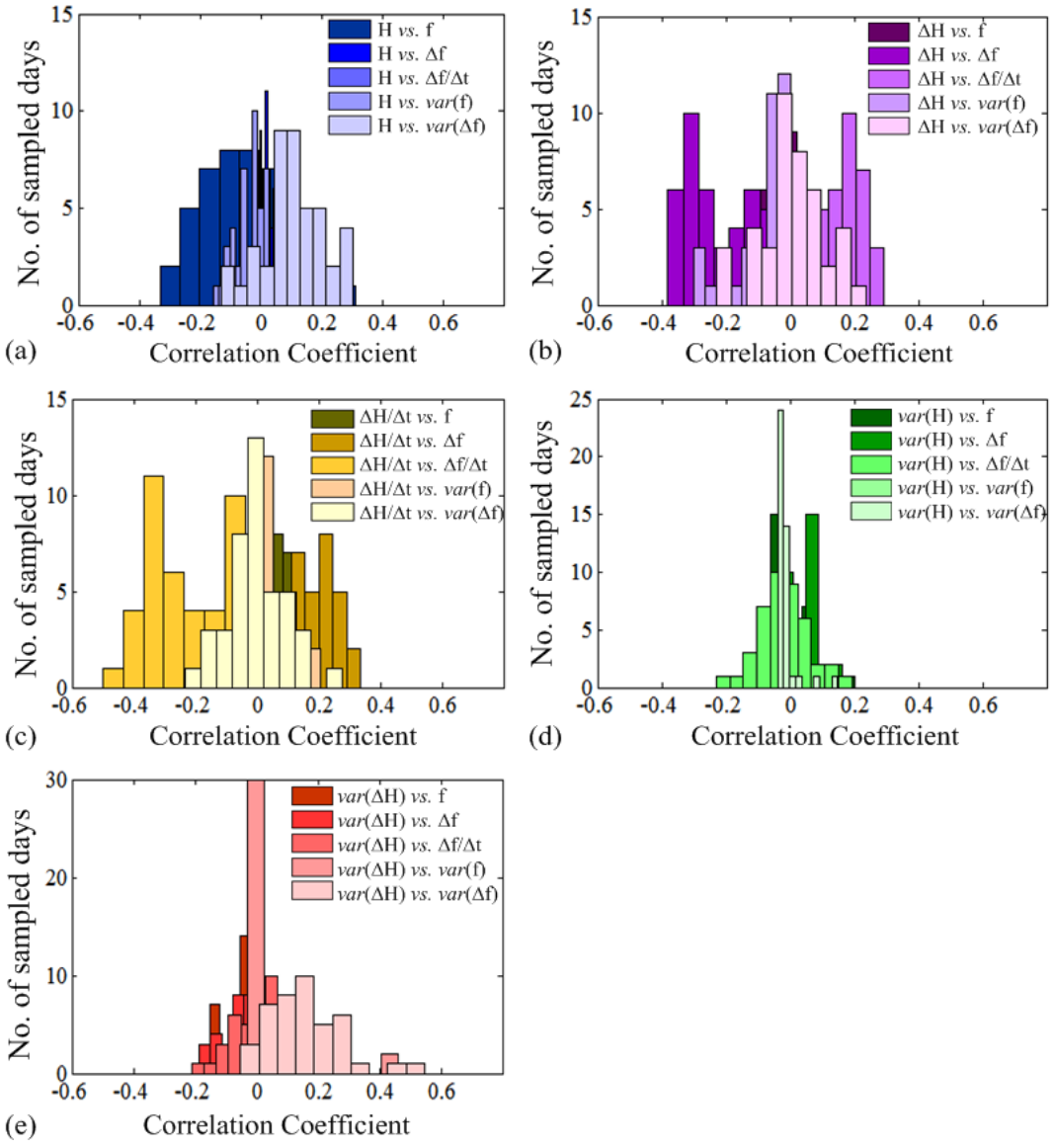

Figure E-1: Histogram of correlation coefficients of 25 combinations of frequency and inertia pair

Appendix F. Rise Assessment Data

Table F-1: Number of DGs in each defined study zone [160, 163]

Study Zone	N1	N2	N3	N4	S1	S2	S3	S4	S5	S6	S7
No. of SG in each zone	4	3	3	14	21	21	18	16	27	51	10

Table F-2: NDR over 3 load profiles – worst case scenario [18]

Setting Type	P_{LOM_1DG} PV controlled G	P_{LOM_1DG} Pf controlledG
0.12Hz+0ms	9.14E-09	0.00E+00
0.13Hz+0ms	1.22E-08	0.00E+00
0.2Hz+0ms	2.65E-08	0.00E+00
0.5Hz+0ms	1.04E-07	0.00E+00
1Hz+0ms	2.13E-07	0.00E+00
1Hz+500ms	2.37E-07	1.57E-10

Table F-3: Equations of 2nd-order polynomial fitting in zones

Study Zone	Equations
N1	$Prob = -1.339e^{-7} \cdot x^2 + 1.081e^{-6} \cdot x - 9.416e^{-8}$
N2	$Prob = -1.005e^{-7} \cdot x^2 + 8.105e^{-7} \cdot x - 7.066e^{-8}$
N3	$Prob = -1.005e^{-7} \cdot x^2 + 8.105e^{-7} \cdot x - 7.066e^{-8}$
N4	$Prob = -4.935e^{-7} \cdot x^2 + 3.808e^{-6} \cdot x - 3.328e^{-7}$
S1	$Prob = -6.897e^{-7} \cdot x^2 + 5.654e^{-6} \cdot x - 4.92e^{-7}$
S2	$Prob = -6.897e^{-7} \cdot x^2 + 5.654e^{-6} \cdot x - 4.92e^{-7}$
S3	$Prob = -5.999e^{-7} \cdot x^2 + 4.855e^{-6} \cdot x - 4.224e^{-7}$
S4	$Prob = -5.113e^{-7} \cdot x^2 + 4.297e^{-6} \cdot x - 3.738e^{-7}$
S5	$Prob = -9.171e^{-7} \cdot x^2 + 7.308e^{-6} \cdot x - 6.374e^{-7}$
S6	$Prob = -1.603e^{-6} \cdot x^2 + 1.370e^{-5} \cdot x - 1.193e^{-6}$
S7	$Prob = -3.348e^{-7} \cdot x^2 + 2.702e^{-6} \cdot x - 2.355e^{-7}$

Table F-4: Ratios of NDR comparing the proposed zonal adaptive settings against the 1Hz/s+0ms and 1Hz/s+500ms protection settings (averaged over three valid cases [18])

Settings Renewable Level / (System Inertia Constant)		Adaptive *vs.* 1Hz+0ms			Adaptive *vs.* 1Hz+500ms		
		0%~30% (6 s ~ 4.2 s)	30%~50% (4.2 s ~ 3 s)	50%~70% (3 s ~ 1.8 s)	0%~30% (6 s ~ 4.2 s)	30%~50% (4.2 s ~ 3 s)	50%~70% (3 s ~ 1.8 s)
Study Zone	N1	0.79	0.62	0.18	0.82	0.67	0.29
	N2	0.79	0.62	0.20	0.82	0.67	0.30
	N3	0.79	0.62	0.22	0.82	0.67	0.32
	N4	0.80	0.66	0.32	0.83	0.70	0.41
	S1	0.84	0.73	0.42	0.86	0.77	0.50
	S2	0.89	0.74	-0.05	0.91	0.78	0.09
	S3	0.92	0.78	0.17	0.93	0.81	0.28
	S4	0.87	0.66	-0.40	0.89	0.70	-0.22
	S5	0.91	0.72	-0.37	0.92	0.76	-0.19
	S6	0.88	0.63	-0.62	0.90	0.68	-0.41
	S7	0.89	0.73	-0.45	0.91	0.77	-0.25
National Average		0.85	0.68	-0.03	0.87	0.72	0.10